Doctoral theses at NTNU, 2020:66

Alberto Luis Bila

Experimental investigation of surface-functionalised silica nanoparticles for enhanced oil recovery

Doctoral thesis

ISBN 978-82-326-4484-1 (printed ver.)
ISBN 978-82-326-4485-8 (electronic ver.)
ISSN 1503-8181

NTNU
Norwegian University of
Science and Technology

NTNU
Norwegian University of Science and Technology
Thesis for the Degree of
Philosophiae Doctor
Faculty of Engineering
Department of Geoscience and Petroleum

Doctoral theses at NTNU, 2020:66

NTNU

NTNU
Norwegian University of
Science and Technology

Alberto Luis Bila

Experimental investigation of surface-functionalised silica nanoparticles for enhanced oil recovery

Thesis for the Degree of Philosophiae Doctor

Trondheim, March 2020

Norwegian University of Science and Technology
Faculty of Engineering
Department of Geoscience and Petroleum

NTNU
Norwegian University of
Science and Technology

NTNU
Norwegian University of Science and Technology

Thesis for the Degree of Philosophiae Doctor

Faculty of Engineering
Department of Geoscience and Petroleum

ISBN 978-82-326-4484-1 (printed ver.)
ISBN 978-82-326-4485-8 (electronic ver.)
ISSN 1503-8181

Doctoral theses at NTNU, 2020:66

Printed by NTNU Grafisk senter

Dedication

I wish to dedicate this thesis with my deepest gratitude and affection to

my daughter Larissa Kyandra Bila

to my wife Patricia Bila

and to my grandmother (in memoriam)

in the hope that it will be a source of knowledge and inspiration.

Abstract

Enhanced oil recovery (EOR) using nanoparticles (NPs) has been proposed as a solution in the petroleum industry to overcome declining production rates. Research has shown that commercially available hydrophilic silica NPs, manufactured by Evonik Industries, as additives to water flood can increase oil production from oil reservoirs. However, recent advances show that surface modification can further improve the microscopic sweep efficiency of NPs due to improved solubility and stability, greater stabilisation of emulsions, and low retention on porous medium compared with bare nanoparticles. The hypothesis above was the initiation of the present project. Evonik Industries developed twenty-three different types of silica nanoparticles with surface functionalities for oil recovery applications. The NPs were supplied to us as special research and development products under the name AERODISP®, or more precisely AEROSIL® particles in liquid solution.

Twenty-three unique glass micromodel injection configurations were conducted as a preliminary NPs screening step in the secondary recovery mode. The NPs with the greatest EOR potential were further evaluated using water-wet and neutral-wet Berea sandstone rocks, totalling sixty-seven successful core flooding configurations. Finally, the most promising samples were tested at a minimal reservoir temperature of 60 °C in tertiary recovery mode. Experimental nanofluids stability, interfacial tension and wettability tests, as well as the analyses of the differential pressure throughout the core, were performed to gain insight into the mechanisms by which nanofluids increased oil recovery. The nanofluids were prepared at 0.1 wt% concentration in seawater. Crude oil was obtained from a North Sea field.

The overall screening process identified four types of silica NPs with the greatest oil production potential. Interestingly, all NPs were coated or modified with polymer molecules, resulting in polymer-coated nanoparticles. The NPs were stable at room temperature (22 °C) for over four months in seawater, but they failed to hold long-term stability at the assumed reservoir temperature (60 °C). They remained stable for up to four days storage-time at reservoir temperature. Never-

theless, flooding experiments demonstrated that the NPs can mobilise residual oil and increase oil recovery. In addition, the experiments revealed that the NPs were more efficient in enhancing oil recovery from water-wet Berea sandstone, and the recovery was greatest at high temperature. The oil recovery factor greater than 5% of OOIP was only achieved at the expense of large pore volumes of injected nanofluids.

An analysis of displacement mechanisms due to nanofluid injection suggested that oil recovery occurred through synergistic effect of reduced interfacial tension, increased structural disjoining pressure and wettability alteration, generation of *in-situ* oil emulsion droplets and microscopic flow diversion due to clogging of the pores. At present, the contribution of these displacement parameters may not be fully isolated. However, the formation of NP-stabilised emulsion and log-jamming effect appeared to be the main influencing parameters for oil recovery from water-wet Berea sandstone rocks; While wettability alteration was the most relevant oil drive mechanism for any of the NPs in neutral-wet Berea sandstone.

Future studies are recommended to focus on the characterisation of surface activity and reactivity of the surface/coating additive materials at reservoir conditions to predict their interactions with base fluids, the binding with NPs, and with the reservoir rock. This will further improve the understanding of how NPs contribute to the mobilising of residual oil.

Preface

This thesis was submitted in partial fulfilment of the requirements for the degree of Doctoral of Philosophy (Ph.D) in Reservoir Engineering at the Norwegian University of Science and Technology (NTNU).

The research work presented herein was carried out for Evonik Industries as part of the nanoparticles for enhanced oil recovery project under the supervision of Dr. Ole Torsæter and Dr. Jan Ågen Stensen.

This project was funded by the Norwegian Programme for Capacity Development in Higher Education and Research for Development within the Fields of Energy and Petroleum (EnPe 2016-2019), with additional financial support from Evonik Industries. All experimental work was carried out at the Department of Geoscience and Petroleum at NTNU, Trondheim-Norway.

Acknowledgements

First of all, I thank Almighty God for giving me the strength and knowledge to undertake the "endless" research study and complete this doctoral step.

I would like to express my gratitude appreciation to my esteemed advisers Prof. Ole Torsæter from NTNU and Dr. Jan Åge Stensen from Sintef Industry for the support, guidance, and motivation throughout my doctoral research. Their immense knowledge and guidance have always been the backbone of my research stages. I could not have imagined having better advisers and mentors for my PhD study.

I am also grateful to Pål Skalle for copy-editing this thesis.

Special thanks extend to Dr. Ulrich Fischer and Dr. Maximilian Cornelius from Evonik Industries for their fruitful discussions and ideas that helped to build solid knowledge on nanoparticle technology for oil production.

I gratefully acknowledge the substantive contributions from, Dr. Georg Voss, Erik Kjørslevik, Mohamed Omran and Salem Akarri for helping me conducting part of the flooding experiments and particle size measurements. I thank Reidun Cecilie Aadland and Hamid Hosseinzade Khanamiri for helpful discussions to build the flooding rig and understanding its workflow, especially at elevated temperature.

Finally, I would like to thank my family for their unconditional support.

A.B.

List of Papers

This work resulted in the publication of five main papers and one poster. Additional two articles are under preparation for publication. The author has also contributed to other research activities that will result in the publication of two articles.

Papers	Description
P#1	**Bila, A., Stensen, J. Å., & Torsæter, O**. (2019, May 13). Experimental Evaluation of Oil Recovery Mechanisms Using a Variety of Surface-Modified Silica Nanoparticles in the Injection Water. *Society of Petroleum Engineers. doi:10.2118/195638-MS*.
P#2	**Bila, A., Stensen, J. Å., & Torsæter, O**. (2019). Experimental Investigation of Polymer-Coated Silica Nanoparticles for Enhanced Oil Recovery. *Nanomaterials (Basel, Switzerland), 9(6), 822. doi:10.3390/nano9060822*.
P#3	**Bila, A., Stensen, J. Å., & Torsæter, O**. An experimental investigation of surface-modified silica nanoparticles in the injection water for enhanced oil recovery. *This paper was prepared for presentation at the International Symposium of the Society of Core Analysts held in Pau, France, 26-30 August 2019. SCA2019-012*.
P#4	**Bila, A., Stensen, J. Å., & Torsæter, O**. Polymer-coated silica nanoparticles for enhanced oil recovery in water-wet Berea sandstones. *This paper was prepared for presentation at the 2^{nd} Conference of the Arabian Journal of Geoscience (CAJG) held in Sousse, Tunisia, 25-28 November 2019*.
P#5	**Bila, A., Stensen, J. Å., & Torsæter, O**. (2020). Polymer-functionalized silica nanoparticles for improving water flood sweep efficiency in Berea sandstones. *In E3S Web of Conferences (Vol. 146, p. 02001).* EDP Sciences. https://doi.org/10.1051/e3sconf/202014602001.

Poster	**Bila, Alberto, Kjørslevik, Erik and Torsæter, Ole.** (2018). Microfluidic and Core-flood Methods for Screening Nanoparticles for EOR process. *This poster was prepared for presentation at the IOR conference held in Stavanger, Norway, 23-24 April 2018.*

Table of Contents

List of Tables

List of Figures

Nomenclature and Abbreviations

A Cross sectional area

AERODISP® Aqueous dispersion of hydrophilic silica nanoparticles poduced by Evonik Industries

AEROSIL® Hydrophilic silica nanoparticles produced by Evonik Industries

BPR Back pressure regulator

BT Breakthrough

D$_{ave.}$ Average nanoparticle diameter

DLS Dynamic light scattering

DSA Drop Shape Analyser

dP Differential pressure

E$_V$ Macroscopic displacement efficiency

E$_D$ Microscopic displacement efficiency

EOR Enhanced oil recovery

g Gravitational acceleration

HT High temperature

I$_w$ Amott water index

I$_o$ Amott oil index

IOR Improved oil recovery

IFT Interfacial tension

k Permeability

k_{rw} End-point relative permeability to water

k_{ro} End-point relative permeability to oil

l Length of the rock core plug

M Mobility ratio

NTNU Norwegian University of Science and Technology

NCS Norwegian Continental Shelf

NPD Norwegian Petroleum Directorate

NF Nanofluid

NP Nanoparticle

N_c Capillary number

OOIP Original oil in place

PSD Particle size distribution

PV Pore volume

P_c Capillary pressure

PTFE Polytetrafluoroethylene

$Q_{inj.}$ Injection flow-rate

r Pore radius

RT Room temperature

RF Recovery factor

rpm Revolution per minute

SEM Scanning electron microscope

SDP Structural disjoining pressure

SARA Saturates, Aromatics, Resins and Asphaltens

SI Spontaneous imbibition

SSW Synthetic Seawater

$\mathbf{S}_{oi}$ Initial oil saturation

$\mathbf{S}_{or}$ Residual oil saturation

$\mathbf{S}_{orw}$ Water flood residual oil saturation

$\mathbf{S}_{o}$ Oil saturation

$\mathbf{S}_{wi}$ Initial water saturation

TDS Total dissolved salts

$\mathbf{V}_{b}$ Bulk volume

$\mathbf{V}_{o}$ Volume of oil

$\mathbf{V}_{o1}$ Volume oil produced by spontaneous water imbibition

$\mathbf{V}_{o2}$ Volume oil produced by forced drainage

$\mathbf{V}_{w1}$ Volume water produced by spontaneous oil drainage

$\mathbf{V}_{w2}$ Volume oil produced by forced drainage

$\mathbf{V}_{b}$ Bulk volume

WF Water flood

WI Wettability index

XRD X-ray diffraction

γ Interfacial tension

$\Delta\rho$ Fluid density

$\Delta\mathbf{P}$ Laplace pressure across the fluid interface

θ Contact angle

μ**CT** Micro Computed tomography

μ Fluid viscosity

ν Fluid velocity

ρ Fluid density

ϕ Porosity

CHAPTER 1

Introduction

1.1 Background and Motivation

The world population is expected to rise to nearer 10 billion by 2050, and the need for energy is to increase as a function of population (Baron et al. 2008). The estimate assumes that the present population has enough energy to meet its needs. Today, energy consumption is largely met by the combustion of hydrocarbons. However, the discovery of new oil fields have been scarce (Muggeridge et al. 2014, Sun et al. 2017), and most of the existing fields have reached or are nearing the abandonment phase while leaving more than 50% of original oil in place (OOIP) buried in the reservoir (Fletcher and Davis 2010), which in some cases is producible under tertiary or enhanced oil recovery (EOR). State-of-the-art of currently available technologies, such as thermal recovery, gas injection and chemical methods, have limited success due to high costs or inefficient recoveries. Therefore, the oil industry is seeking for innovative technologies to extend the life of existing fields while running the production more economically and environmentally friendly.

Norway is the largest oil producer in Europe and the eighth largest producer in the world (Smalley et al. 2018). On the Norwegian Continental Shelf (NCS), most of the production is developed by water or gas flooding (Smalley et al. 2018). Despite high average oil recovery factor, 47% of OOIP (Smalley et al. 2018), about half of the oil resources cannot be produced with current technology. Figure 1.1 shows that many fields still contain large oil volumes above those covered by production plans and will be shut down with large quantities of residual oil in their reservoirs (NPD 2019). This example provides a practical estimation of oil remaining in the

reservoir after primary and secondary oil production stages, and obviously this oil calls for EOR techniques, so that all commercially resources get produced.

Nanoparticles are believed to have enormous potential to improve the microscopic sweep efficiency of water flood on the NCS fields. The small diameter (1-100 nm) and large surface area-to volume ratio make the NPs appropriate for EOR application. These properties increase the mobility and surface reactivity of the NPs, especially at high temperature, while travelling through reservoir pores, thereby modifying fluid-rock properties (Ayatollahi and Zerafat 2012, Bennetzen and Mogensen 2014, Sun et al. 2017). Furthermore, NPs can travel along with water through and reach untouched zones of reservoir with no severe impact to the rock permeability (Hu et al. 2016, Bennetzen and Mogensen 2014, Sun et al. 2017), being the main outcome the mobilisation of capillary trapped oil and that bypassed during water flooding.

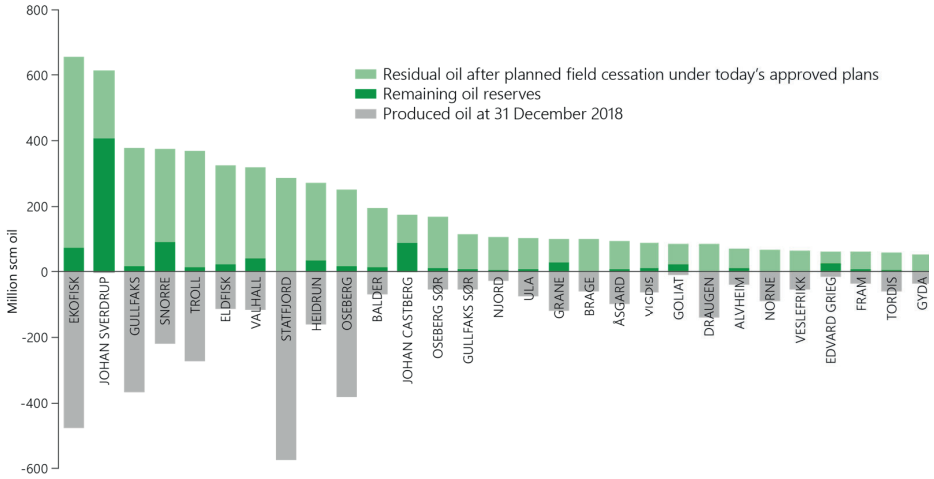

Figure 1.1: An overview of 27 oilfields on the Norwegian Continental Shelf: Produced oil (grey) at December 2018, remaining reserves (dark green) and residual crude oil after planned shut-in (light green) (NPD 2019); 1 Sm^3 = 6.29 barrels.

This thesis expands on the work of Aurand (2017), in which the conditions required for silica NPs to improve the performance of water flood on the NCS fields were experimentally investigated. Aurand's work resulted in the development of silica NPs with surface that was modified/functionalised with different material additives to meet some of the field conditions found on the NCS to increase oil recovery. These NPs are investigated in the present thesis. The most promising NPs samples are highlighted, and their underlying oil recovery mechanisms are proposed. Finally, recommendations are outlined for future developments/works.

1.2 Formulation of the Problem

Nanoparticles play an important role for crude oil/brine/rock interfaces, which can be advantageous for oil production. However, the complex nature of the interactions occurring at the interfaces still pose many challenges to formulate homogeneous suspension of NPs and to grasp the underlying mechanisms of NPs for oil production. Nevertheless, there is a growing evidence that NPs can improve water flooding oil production at least from 5 to 15% of OOIP (Bera and Belhaj 2016). The surface modification may further improve NPs oil recovery efficiency due to improved solubility and stability, greater stabilisation of emulsions, and low retention on porous medium compared with bare nanoparticles (ShamsiJazeyi et al. 2014, Gbadamosi et al. 2018). This thesis experimentally unleashes the potential of surface-modified silica NPs and attempts to reduce uncertainties on their application for oil production.

Norwegian Continental Shelf data, according to Bjorkum and Nadeau (1998), show that most of the discovered resources occur at temperatures greater than 60 °C. Stable NPs dispersion at 60 °C can be applicable in shallower reservoirs (Aurand 2017). This work seeks to answer the following questions:

1. Are the surface modified silica NPs stable stable in seawater at 60 °C?

   Hamon (2016) suggested that tertiary core flooding tests should produce oil at the core outlet at approximately 0.5-0.6 of pore volumes (PVs) injected or additional oil recovery should be at least 5% of OOIP after 1 PV. This criterion is used in the present work to determine the viability of NPs during core flood experiments. This raises the second research question:

2. Do surface-modified silica NPs increase oil recovery? When or how much oil is produced and how many PVs are needed to induce production?

   Oilfields are unique and may behave differently to EOR fluid injection. Thus, it is important to understand why and how the injectants induce oil production. The outcome is extremely critical for the design and execution of an effective EOR strategy. Therefore, the third research question is:

3. What are the main EOR mechanisms of surface-modified silica NPs?

1.3 Research Objectives

Nanoparticle are often injected into oil and gas wells and are subjected to reservoir conditions such as high pressure, high temperature, high salinity and the presence of contaminants (Khalil et al. 2017). Undoubtedly, these conditions prevent the

NPs from playing their designated roles in the reservoir. In order to overcome these limiting conditions and ensure a successful application of the particles, the modification and functionalization of the surface of the particles can be created to improve stability and dispersibility, stabilisation of the emulsion, fluidity in porous media and improve microscopic sweep efficiency of water flood. This thesis expands on the work initiated by Aurand (2017) that investigated the conditions required for the development of silica NPs for EOR applications. Aurand's recommendations resulted in the development of tailored NPs for specific oil field characteristics by creating surface functionalities on the particle's surface using a variety of surface material additives. The main objectives of this thesis were therefore to:

- Identify the nanoparticles with the highest oil recovery potential; and
- Determine the underlying oil production mechanisms of the nanoparticles.

1.4 Limitations of the study

The nanoparticles used in this work were supplied to us as special research and development (R&D) products by Evonik Industry.

The experiments were conducted to evaluate the applicability of the NPs in EOR in reservoirs such as that of North Sea sandstone and unleash the underlying mechanisms by which the NPs increase oil recovery. Initially, the experimental materials and research methodology were proposed by the nanomaterials supply company; The number core flooding experiments required, coupled with the need to deliver results on time, left little time for additional studies/tests. The most limiting factor concerned the characterisation of the supplied nanomaterials; the physicochemical mechanisms governing the surface modification of the NPs were not revealed by the manufacturer. Furthermore, relevant information such as type and surface functional group characteristics of the surface additive materials, surface area, particle composition, physicochemical interactions between the surface additives and silica NPs etc. were not made clear by Evonik Industries. This was because the company would need to file patent in order to protect intellectual property, proved that the nanoparticles can increase oil recovery. This has largely limited a deep interpretation and discussion of the results obtained in this thesis.

All experiments were carried out at core analysis laboratory at the Department of Geoscience and Petroleum at NTNU using the available equipment.

1.5 Outline of the Thesis

This thesis consists of seven Chapters. The organisational structure is given in Table 1.1.

Table 1.1: Organisational structure of the thesis.

Chapter	Description
#1	This chapter provides an introduction of the research topic and establishes the background and motivations of the present work.
#2	It introduces the main concepts of enhanced oil recovery. This includes the fundamentals of oil production, the main reservoir parameters that affect oil recovery. This chapter also presents the definition of the main reservoir engineering terminology used throughout this work.
#3	An overview of the experimental material that used throughout this work is described in this chapter.
#4	This chapter provides additional characterisation of experimental material and description of the methods adopted to perform the experiments.
#5	Presents the main experimental findings of this thesis.
#6	This chapter is devoted to the discussion of the main results achieved in this thesis.
#7	This chapter concludes the present thesis and summarises overall findings and outlines some recommendations for future developments/works.

CHAPTER 2

Concepts of enhanced oil recovery

2.1 Introduction

Reservoir engineering is a branch of petroleum science that provides and applies scientific principles for the maximum recovery of reservoir hydrocarbons at lowest cost possible. Enhanced oil recovery involving nanoparticles is an emerging technology across the petroleum industry. The purpose of present Chapter 2 is to provide background information on how the nanoparticles can enhance oil recovery. To build a comprehensive understanding for the reader, the present Chapter describes the main reservoir parameters that are influenced by nanoparticles and the main enhanced oil recovery mechanisms of NPs. The main reservoir engineering terminology used throughout this work is defined.

2.2 Fundamental properties of reservoir and fluids

A reservoir is composed of rock and fluids (water, oil, and gas) that occupy the pore spaces. The volume of interconnected pore spaces is termed *pore volume* (PV); it is a product of the reservoir *bulk volume* (V_b) and the *effective porosity* (ϕ_e). A porosity of a reservoir is the property that measures how porous a rock is and its fluid storage capacity. There are two main types of porosity, the total and the effective porosity; the latter affects the amount of hydrocarbons that can be produced, so it is the most important for reservoir engineers.

$$\phi_e = \frac{PV}{V_b} = \frac{V_{bulk} - V_{grain}}{V_{bulk}} \tag{2.1}$$

A reservoir can be porous without being permeable. It is said permeable if and only if there is an effective communication between the pore spaces establishing pathways through which fluids can flow and be produced. This is *permeability*. In other words, it defines how well a porous media can conduct or transmit fluids under a potential pressure gradient. The most used definition of permeability follows the Darcy's law:

$$\frac{q}{A} = \frac{k}{\mu}\frac{\Delta P}{L} \tag{2.2}$$

where q is the flow rate, A is the flow cross section area, k is the absolute permeability, and μ and ΔP/L are fluid viscosity and the pressure drop per unit length.

Equation 2.2 was developed under the assumptions of neutral fluid (no chemical reaction with the porous media), incompressible fluid, and isothermal conditions. The flow is horizontal, and the fluid is assumed single flow and liquid, which is subjected to laminar flow (Lock et al. 2012, Dandekar 2013). There are three types of permeability, the absolute, the effective, and relative permeability. The concept of *absolute permeability* applies if and only if one fluid flows through the rock as described by Equation 2.2. It is a constant for a specific porous media, regardless of the type of fluid flowing through it. In a reservoir, there are more than two and immiscible fluids flowing through it. Therefore, the concept of *effective permeability* of each fluid phase i (water, oil or gas) (k_i) is introduced to account for the ability of one fluid to flow through that media in the presence of other immiscible fluids. It plays a major role in the production of hydrocarbons by primary recovery mechanism or immiscible displacement methods involving the injection of gas or water (Dandekar 2013). The effective permeability is usually normalised by absolute permeability to reflect possible combinations of fluid saturation for a single porous media. This results in *relative permeability* (k_{ri}), the ratio of effective permeability to absolute permeability.

$$k_{ri} = \frac{k_i}{k} \tag{2.3}$$

Relative permeability is mostly influenced by fluid saturation, capillary, viscous and gravity forces, wettability of the rock, temperature and pore geometry (Craig 1971). More importantly, relative permeability is required in various reservoir engineering calculations, reservoir simulations such as assessing efficiency of displacement mechanism and ultimate recovery of hydrocarbon from petroleum reservoir (Dandekar 2013). Estimation of hydrocarbons present in petroleum reservoir is also based on the ability to estimate saturation of each fluid in it. The saturation of each fluid phase (gas, oil or water), S_i, is defined as the volume ratio of a particular fluid, V_i, to the pore volume according to Equation 2.4. The summation of all fluid saturation in a reservoir is 100%.

$$S_i = \frac{V_i}{PV} \tag{2.4}$$

In the present thesis, the reservoir rock was prepared to be saturated by two fluids, water and oil. The gas phase was therefore not included. Both initial oil saturation (S_o) and residual oil saturation (S_{or}) were the principal targets for secondary and tertiary EOR processes, respectively. The reservoir saturating fluids interact differently with each other and with the rock system. The resulting interactions play a major role for the recovery in the recovery of oil. Therefore, it is important to characterise the involved interaction forces and how they can be modulated in the presence of nanoparticles for enhancing oil recovery.

2.3 Forces and interactions between reservoir rock and fluids

In the reservoir, more than two fluids compete for the same pore space. Capillary are the governing forces that define the dynamic flow conditions (competition) between interfaces of the phases. These forces are therefore a combined effect of interfacial tension, pore size and geometry, capillary pressure, and the wetting characteristics of the rock system. In oil recovery process, capillary forces resist externally applied viscous forces and hence, being responsible for trapping large portion of the hydrocarbons within the interstices or pores space. A transition between the displacement process dominated by capillary or viscous forces is correlated by the capillary number (N_c):

$$N_c = \frac{\text{Viscous forces}}{\text{Capillary forces}} = \frac{\mu v}{\gamma \cos\theta} \tag{2.5}$$

Here, μ and v represent the viscosity and velocity of the displacing fluid, respectively. The γ is the IFT between the displacing and the displaced fluid.

To accelerate oil recovery, N_c should be increased either by increasing the viscous forces or by decreasing the capillary forces. Applying sufficient pressure gradients between wells when injecting viscous fluids to significantly increase viscous forces is the major challenge (Muggeridge et al. 2014), as it can fracture the reservoir. Therefore, reservoir engineers rely on decreasing the capillary forces. Low capillary forces increase the mobility of the oil phase by deforming and breaking large oil drops into small ones that can flow easily through the pore throats toward the production wells (Mohammadi 2013, Sheng 2015). Equation 2.5 shows that capillary forces acting against oil recovery can be weakened by decreasing IFT, which increase N_c, or by manipulating the rock wettability to a more favourable oil recovery condition. The critical capillary number for the onset of mobilisation of residual oil is of orders of 10^{-5} (Humphry et al. 2014, Muggeridge et al. 2014), above which a complete mobilisation of oil may occur. This requires that any EOR

fluid should be able to change the fluid-fluid and fluid-rock interfaces properties to a favourable condition for oil recovery.

2.3.1 Surface and interfacial tension

At the interface of two dissimilar fluids, such as oil and water, the forces acting on the molecules of each of these fluids are not the same as within each phase (Dimri et al. 2012). This gives rise to *interfacial tension* (IFT), and it behaves like a membrane separating the two phases. If one of the phases is gas, the interfacial force is termed *surface tension*. The focus in present work is the interfacial tension because no gas phase saturation was included in oil recovery experiments. Interfacial tension is a measure of the force acting on the surface of a liquid and tend to minimise the area of its surface, resulting in liquid forming droplets with spherical shape (Dimri et al. 2012). It is expressed as the force per unit length (mN/m, which is equivalent to dynes/cm) and is denoted by γ (Dimri et al. 2012, Dandekar 2013). Together with viscosity, the IFT provides a qualitative indication of how, and to what extent, oil will flow through the pore spaces of the rock matrix. Interfacial tension for most crude oil and seawater systems is typically between 20 to 30 mN/m (Dimri et al. 2012, Dandekar 2013, Sheng 2015). This results in high capillary forces. The oil phase will therefore resist the mobilising viscous forces stemming from pressure gradient during oil recovery process (e.g. water flood). To mobilise substantial volumes of capillary trapped oil, the IFT should be reduced to $\leq 10^{-3}$ mN/m (Sheng 2015). Measurement of IFT is required for evaluating the potential of any EOR fluid where lowering of IFT is the mean of oil recovery. Water with added NPs or nanofluid was the EOR fluid used to increase oil recovery through the reduction of IFT in present work. The resulting effect of surface functionalised silica nanoparticles on the oil-water interface is described in Section 2.6.1.

2.3.2 Wettability and contact angle

In addition to forces acting at fluid-fluid interfaces, the forces at fluid-solid interface are also of vital importance for oil production and optimisation of EOR process. A force balance between adhesive forces (acting at liquid-solid interface) and cohesive forces (acting in the wetting liquid) determines the degree of wettability of a reservoir rock. These forces may act to bring the interfaces close together or to hold them separated; its contribution include van der Waals, electrostatic, and structural or solvation forces (Schramm 2000). A net force is expressed as force per unit area, termed disjoining pressure; a positive disjoining pressure tends to hold the interfaces apart while the negative attracts or brings the interfaces close together (Schramm 2000). The latter contributes to enhancing wetting properties of the rock. *Wettability* is therefore defined as the preference of a solid to be

contacted/coated by one fluid rather than another (Abdallah et al. 1986, Dandekar 2013). This results in wettability being the major parameter that controls the location, flow, and distribution of fluids in a reservoir; it affects relative permeability, capillary pressure (Abdallah et al. 1986, Anderson 1987, Bera and Belhaj 2016), the amount of oil that can be produced at pore level (Abdallah et al. 1986, Bera and Belhaj 2016).

In a porous rock saturated with oil and water, wettability can be *water-wet* where the rock surface prefers contact with water; water occupies the small pores while oil is found in the centre of the larger pores. *oil-wet*: the rock has much affinity for oil rather than water and oil occupies the small pores while water is found in the centre of the larger pores. In between is the *mixed-wet* condition, i.e. the surface have a variety of preferences. The mixed-wet system may possibly include *intermediate-wet* or *neutral-wet* surfaces, which means lack of wetting preference. Figure 2.1 shows the distribution of fluids within the reservoir for different wettability. Reservoir rocks are complex structures composed of a variety of mineral types, each exhibiting its own wetting preferences. Reservoir wettability depends on the rock mineralogy, crude oil composition, connate water composition and pore size distribution (Buckley et al. 1998, Muggeridge et al. 2014). It is generally accepted that changing the wettability of an oil-wet reservoir is favourable for oil recovery. However, there is less agreement as to which alteration, water-wet or neutral-wet, lead to the maximum oil recovery.

In the present thesis, water-wet and neutral or intermediate-wet system were used for the evaluation of oil the recovery process. Wettability was changed by ageing naturally water-wet rock cores in crude oil. Then, it was evaluated using Amott-Harvey test (the procedure is described in Section 4.5).

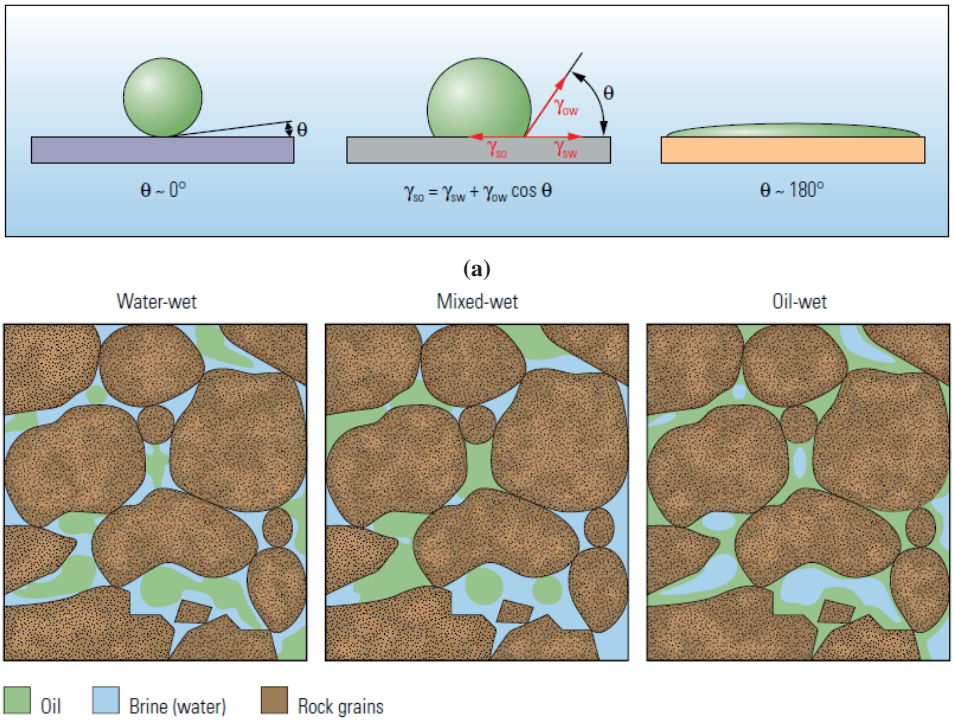

Figure 2.1: Wettability regimes of a reservoir rock saturated with water and oil: (a) The contact angle is $\theta \approx$ zero for an oil drop surrounded by water on a water-wet surface. On oil-wet surface, the drop spreads, forming an angle of about 180°. In neutral-wet surfaces, the θ derives from a force balance between the interfacial tension forces; (b) In water-wet surfaces, oil remains in the center of the pores. The reverse is true in oil-wet surfaces. In mixed-wet surfaces, oil has displaced water from some pores, but is still in the center of the water-wet pores (Abdallah et al. 1986).

2.3.3 Capillary pressure

The interactions between two immiscible fluids give rise to *capillary pressure*, P_c due to curved interfaces of the fluids. This means that each immiscible fluid has a different pressure, thus keeping the interfaces separated. The pressure difference across the interface is defined as the pressure of non-wetting phase (P_{nw}) minus pressure of wetting phase (P_w), mathematically expressed as:

$$P_c = P_{nw} - P_w \tag{2.6}$$

Equation 2.6 suggests that the greater pressure occurs in the non-wetting phase. Capillary pressure can be either positive or negative on the curvature of the surface.

As noted previously, capillary forces are manifestation of interfacial tension, pore size, and wettability. Therefore, capillary forces can be expressed in terms of capillary pressure as:

$$P_c = \frac{2\gamma \cos\theta}{r} \tag{2.7}$$

where r is the pore radius.

There are two types of capillary pressure processes, the *drainage*, and *imbibition*. Drainage refers to a process where the non-wetting phase displaces the wetting-phase. An example of drainage is water flood of an oil reservoir that is oil-wet. The reverse process refers to imbibition; an example is the water flood of an oil reservoir that is water-wet. Capillary pressure curves can provide data necessary for estimating oil recovery parameters such as irreducible water saturation, residual oil saturation and rock wettability.

2.4 Oil production process

In an oilfield, there are three chronological stages describing the progress of oil production from its inception to the point where production is no longer economical. These processes are known as primary, secondary and tertiary oil production processes as presented in Figure 2.2.

Typically, the first wells drilled in a reservoir become pressure driven production wells because the reservoir pressure is above bubble point (Muggeridge et al. 2014). The production energy originates from dissolved gas, expansion of gas cap, or the influx of water (Stosur et al. 2003, Shepherd 2009). The first stage, in which production occurs from natural energy, is termed *primary oil recovery*. The reservoir pressure declines with production over time and it can reach uneconomic levels if no additional energy is added to the reservoir. Additional energy can be added in the form of water or gas injected through injection wells to maintain reservoir pressure (Stosur et al. 2003, Muggeridge et al. 2014). This marks the *secondary oil recovery*. If water is used, the process is termed *water flooding*, otherwise *gas flooding*. Water flood is implemented by injecting water into wells where it flows into the pore spaces previously occupied by oil. Due to the applied pressure, water displace oil from the pores to the producer wells. The produced gas is normally re-injected into the gas cap to maintain reservoir pressure rather than to displace oil. In the present work, water flood was implemented to mimic the secondary recovery process. Because oil is normally more viscous than water, water tend to finger through continuous oil and breaking early through to the production wells. This lead to water by-passing significant portion of the initially mobile oil. Even if large quantities of water are flown through the reservoir, oil is held in the pore spaces by capillary forces (see Section 2.3). The remaining oil

in the reservoir after secondary recovery process is called *residual oil saturation* (S_{or}). This oil is target for *tertiary oil recovery* process, which is conducted when secondary recovery is no longer economic. Tertiary recovery processes are also referred to as *enhanced oil recovery* (EOR) processes (Stosur et al. 2003, Shepherd 2009) (see Figure 2.2). A thermal process involving steam, hot water, or combustion has the greatest probability of success and is applied in about 70% of EOR processes worldwide (Lake and Venuto 1990, Green and Willhite 1998, Shepherd 2009). Thermal methods give the highest oil recoveries at the lowest cost (Lake and Venuto 1990). Processes such as microbial, nanotechnology and some other novel proposals are still in the laboratory phase.

The term improved oil recovery (IOR) was introduced in the literature to refer to any practice to increase oil recovery (Stosur et al. 2003). The term "IOR" is not used in this work. Oil production process as shown in Figure 2.2 may not always be conducted in chronological order. For example, if primary and secondary processes fail to produce oil at economic level, thermal techniques, which decreases oil viscosity, can be used from start of the production phase.

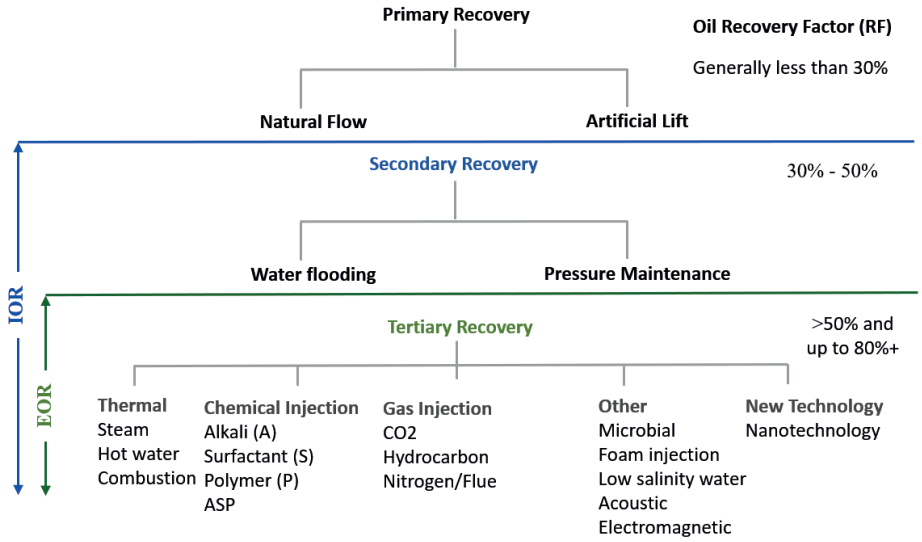

Figure 2.2: Oil production stages and distinction between EOR and IOR terms. Figure modified after (Stosur et al. 2003).

In other situations, the so-called tertiary recovery process may be applied as secondary recovery in a lieu of water flood depending on factors such as the nature of tertiary process, availability of injectants, and economics (Green and Willhite

1998). Because of such situations, the term *tertiary oil recovery* fell into disfavour in the petroleum industry, and EOR is accepted (Green and Willhite 1998).

Enhanced oil recovery processes focus on the rock/oil/injectant to create favourable conditions for oil recovery. Fluids are injected to interact with the reservoir system to release oil from the rock surface. Such interactions might be, for example, reduction of the interfacial tension between oil and water, oil swelling, oil viscosity reduction, wettability alteration, or phase behaviour (Green and Willhite 1998).

The term "EOR" is used throughout this thesis to describe the application of nanotechnology to increase water flood sweep efficiency. The EOR operation performed in this thesis will be specified, whether it is a secondary or tertiary oil recovery process.

2.4.1 Overall Recovery Efficiency

Inspection of Equation 2.5 shows that oil recovery is largely influenced by viscous forces, at macroscopic level, and by capillary forces at microscopic level. Enhanced oil recovery techniques are therefore designed to overcome one of two influencing factors: improve macroscopic displacement efficiency or improve microscopic sweep efficiency of oil. The overall recovery efficiency, E, or oil recovery factor, RF, is given by the product of the *macroscopic*, or *volumetric*, *displacement efficiency* (E_V) and *microscopic sweep efficiency*, E_D. The RF is measured at surface conditions.

$$RF = E_V E_D \tag{2.8}$$

E_V is a fraction of reservoir pore volume that has been contacted by the injected fluid, both areally and vertically, as well as how effectively the injected fluid moves the oil to production wells (Green and Willhite 1998, Muggeridge et al. 2014). Factors that affect E_V include geological characteristics of the reservoir, the fluid properties, the physical arrangement of injection and production wells (Green and Willhite 1998). Macroscopic sweep efficiency is inversely proportional to the *mobility ratio*, M.

$$M = \frac{\text{Mobility of the displacing fluid}}{\text{Mobility of the displaced fluid}} = \frac{k_{rw}/\mu_w}{k_{ro}/\mu_o} \tag{2.9}$$

In Equation 2.9, the displacing and displaced fluids are water and oil, respectively. E_V increases as the M decreases. An ideal EOR fluid, thus, is one that can decrease the oil viscosity or increasing viscosity of injection water throughout the oil recovery process.

Microscopic sweep efficiency is the mobilisation of oil at pore scale. It measures the effectiveness of injected fluids to mobilising residual oil. To increase the E_D, an ideal EOR fluid is one that decreases the IFT and change the wettability to a favourable oil recovery condition during recovery process.

In the present thesis, the EOR process was designed to overcome capillary forces and increase oil mobility. This was accomplished by addition of nanoparticles in the injection water. Laboratory studies were therefore conducted in core floods to investigate the expected performance of the technique. Scaling up the lab-tests to reservoir dimensions represents the major challenge and it is not discussed at present. However, if EOR fluid injection succeeds at core scale, the likelihood of success at reservoir field scale increases.

2.4.2 Laboratory scale enhanced oil recovery

Ensuring successful EOR techniques depend on careful planning and design of EOR fluids specific to the properties of the oil, reservoir conditions, and the availability of injectants. Laboratory studies are widely used to screen the proposed EOR fluids in glass micromodels and/or in core plugs simulating reservoir rock conditions of temperature, pressure, fluids and fluid velocity; These techniques are referred to as *micromodel flooding* and *core flooding*, respectively. At laboratory scale, oil production is collected step wise while paying attention to *how much* oil is produced, *when*, *why*, *how*, etc. to evaluate the performance of EOR fluid relative to conventional water flood. Oil recovery factor (RF) can be obtained by re-writing Equation 2.8:

$$RF = \frac{\sum V_o}{OOIP} = \frac{S_{oi} - S_{or}}{S_{oi}} \tag{2.10}$$

The physical properties of natural rocks often vary, resulting in different pore volume even for the same size of rock cores. Therefore, the injection time is normalised by bulk volume to better compare with other rock core tests. The normalised time or pore volume (PV) is given by Equation 2.11:

$$PV = \frac{Qt}{V_b} \tag{2.11}$$

In Equation 2.11, PV is dimensionless; Q is the injection flowrate, t is the injection time, and V_b is the rock bulk volume.

Oil recovery is then plotted against normalised time or PV (see Figure 2.3). When evaluating an EOR fluid at laboratory scale, a set of duplicate core plugs with similar properties should be used to ensure reproducible results and to better compare the EOR fluid with water flood results. The re-use of the cores after any stage of

oil production is not recommendable due to difficulties in removing crude oil and EOR fluid.

If an EOR process is applied as secondary operation, the ultimate recovery factor must be better than for traditional secondary water flooding to ensure economic attractiveness of the secondary EOR process (Green and Willhite 1998). In this case, oil recovery from EOR fluid is expected to increase by *percentage point*, which is a difference between the ultimate oil recoveries from secondary EOR fluid and water flood processes. It measures the efficiency of applying an EOR fluid compared to water flood. This is depicted in Figure 2.3(a).

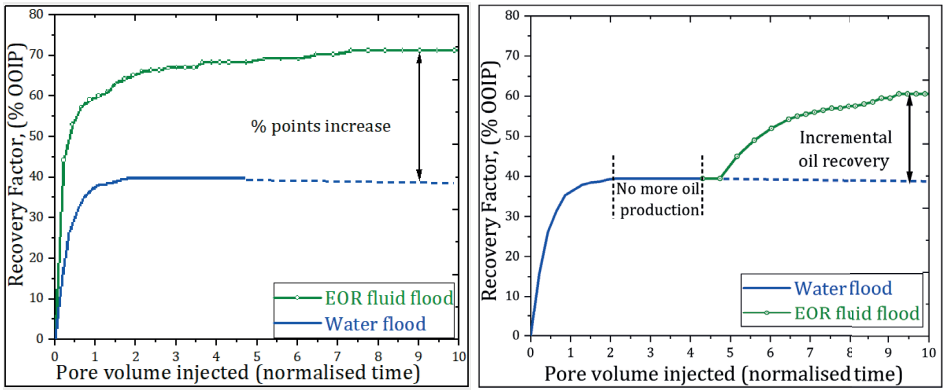

Figure 2.3: Comparison of oil recovery factors from water flood and EOR fluid flood: (a) Water and the EOR fluid are separately injected (at S_{wi}) in secondary recovery mode; (b) water flood is followed by EOR fluid flood.

If an EOR process is applied as tertiary recovery operation, then a criterion must be adopted to ensure that a reservoir rock has been water flooded enough to reach true residual oil saturation and capillary end-effects are mitigated. Hamon (2016) proposed criteria for assessing tertiary process. In his study, the EOR fluid was low salinity water. Hamon's criteria assume that a realistic or positive effect of any EOR fluid is that which produces the first oil bank at core outlet after injection of 0.6 PV or oil recovery is at least 5% of OOIP after 1 PV is injected. As noted earlier, an EOR fluid can induce oil recovery through fluid-fluid and fluid-rock interactions. The nature of the interactions may be fluid type, reservoir system and time dependent. Furthermore, Equation 2.11 shows that PV is a function of flowrate, time and core size. This means that, for instance, it is possible to flood 1 PV through the core within one hour. Under some circumstances, this may not be enough time for the interactions needed to mobilise residual oil to occur.

Therefore, one should consider these factors when evaluating any EOR fluid using Hamon' criteria.

A plot showing a tertiary oil recovery process in a chronological sense, i.e. water flood followed by EOR fluid injection, is presented in Figure 2.3(b). Additional oil produced by EOR fluid is termed *incremental oil* and is expressed as % of OOIP.

2.5 Nanoparticles for enhanced oil recovery

This Section defines and characterises the nanoparticle, as well as how it is injected into the reservoir to accelerate oil recovery. Present Section also focuses on studies that evaluated silica NPs for oil recovery and describes the most relevant oil recovery mechanism.

2.5.1 Nanoparticle and nanofluids

Nanoparticles are the collections of atoms bonded together with size ranging from 1 to 100 nm (Bera and Belhaj 2016). Nanoparticles (NPs) are of great scientific interest as they bridge bulk materials and atomic or molecular structures. Bulk materials exhibit constant physical properties regardless their size; unlike nano-sized materials, the properties are often size dependent. A NP is composed of two entities as shown in Figure 2.4: the *core* and the *shell* or *coating* (Das et al. 2006).

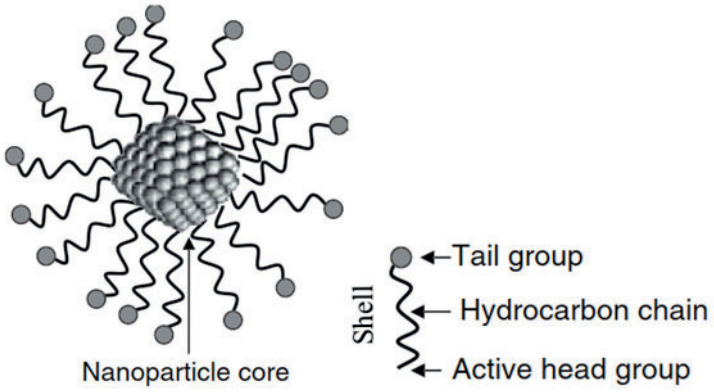

Figure 2.4: Schematic of a nanoparticle, showing the core and the shell (Das et al. 2006).

The *core* (often ceramic, metallic, or polymeric) determines the properties of a nanoparticle whereas the *shell* (ionic, molecular, polymeric, ceramic, or metallic) provides a protective layer and determines the solubility or binding affinity of the nanoparticles (Das et al. 2006). For instance, if NPs are hydrophilic with hydroxyl functional group (-OH) as shell layer (or surface molecules), they can disperse

easily in polar liquid (e.g. water, alcohol, etc.), unlike hydrophobic with lipophilic shell layer, they disperse in non-polar liquid-like oil or toluene.

For EOR applications, the interest in NPs arises from its small size, usually two to three orders of magnitude smaller than reservoir pore throats (Zhang et al. 2015, Kokubun et al. 2019), and high surface area-to-volume ratio. The small size gives good mobility properties while the latter makes the NPs very reactive with other molecules (reactions normally occur on the surface). More importantly, the surface of NPs can be modified and tailored to meet different oil reservoir characteristics (Miranda et al. 2012, Bennetzen and Mogensen 2014). Figure 2.5 tries to make it memorable for the reader about how small a NP is compared to other common material scales. A common example is that the diameter of NP is 10^5 times smaller than that of a strand of human hair. The mall size makes the particles to perform entirely different compared to their larger scale counterparts. This unique property extends the application of NPs into many fields of science.

To accelerate oil recovery, NPs are mixed with fluids that are injected into the reservoir. The resulting mixture is called *nanofluid*. Nanofluids must travel deep into the reservoir subject to high pressure, high temperature, high salinity and uneven reservoir mineralogy and composition, which increases the likelihood of NP collision and the tendency to aggregate/agglomerate. This also happen due to large surface free energy induced by nanoparticles small size and large surface area (Yu and Xie 2012). The formation of aggregates or *unstable* nanofluids diminishes surface functionalities of NPs at the fluid-rock interfaces resulting in poor oil recovery. Furthermore, the aggregates can block reservoir pore channels and increase the pressure and oil production costs. To address this problem and achieve *stable* nanofluids, surface modification can be created on the primary NP surface. The resulting NPs are referred to as *surface-modified nanoparticles* and may possess additional surface functionalities such as stabilisation of emulsion, transportable through the pores with low retention, etc. (ShamsiJazeyi et al. 2014, Gbadamosi et al. 2018). These types of NPs are the main focus in present work. The commonly reported mechanisms for improving nanofluid stability are *electrostatic stabilisation* and *steric stabilisation*. They have been developed to increase repulsive inter-particle interaction, which can count balance the attractive van der Waal dispersion force (Yu et al. 2017). The stabilisation mechanisms of NPs are not discussed in this work. The reader is directed to (Yu and Xie 2012) and (Yu et al. 2017) for details of preparation and improving nanofluid stability.

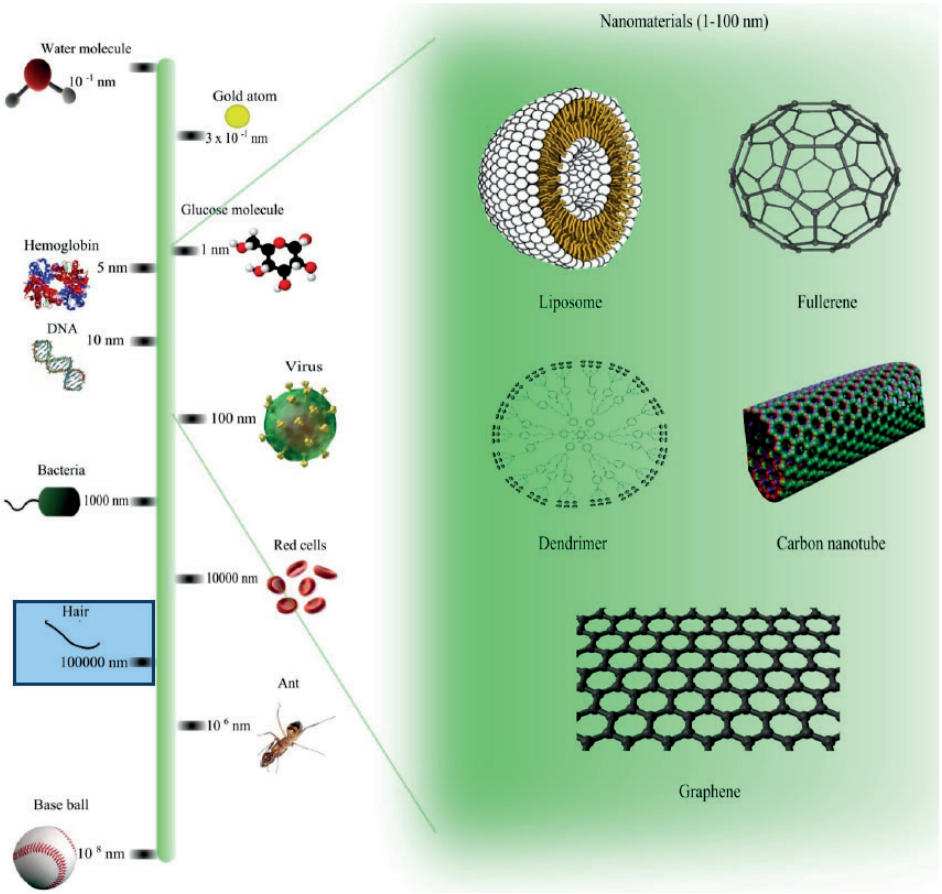

Figure 2.5: Comparison of the sizes of NPs with those of other common materials (Panneerselvam and Choi 2014).

2.5.2 Oil production from nanoparticles injection

There are three categories of nanoparticles for EOR applications: metal oxide, organic and inorganic particles (Negin et al. 2016). The inorganic particles, particularly silica nanoparticles, are the most studied nanomaterials for EOR applications (Negin et al. 2016, Bera and Belhaj 2016). Readers are directed to Negin et al. (2016), Bera and Belhaj (2016), Fakoya and Shah (2017) for details on the use of different types of NPs in various disciplines of petroleum industry, especially in oil recovery. In the petroleum industry, silica (SiO_2) NPs are of interest because of its abundance in nature in the form of sand or quartz (Negin et al. 2016). It is the principal constituent of sandstone rocks such as used in this work. This makes silica nanoparticles environmentally friendly and cost-effective. Miranda et al.

(2012) have discussed other advantages of using silica NPs for EOR purposes. This include the easiness to engineer desired surface functionalities on SiO_2 NPs to improve some properties such as fluidity through the pores, stability, stabilisation of emulsion, etc. A comprehensive review of the application of SiO_2 NPs across the petroleum industry is presented by Fakoya and Shah (2017). Present work focuses on silica NPs whose surface has been modified with various material additives, being the main hypothesis to improve the microscopic sweep efficiency of water flood.

Transportability: The transport and delivery of NPs to where oil exists deep within the reservoir are prerequisites for oil production. For this, Rodriguez et al. (2009) conducted flooding experiments to investigate the transport of polymer-coated silica NPs dispersed in 3 wt% NaCl (5 and 19 wt%) in limestone (10 to 15 mD) and sandstone (421-921 mD) cores. The authors concluded that NPs can travel through reservoir pores of various permeability with little retention. This was attributed to reversible adsorption of NPs as opposed to straining and filtration for colloidal dispersion, the size and the surface coating of the NPs that improved stability in water. Similarly, Yu et al. (2012) carried out core flood tests with bare silica NPs diluted with 2% NaCl to 0.5 wt% concentration to study transport behaviour in sandstone, limestone and dolomite rocks. Their results indicated good transport properties of silica NPs through sandstone cores; little adsorption was observed in limestone and dolomite cores, but the permeability was not changed. Zhang et al. (2015) investigated the effect of experimental conditions on the transport of polymer-coated silica NPs. The authors used core plugs and columns packed with crushed sedimentary rock and systematically varied the flow rate, the particle concentration in 3 wt% NaCl brine and properties of porous media. They concluded that NP retention depends on operating conditions (concentration, flow rates) as well as material properties (clay content in porous media, type of NPs and surface coating). Likewise, Rodriguez et al. (2009) and Zhang et al. (2015) argued that silica NPs coated with polymer chains have remarkable mobility through the pores. In summary, the above mentioned advantages make SiO_2 NPs suitable for EOR applications; In the literature, promising oil recoveries have been reported in the literature under various operating conditions.

Secondary oil production: El-Diasty (2015) evaluated the effect of silica NP concentration (0.01 to 3 wt%) and size (5 to 60 nm) on the displacement of mineral oil (unspecified) in water-wet Bahariya sandstone. The authors reported oil recovery increase by 34% point, that is, from 44.6% by reference water flooding to 79% OOIP by nanofluid flooding. The authors also found that oil recovery increased with NP concentration. However, no correlation was reported with particle size. The recommended concentration of NP (20 nm) in NaCl water (65,000 ppm) was

3 wt% for oil recovery. Torsater et al. (2012) and Youssif et al. (2018) investigated similar type of commercial silica NPs dispersed in 3 wt% NaCl for EOR in water-wet sandstone. Torsater et al. found that NP dispersion (0.01 wt%) can increase paraffin oil recovery by 8% point, while experiments conducted by Youssif et al. revealed a 13% point increase crude oil recovery. Zallaghi et al. (2018) reported that silica NPs, at 0.2 wt% in NaCl water, could increase crude oil recovery by 18% point compared with reference water flood in oil-wet reservoirs. Choi et al. (2017) grafted polymer shell layers on the surface of silica NPs to improve stability. The flood tests showed that, when the grafted NPs were injected into Berea sandstone cores, 74.1% of OOIP could be recovered, which was quite comparable to "pure" water flood (68.9%) and unmodified silica NPs. The nanofluids consisted of 45 wt% NPs in 3 wt% NaCl brine. The potential application of SiO_2 NPs for oil recovery have also been demonstrated with glass micromodels (Behzadi and Mohammadi 2016, Dehaghani and Daneshfar 2019).

Many studies (Torsater et al. 2012, Li and Torsæter 2014, Ragab and Hannora 2015, El-Diasty 2015, Youssif et al. 2018) have shown that oil recovery increases with NP concentration up to an optimal value, above which it decreases. The optimal concentration and the recovery differ from several studies. There is no clear influence of particle size on oil recovery. It appears that a direct injection of NPs, (i.e. secondary mode) requires more pore volumes to produce oil out of the core, which can be economically unfeasible for field scale applications (Zallaghi et al. 2018, Youssif et al. 2018). Therefore, NPs have been tested after conventional water flooding.

Tertiary oil production: Core flood experiments have shown no mobilisation of residual oil by injecting SiO_2 NPs in water-wet sandstone rocks (Skauge et al. 2010). However, the same effect is not true for others who reported incremental oil recovery up to 32% of OOIP (Roustaei et al. 2012, Torsater et al. 2012, Li et al. 2013, Hendraningrat et al. 2013a;c;b, Hendraningrat and Torsaeter 2014, Hendraningrat and Torsæter 2014, Aurand et al. 2014, El-Diasty 2015, El-Diasty and Aly 2015, Hendraningrat and Torsæter 2016, Zallaghi et al. 2018, Youssif et al. 2018).

Other studies investigated the EOR potential of silica NPs in carbonate rocks. Roustaei and Bagherzadeh (2015) reported an incremental oil recovery of about 17% of OOIP by injecting SiO_2 NPs at a concentration of 4 g/litre in 5 wt% NaCl water in carbonate rocks. Other authors found an additional oil recovery of about 8-9% of OOIP by injecting SiO_2 NPs at a concentration of 30,000 ppm in seawater (Nazari Moghaddam et al. 2015).

Previous research has also focused on the application of surface-treated NPs de-

signed to improve surface properties and overcome stability issues commonly reported with bare NPs, especially in harsh reservoir conditions. To this end, Roustaei et al. (2012), Mohammadi (2013) and Roustaei (2014) studied *hexadecylsilane*-treated SiO_2 NPs for improving oil recovery from light and intermediate reservoirs. Significant incremental oil recovery of about 28.57% OOIP was reported by Roustaei (2014), despite large aggregation of NPs at core inlet. Early studies conducted by the same group of researchers, Roustaei et al. (2012) and Mohammadi (2013), have shown an oil recovery of about 32.2% of OOIP and 25.43% of OOIP, respectively. Mohammadi (2013) concluded that their NPs are efficient in light oil reservoirs. Both studies proposed optimum concentration of 4g/l.

Ponnapati et al. (2011) evaluated oil recovery from polymer (*Poly-(oligo(ethylen oxide) monomethyl ether methacrylate)*-grafted SiO_2 NPs injection in Berea sandstone. The NPs propagated through Berea cores and mobilised residual oil and yielded 7.9% of OOIP. Behzadi and Mohammadi (2016) found that polymer-coated silica NPs can modulate oil and water interfacial tension and change the wettability of the oil-wet glass micromodel to more water-wet, resulting in higher EOR than unmodified silica nanoparticles.

Most of the studies were conducted with SiO_2 NPs dispersed in NaCl water (1-5 wt % concentration) or in non-aqueous solution (Ogolo et al. 2012). The concentration of NPs dispersion is often varied from 0.01 to $\geq$ 0.1 wt% in injection water or brine. The wettability of the rocks is changed by ageing water-wet cores in crude oil (Hendraningrat et al. 2013c, Roustaei and Bagherzadeh 2015, Zallaghi et al. 2018) or in *SurfaSil*™solution (Hendraningrat and Torsæter 2016). Other studies have aged the cores without having initial water saturation established in the cores (Aurand 2017). The non-wetting phase used for the experiments varied from crude oil (Hendraningrat et al. 2013a, Youssif et al. 2018, Ponnapati et al. 2011) to mineral oil (El-Diasty 2015, El-Diasty and Aly 2015, Torsater et al. 2012). The injection flowrate, temperature and evaluation criteria of oil recovery are also varied in many studies.

The variation in the oil recovery parameters further complicates the evaluation of nanoparticles effect on oil recovery. For instance, the salinity and ionic composition of injection water can influence the amount of oil that can be produced by NPs (Hendraningrat and Torsæter 2016). With increasing concentration of nanofluids, the reservoir permeability can be decreased; The injection flowrate and differences in fluid density can cause NPs to settle down and clog the pores (Youssif et al. 2018), resulting in decreased nanofluid flooding efficiency. There are few studies in the literature that compare the efficiency of nanofluid flooding in oil recovery with different rock wetting systems. However, it is reported that oil recovery by SiO_2 NPs is greatest at neutral-wet condition and increases with temperature

(Hendraningrat et al. 2013c, Hendraningrat and Torsæter 2016).

Variation of the experimental conditions, briefly reviewed here, mirrors the large variations in nanofluid flood results reported in the literature. However, the results show that SiO_2 NPs have enormous potential for recovery of oil, but more studies are needed to reproduce the results to make the nanoparticle technology robust for field scale application.

2.5.3 Summary

From the above review, it becomes apparent that under variable operating conditions such as rock lithology and wettability, concentration, experimental conditions and procedure, composition of base fluid, etc., laboratory experiments reveal promising application of SiO_2 NPs for oil recovery. The incremented oil recovery is as high as 32% of the OOIP, but the most frequent by the range is 5% (Ding et al. 2019). It is difficult to evaluate how effective SiO_2 NPs are for EOR due to variation of experimental conditions and lack of experimental repeatability.

This calls for a standardised procedure for evaluation of oil recovery on a laboratory scale. For instance, the NPs are either evaluated as secondary or tertiary recovery agents, the oil-wetness of the porous media is achieved using various methods, which in some cases might have an issue of wettability steadiness. Most of the conditions under which the NPs are evaluated may not mimic that of an oilfield.

For practical considerations, some studies argue that it is preferable to use NPs during secondary recovery operation (Torsater et al. 2012, Hu et al. 2016), while others believe that it is economically feasible to inject NPs after water flooding process (Zallaghi et al. 2018, Youssif et al. 2018). A model that can upscale core flood results for application in reservoir scale is required. This would facilitate economical evaluation and feasibility application EOR fluid on a field scale. An assessment of nanoparticles focusing on a specific oilfield application is recommended because it may reduce the widespread interpretation of nanoparticle oil recovery potential.

2.6 The EOR mechanisms of silica nanoparticles

Aside from i) interfacial tension reduction (IFT) and ii) wettability alteration, which are the most two proposed enhanced oil recovery (EOR) mechanisms of silica nanoparticles (NPs) (Ding et al. 2019), other operating mechanisms include iii) generation of emulsion, iv) disjoining pressure, and v) log-jamming effect. The theory behind these five mechanisms is discussed in the following sections.

2.6.1 Interfacial tension reduction

Microscopic sweep efficiency of oil can be improved by decreasing the IFT between the flowing aqueous phase and oil phase. Interfacial tension is reduced through the migration and arrangement of NPs into oil and water interface due to the ultra-small size and large surface area. The migration to the oil or water phase is determined by hydrophilic and hydrophobic nature of the particles (Bera and Belhaj 2016, Agi et al. 2018). Nanoparticle designed to be wetted by both phases, thus be partly hydrophilic and partly hydrophobic, can reduce IFT markedly (Peng et al. 2017).

Interfacial tension determines fluid movement in porous media. A reduction of IFT to $\leq 10^{-3}$ mN/m can lead to a significant production of capillary trapped oil (Sheng 2015). At low capillary forces oil flows within water phase to the production wells in the form of disconnected small droplets.

Most studies reported IFT reduction in the presence of SiO_2 NPs in injection fluid (Ponnapati et al. 2011, Roustaei et al. 2012, Torsater et al. 2012, Hendraningrat et al. 2013a;c;b, Hendraningrat and Torsaeter 2014, Hendraningrat and Torsæter 2014, Li et al. 2013, Aurand et al. 2014, Ragab and Hannora 2015, El-Diasty 2015, Hendraningrat and Torsæter 2016, Agi et al. 2018). Interfacial tension has been shown to decrease with increasing NPs concentration up to an optimum value (Li et al. 2013, Zallaghi et al. 2018). Other studies have found that silica NPs are more effective in reducing IFT of light oils than heavy crude oil (Mohammadi 2013, Huibers et al. 2017).

In summary, the IFT reduction reported in the literature is not in the orders of magnitude required for significant mobilisation of oil. Therefore, it is not the main parameter driving oil recovery during SiO_2 NPs injection. When significant IFT reduction is observed due to NPs, it is often explained by adsorption of NPs at the liquid-solid interface or change in wettability (Behzadi and Mohammadi 2016). Characterisation of the interactions between the NPs and base fluids, the binding effect with surface additive materials, with rock mineral, etc. is often missed in most studies. This makes it unclear whether the reduction of IFT is due to NP itself or combination various parameters. Therefore, studies investigating the influence of particles with their constituents in reducing IFT are needed to give an explicit understanding of the behaviour of NPs at the fluid-fluid interface.

2.6.2 Generation of emulsion

Addition of NPs to the oil-water system can create synergistic effect for the formation and stabilisation of emulsions. This requires partial wetting of NPs by water and oil so that they can irreversibly attach to the oil-water interface, stabilise

emulsion droplets and reduce the interfacial tension. This attachment/adsorption is a matter of balance between the three interfacial energies: nanoparticle-water, nanoparticle-oil and oil-water (Chevalier and Bolzinger 2013). The highly hydrophilic surface of the NPs would be completely water-wet, just as oil would completely wet the highly hydrophobic particles (Chevalier and Bolzinger 2013). Meanwhile, the particles would avoid the interface and would be dispersed in one of the phases. An excellent review of the fundamentals of NPs adsorption at interfaces is given by Chevalier and Bolzinger.

For EOR applications, emulsions can be generated in-situ or injected into the reservoir, in both cases lead to favourable mobility ratio, thereby improving oil recovery efficiency. Emulsion when generated in-situ or injected have the capacity to divert flow to the by-passed oil by blocking swept pores (Chevalier and Bolzinger 2013). It also helps to entrain oil into the mobile aqueous phase (oil-in-water emulsion) and increase the viscosity of the aqueous phase (DiCarlo et al. 2011, Chevalier and Bolzinger 2013); likewise, emulsions can increase the viscosity of the oil phase for water-in-oil emulsion (Aurand 2017). Both cases lead to favourable mobility ratio and to a better sweep efficiency. Nanoparticles are hundred times smaller than emulsion droplets (Chevalier and Bolzinger 2013), meaning emulsions stabilised by NPs can travel long distance in a reservoir without much retention (Zhang et al. 2010, Suleimanov et al. 2011, ShamsiJazeyi et al. 2014). Furthermore, emulsion stabilised by NPs can withstand hard reservoir conditions to remain stable.

In-situ emulsion droplets can be studied via core flooding effluent, differential pressure through the core, and through visual observation using glass micromodels or microscope.

Binks and Whitby (2005) and Kim et al. (2016) studied the influence of silica particle size for the stabilisation of emulsion droplets generated by sonication and core flood in sandpack column. The results demonstrated that small particles are beneficial for emulsion stability. Small NPs can migrate to the oil-water interface more efficiently than their larger counterparts. The impact of SiO_2 NPs on emulsion stability under reservoir conditions was also studied by Binks and Whitby (2005). They concluded that controlling pH or adding electrolyte is essential to reach stability as well as increasing oil phase polarity (the polar oil species adsorb onto surfaces of the silica particles). Zhang et al. (2010) and DiCarlo et al. (2011) reported very stable oil-in-water emulsion generated in-situ during core flooding experiments using aqueous suspensions of surface-treated SiO_2 NPs. Moreover, the authors found that the displacement front was spatially uniform, and with later breakthrough when compared to controlled displacement with no in-situ NPs. A uniform displacement front is an important requirement for improving oil recovery sweep efficiency.

The phenomena of in-situ emulsion generation have also been observed with glass micromodels (Hendraningrat et al. 2012, Li et al. 2013, Pei et al. 2015). Li et al. (2013), Hendraningrat and Torsæter (2014). It was observed that injection of aqueous suspensions of SiO_2 NPs at 0.1 wt% could deform and break oil droplets while assisting oil recovery. This was interpreted as formation of emulsion due to NPs injection. Other studies visually observed that adding NPs increased the thickness of the emulsion layer and improved oil mobility by preventing the oil from contacting the rock surface (Hendraningrat et al. 2012, Li et al. 2013, Pei et al. 2015).

Optical microscope was used in the present work to detect emulsions generated in-situ during core flooding experiments at high temperature. While it was not possible to quantify size distribution of the emulsion droplets, Figure 2.6 shows oil droplets emulsions temporarily stabilised by 0.1 wt% SiO_2 NPs in seawater. This emulsion assisted oil recovery by increasing relative permeability to oil.

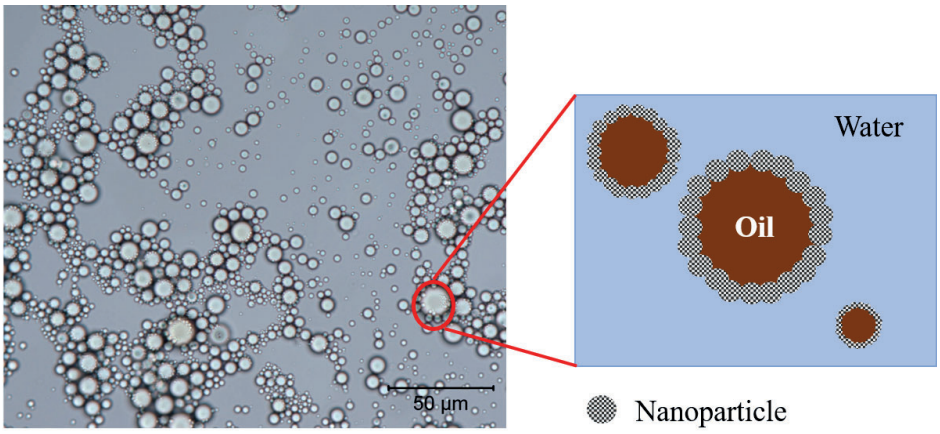

Figure 2.6: Optical image of oil-in-water emulsion droplets collected from nanofluid core flood effluent. The oil droplets were temporarily stabilised by SiO_2 NPs at 0.1 wt% in seawater solution (also refer to Figure 5.24).

2.6.3 Wettability alteration

Wettability of a reservoir is directly related to fluid-fluid and fluid-rock interactions (Bera and Belhaj 2016); For EOR purposes, it refers to the restoration of wettability back to its original state, which is presumed to be water-wet (Mohammed and Babadagli 2015).A water-wet reservoir would have oil easily extracted from it than an oil-wet formation (Ogolo et al. 2012, ShamsiJazeyi et al. 2014); that is because changing an oil-wet reservoir to water-wet, the role of capillary pressure (negative

capillary pressure) shifts from a barrier force to a driving force, which increases capillary imbibition (Afolabi and Yusuf 2019) and relative permeability of the oil phase. Therefore, wettability alteration is one of the most effective methods of EOR. Reservoir wettability can be evaluated by contact angle, spontaneous imbibition tests, Amott test, surface imaging tests or other techniques reported elsewhere (Anderson 1986, León-Pabón et al. 2014, Mohammed and Babadagli 2015).

The mechanism governing the alteration of rock wettability by NPs is complex. However, the effect of nanofluids on wettability alteration depends on how NPs will affect crude oil-brine-rock properties. The mechanisms of reservoir oil interactions with brine for each petroleum reservoir are unique and depend on crude oil and brine composition, rock mineralogy, and other reservoir properties (Morrow 1990, Mohammed and Babadagli 2015).

In oil-wet reservoirs, the surface is covered by oil films; When NPs flow through it, some of the NPs may adhere to the oil-water interface, while others may adsorb on the rock surface. The adsorption of NPs on the surface changes the rock surface energy and allows the formation of nanotextures and new surface roughness. This disrupts whatever molecular attachment amongst the rock surface and the oil molecules accountable for the oil-wet condition (Afolabi and Yusuf 2019). Moreover, the charged NPs on the rock surface form hydrogen bonds with water molecules, thereby attracting water to the rock surface; this reduces the interfacial tension between rock surface and water and allows water-wet condition to be achieved (Roustaei and Bagherzadeh 2015, Afolabi and Yusuf 2019).

Summarily, the wettability of an oil reservoir can be changed by the addition of NPs in the carrier fluid (Mohammadi 2013, Roustaei and Bagherzadeh 2015, Behzadi and Mohammadi 2016, Huibers et al. 2017), which lead to an increased oil recovery. The extent of wettability alteration by NPs depends on the volume fraction of NPs, the size and properties of the particles, and rock surface type (Lim et al. 2015). Additional parameters include salinity of base fluid and nanofluid exposure time on the rock surface.

2.6.4 Change in structural disjoining pressure

The concept of *structural disjoining pressure* (SDP) was introduced by Wasan and Nikolov (2003) to explain oil recovery and wettability alteration towards water-wet due to the injection of nanoparticles. Since then, many studies have relied on this concept to explain their experimental results. For instance, the SDP mechanism has been proposed to be responsible for oil recovery and changing wettability of water-wet sandstone (Hendraningrat et al. 2013a, El-Diasty 2015, El-Diasty and Aly 2015, Choi et al. 2017), oil-wet sandstone (Dai et al. 2017), and oil-wet car-

bonates (Nazari Moghaddam et al. 2015) to more water-wet condition. The noteworthy point is that, water coats the rock surface of water-wet reservoirs and oil is trapped in the center of the pores; as shown in Figure 2.1 in Section 2.3.2, for oil droplet surrounded by water the contact angle is zero (see also Figure 2.7). This is favourable for the formation of a wedge-like region in the vicinity of three-phase water-oil-rock contact line. This is essentially the basis of the Wasan and Nikolov's theory. Driven by injection pressure, NPs tend to self-assemble into well-ordered wedge-like structures (see Figure 2.7) resulting in i) an increase in NPs concentration in the wedge film; the concentration gradient creates an osmotic pressure that attempts to separate the oil from the rock surface; ii) as the film tension increases toward the vertex of the wedge film, an extra force or *structural disjoining pressure*, develops and enhances the spreading of NPs on the surface; this induce a nonuniform surface roughness that change the rock wettability.

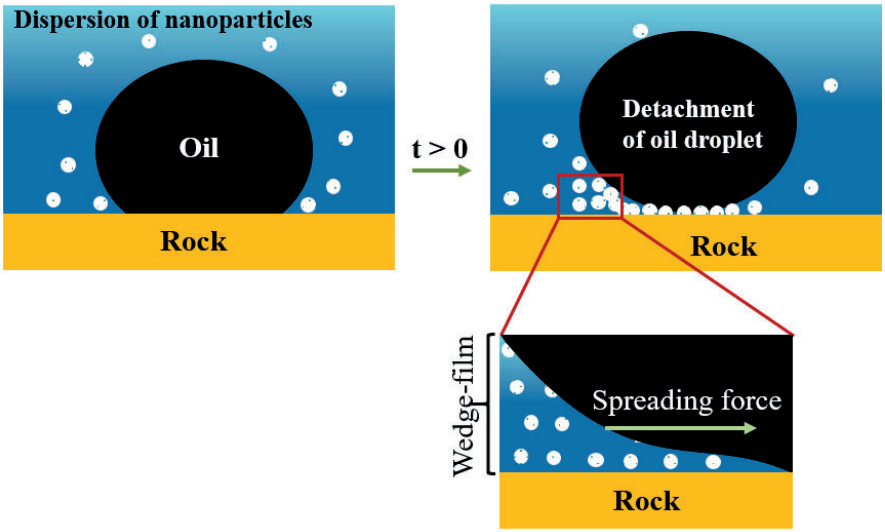

Figure 2.7: Schematic illustration of self-ordering of NPs in the wedge-like region. This increases SDP that attempts to detach the oil droplet from the surface and enhances spreading of NPs on the rock surface, resulting in wettability alteration (modified from Wasan and Nikolov (2003)).

The SDP mechanism was further investigated by Chengara et al. (2005) and Kondiparty et al. (2011). The authors observed that SDP is a long-range force, it requires high volume concentration of NPs (> 30 vol%) to be effective in enhancing oil recovery and to change wettability. The SDP mechanism increases with decreasing NP size. Small NPs can easily fit into well-ordered wedge-like structures than their large counterparts (Kondiparty et al. 2011). For this to occur, there should be no

tendency for the NPs to adsorb on the rock surface (Kuang et al. 2018) so that they can migrate and self-organise in a pre-existing wetting-wedge (Sofla et al. 2019).

Therefore, it seems that the concept of SDP cannot be generalised to explain the wettability alteration and oil recovery by virtue of nanofluids.

2.6.5 Mechanical entrapment and log-jamming effect

Mechanical displacement of the by-passed oil can be inferred by characterising transport of NP dispersion in the reservoir rocks. The transport has two components: the mobility and the retention of the NP dispersion in porous media (Rodriguez et al. 2009). The former may indicate propagation of NPs through the pores until the target zone, while the latter indicates the fraction of NPs being trapped in the pores and not reaching the target locations.

Entrapment/retention of NPs in porous media occurs due to physicochemical interactions (Zhang et al. 2015), such as *mechanical entrapment* or *straining*, *log-jamming effect* and chemical adsorption. By straining, particles with larger size can block narrow pore-throats (Skauge et al. 2010). The size of NP is usually two to three orders of magnitude smaller than pore-throat diameter in typical reservoir rocks (Rodriguez et al. 2009, Zhang et al. 2015, Kokubun et al. 2019); Nevertheless, under some circumstances, small NPs can block the reservoir pore throats. This mechanism, which leads to blocking of pores larger than the particle size is known as "log-jamming effect" (Skauge et al. 2010, Kokubun et al. 2019). Log-jamming effect is the most relevant mechanical oil displacement mechanism. This is because the aqueous phase decreases nanoparticles mobility during nanofluid flooding operation, causing them to accumulate at the pore-throat entrance. At the stopping point, the inner pore pressure increases as the injection proceeds, which forces water to flow into neighbouring oil-containing pore channels and mobilises the oil to the production wells (Skauge et al. 2010, Kokubun et al. 2019). The mobility of nanoparticles decreases in the aqueous phase because NPs carry water molecules and become heavier than in dry state. During floods of nanofluids, water molecules accelerate faster than heavier particles, leaving them trapped at the pore entrance. The jamming effect can also occur if NPs aggregate in-situ, becoming larger than the size of the pore throats (Skauge et al. 2010, Kokubun et al. 2019). Then, the pore-throat size is reduced slowly, and eventually blocked (Skauge et al. 2010), as shown in Figure 2.8. The arrows in Figure 2.8 show the diversion of water at microscopic level to the adjacent pores due to increased pressure in blocked pores. The oil trapped in those pores can be mobilised and produced owing to high pressure. After blocking a pore, the accumulated NPs may eventually be re-mobilised, unblocking the pores and restoring water flow in it (Kokubun et al. 2019). This causes pressure drop across the core before the pores are reloaded

with particles and increase the pressure.

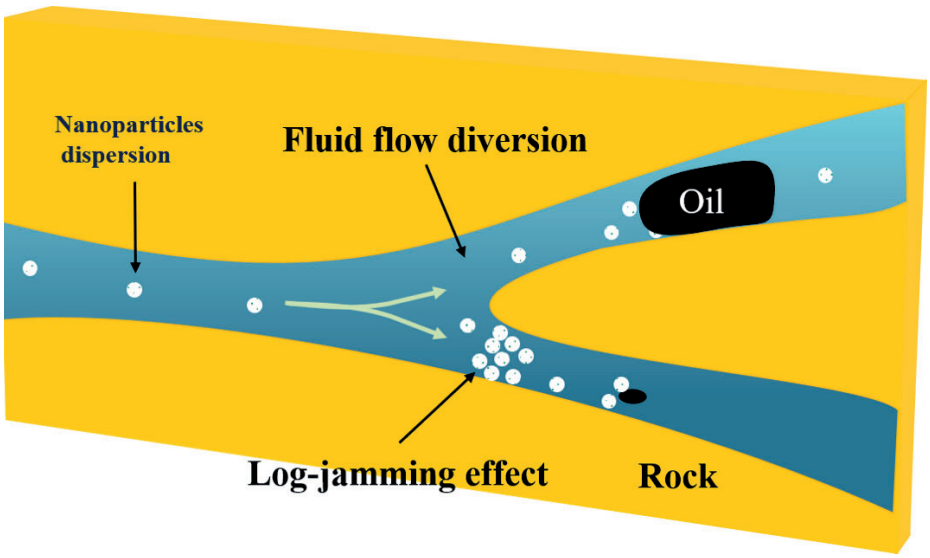

Figure 2.8: Schematic illustration of oil mobilisation due to pore plugging and microscopic fluid flow diversion. The arrows show the direction of NPs carrying water molecules flowing from a large to a narrow rock pore. Due to the reduced velocity, the NPs accumulate at the narrowest pores and block them and increasing pressure. Then, water is rerouted to the adjacent pores where it collides with trapped oil and attempts to push it forward to the production lines (Figure 2.8 adapted from Aurand et al. (2014)).

The microscopic flow diversion mechanism can be studied via differential pressure across the core. If the flow pattern or pore volume available for flow is change by NPs injection, the differential pressure must be much high than that for "pure" water injection. The residual oil saturation, core heterogeneity and blocked pores can result in water flow being redirected to other channels during nanofluid flooding process. However, some pore channels may remain bypassed, if the entrainment of oil does not occur. In this case, a continuous increase in injection pressure may occur, which does not necessarily indicate removal of oil in unswept regions. The jammed NPs may also result in low recovery due to reduced core permeability. Thus, large pressure fluctuations may be a good indication of pore blockage and opening because of mobilisation of residual oil droplets.

Denney (2011) reported that log-jamming effect may not be a sufficient criterion for oil mobilisation by SiO_2 NPs. The microscopic diversion of the flow can play a prominent role in oil recovery, if the EOR fluid does not change the rock wettability (Kokubun et al. 2019). This may be the reason why the oil recovery by

log-jamming is, in most cases, associated with other EOR parameters (i.e. IFT, wettability alteration, etc.).

Besides the mobilisation of by-passed oil, microscopic flow diversion can contribute to the mobilisation of capillary trapped oil (Spildo et al. 2009). The contribution of microscopic flow diversion in the mobilisation of residual oil is not fully addressed in the literature. The main factors governing the jamming effect are the size, concentration of the NPs, pore size distribution of the porous media, and the flow rate (Skauge et al. 2010, El-Diasty and Aly 2015, Kokubun et al. 2019).

2.6.6 Summary

It appears that the mechanisms of nanoparticles oil recovery are not yet fully understood, and more studies are needed. This arises due to the diversified experimental conditions and lack of experimental repeatability, leading to different levels of the interpretation of enhanced oil recovery mechanisms. It is apparent that additional oil recovery results from a synergistic effect of both NPs type and surface additive materials and it depends on the resulting solutions and interactions with an oil reservoir system. Future studies are therefore recommended to characterise the surface activity and reactivity of nanoparticles additive materials to predict their interactions with the base fluids, their binding effect with NPs, and with reservoir rock during EOR process.

The contribution of different mechanisms to oil recovery by silica nanoparticles may not be isolated, more than one mechanism is likely associated with oil recovery. However, to determine which mechanism is contributing more than others in EOR needs to be systematically addressed, particularly for a specific oilfield conditions, in order to single out the relevant mechanism of nanoparticle oil drive.

CHAPTER 3

Experimental Materials

3.1 Introduction

This chapter describes all material used in the experiments this work. Relevant materials include fluids, silica nanoparticles, Berea sandstone rocks, core flooding apparatus, centrifuge, and visual glass micromodels. Additional description of the materials can be found in Chapter 4.

3.1.1 Synthetic Seawater

Synthetic Seawater (SSW) was prepared under laboratory conditions with a composition to mimic water from the North Sea. Certain amount of salts were measured and dissolved in certain volume of de-ionized water and stirred using a magnetic stirrer; The prepared North Seawater had a density of 1.024 g/cm^3 and viscosity of 1.025 cP at 21.5 °C. The density and viscosity measured at 60 °C were 1.008 g/cm^3 and 0.53 cP, respectively. The pH and conductivity were 8.01 and -45 mV, respectively, at room temperature. The density was measured with Anton Paar density meter DMA^{TM} 4100 M series; Rotating viscometer (Brook-field, model LVDV-II+P) was used to obtain viscosity; and pH of the solutions was measured using a pH Meter (model pH 1000 L, phenomenal®). The composition of the Total dissolved salts (TDS) in 1 litre bottle of SSW is given in table 3.1 and is 38,318 ppm.

Table 3.1: Composition of the total salts dissolved in 1 litre of synthetic seawater.

Salt components	**Chemical formula**	**Weight (g)**
Sodium Sulphate	Na_2SO_4	4.066
Sodium Chloride	NaCl	28.500
Calcium Chloride Dihydrate	$CaCl_2x2H_2O$	1.625
Magnesium Chloride Hexahydrate	$MgCl_2x6H_2O$	3.162
Strontium Chloride Hexahydrate	$SrCl_2x6H_2O$	0.024
Potassium Chloride	KCl	0.721
Sodium Hydrogen Carbonate	$NaHCO_3$	0.220

3.1.2 Nanoparticles and Nanofluids

Twenty-three different types of hydrophilic nano-structured particles (referred to as nanoparticles in this work) with a variety of surface modifications (silane, polymers and additives modification) were supplied by Evonik Industries. Additional eight samples used in the modification of the NPs were also provided. The nanomaterials are special research and development (R&D) laboratory products from Evonik Industries. They are spherical and amorphous silica products marketed under AEROSIL® trade name and were supplied to us as AERODISP®, which is AEROSIL® particles in liquid solution as shown in Figure 3.1. The properties of selected NPs, as received, are given in Table 3.2.

Figure 3.1: Different types of silica NPs suspended in distilled water (concentrated solutions) as received from Evonik Industries.

The NF stands for nanofluid and the number is used to identify the NP type. The primary size of the NPs was measured with dynamic light scattering technique.

The concentrated solutions of NPs were diluted at a concentration of 0.1 wt% in SSW. The prepared nanofluid (NF) was stirred for approximately 30 minutes using a magnetic stirrer to ensure a homogeneous solution before use. The properties of both concentrated and diluted solutions of NPs are given in Table 3.2.

Table 3.2: Properties of NPs suspended in distilled water (columns 2-5); Columns 6-8 present the properties of diluted solution in SSW to 0.1 wt%, at room temperature.

Sample	**Basis**	**Mod.**	**wt%**	**Size (nm)**	ρ (g/cm^3)	μ (cP)	**pH**
NF02-3	SiO_2 (sol-gel-cationic)	Polymer	38.6	107	1.022	1.021	8.049
NF02-4	SiO_2 (sol-gel-anionic)	Polymer	26.0	32	1.024	1.022	7.812
NF02-6	SiO_2/Al_2O_3/MOX	Polymer	21.6	218	1.025	1.023	7.864
NF02-7	Silica - AE 200	Polymer	21.3	376	1.024	1.022	8.209
NF02-8	SiO_2/Al_2O_3/MOX	Polymer	25.5	145	1.026	1.016	7.735
NF02-9	Silica-AE200	Polymer	28.0	157	1.024	1.015	8.217
NF02-13	Silica-AE200	Polymer	26.5	229	1.025	1.046	8.070
NF-18	SiO_2/Al_2O_3/MOX	Additives	27.0	112	1.026	0.997	7.790
NF-23	Disp. W 1720 EPOMSI	Silane	25.4	112	1.024	1.044	7.791
28	Polymer	Methacryl	-	-	1.025	1.057	-
31	Polymer	Methacryl	-	-	1.024	1.002	-

The density and viscosity of SSW and nanofluid samples NF02-3, NF02-4, NF02-6 and NF02-8 were also measured at 60 °C. For SSW, the density was 1.008 g/cm^3 and 0.53 cP viscosity. For the nanofluid systems, the density varied from 1.007 to 1.009 g/cm^3 while the viscosity ranged from 0.51 to 0.67 cP. As will be explained later in this thesis, these were the only samples injected into the core plugs at high temperature.

3.1.3 Oleic Phase

A dyed *n*-decane with density of 0.73 g/cm^3 and a viscosity of 0.9 cP was used for wettability experiments. Two types of degassed crude oils (A and B) from North Sea fields were used. Both are classified as light to medium crude oils. Table 3.3 reports the density and viscosity of the crude oil measured at different temperatures. Table 3.4 presents the Saturates, Aromatics, Resins and Asphaltens (SARA) analysis performed on both crude oils. The total yield from SARA is 99.3 wt% and 95.21 wt% for crude oil A and B, respectively.

Table 3.3: Density and viscosity of crude oil A and B.

Crude oil	Temperature (°C)	Density (g/cm^3)	Viscosity (cP)
A	20	0.9048	52.5
	60	-	-
B	21	0.886	33.9
	60	0.863	6.0

Table 3.4: Sara analysis for crude oil A and B.

	Weight percent (normalised)			
Crude oil	**Saturates**	**Aromates**	**Resins**	**Asphaltenes**
A	66.21	25.78	7.69	0.32
B	71.57	20.81	7.44	0.18

3.1.4 Porous Media

3.1.4.1 Properties of the Micromodels

Uniform network glass micromodels were used to screen the nanoparticles and visualise the flowing fluids through porous media. All micromodels were water-wet and were purchased from Micronits Microtechnologies. The visual micromodels or microchip had uniform pore-throat network structure with inlet and outlet holes drilled at each end to allow the entering and exiting of the fluids. The porosity of the microchip was 52%, permeability was 2.5 Darcy, and pore volume was 2.1 μL. The arrangement of the pore-throat channels in the micromodels is presented in Figure 3.2. The pore-throat dimensions are given in Table 3.5.

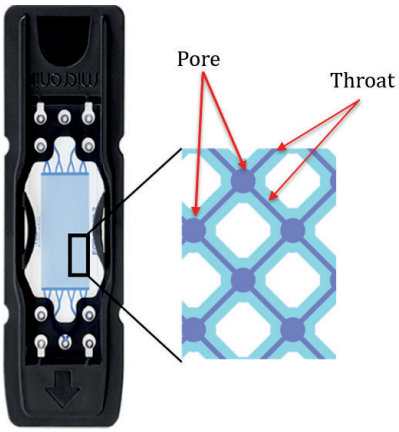

Figure 3.2: Glass micromodel (Micronit 2019).

Table 3.5: Physical properties of the micromodel.

Dimensions (µm)	Throat	Pore
After etching diameter	50	90
Mask width diameter	10	50
Depth	20	20

3.1.4.2 Properties of the core plugs

Berea sandstone core plugs, referred to as "cores" hereafter, were used for all core flooding experiments. The cylindrical core plugs were drilled were drilled from dry/unsaturated block numbered #9 for internal use at NTNU. The cores were naturally water-wet and were prepared to have a standard diameter of 3.75 cm. The length varied from 4.5, 6 and 10 cm (see Figure 3.3). The porosity and permeability ranged from 15% to 25% and 176 mD to 410 mD, respectively. The porosity was measured with both Helium porosimeter and with saturation methods. Permeability was determined with constant head permeameter using nitrogen gas with sleeve pressure held within 18-20 bar. To estimate liquid (water) permeability from the gas permeability measurement, the latter was corrected for the Klinkenberg effect. All core data is presented in Appendix B. To produce neutra-wet cores, the naturally water-wet cores were cleaned and saturated with crude oil to establish initial water saturation, then aged in crude oil at 80 °C. The ageing procedure is described in Section 4.4.2.

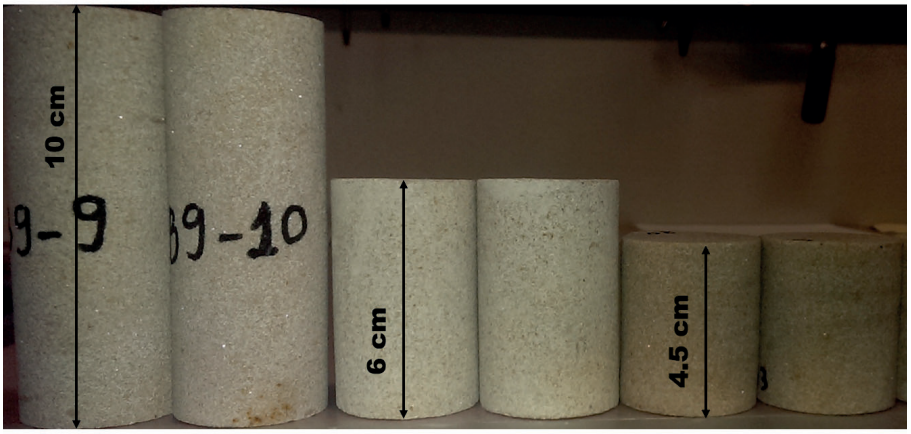

Figure 3.3: Berea sandstone core plugs of different size used for oil recovery process.

The bulk mineral composition was characterised with X-ray diffraction (XRD). Five core samples were analysed. The cores were nearly homogeneous and composed of 93.7 Vol% quartz, 5.0 vol% of Microcline (Alkali feldspar), and Diopside (1.3 vol.%), on average. The XRD analysis for Berea sandstone core plugs is summarised in Table 3.6

Table 3.6: XRD analysis for Berea sandstone core plugs (Aurand 2017).

Content	**Core#1**	**Core#2**	**Core#3**	**Core#4**	**Core#5**	**Average**
Quartz	94.59	93.1	92.99	94.84	93.06	93.7
Microline (Alkali feldspar)	3.94	5.67	5.65	4.07	5.62	5.00
Diopside	1.47	1.23	1.36	1.09	1.32	1.30

CHAPTER 4

Experimental Methodology

4.1 Introduction

This chapter presents the experimental methodology of the main tests conducted in this work for the research questions listed in section 1.2. The experimental procedure described herein includes preparation of porous media and fluids, oil recovery tests with glass micromodels and Berea sandstone core plugs; an investigation of enhanced oil recovery mechanisms through measurements of interfacial tension, Amott-wettability index, analysis of differential pressure from core flood tests and nanofluid flood effluent.

4.2 Evaluation of Nanoparticles Stability

The nanofluid is required to remain stable throughout the duration of EOR process, while maintaining its primary size to allow its mobility and surface reactivity in the reservoir and assist oil recovery. Therefore, predicting the behaviour of the nanofluids is crucial to understand the transport behaviour of the particles and the underlying EOR mechanisms.

The nanoparticles were supplied as suspended concentrates in aqueous solution. The concentrated solutions were diluted to 0.1 wt.% concentration with synthetic seawater. The refractive index of the diluted solution was measured for each nanofluid type. The average refractive index was 1.338. The absorption factor was set to zero due to lack of additional data of the nanoparticles. The properties of the dispersant (SSW) were always adjusted to the desired measurement temperature. The temperature was adjusted to 22 °C or 60 °C to reflect that used during the flood experiments. Three measurements were taken for each sample, and the

average value is reported.

Particle size measurements were conducted four months after the nanofluid solutions were prepared. Then, the measured size was compared with primary size provided by the manufacturer, referred to as reference size. As in the present work, the reference size was characterised with dynamic light scattering (DLS) method.

The following criterion was adopted to assess stability. First, if the measured particle size exceeds the reference size by more than 50%, it suggests that nanoparticles aggregated in solution, otherwise they remained dispersed. Second, if the effluent particle size is smaller than the influent particle size, it provides an indication of nanoparticles aggregation, thus the particles being larger than the pore size and were filtered and retained in the core during the flood experiments. The particles were aggregating. The shortcoming with comparing the sizes is that, it may not always provide reliable results. For example, the effluent collection can be affected by the production of rock fines. Therefore, zeta potential and sedimentation rates of nanoparticles were used to assess the stability. Absolute values of zeta potential greater than 25 mV can provide an indication of stable samples (Yu and Xie 2012). Sedimentation tests were conducted by placing the nanofluid samples in transparent glass vials and visually monitored daily over four months. For the tests conducted at 60 °C, the glass vials containing nanofluids were placed in the oven with the temperature adjusted accordingly.

4.3 Interfacial Tension Measurement

The interfacial tension (IFT) between crude oil and the surrounding phase (water or nanofluid) was determined with pendant drop and spinning drop techniques. The pendant drop measures an asymmetric fluid droplet suspended from a needle, and interactive fitting of the Young-Laplace equation that balances the gravitational deformation of the drop with the restorative interfacial tension (γ) (Berry et al. 2015). At equilibrium, the pendant drop obeys the Young-Laplace Equation 4.1:

$$\Delta P = \gamma(\frac{1}{R_1} + \frac{1}{R_2}) \tag{4.1}$$

where R_1 and R_2 are the principal radii of curvature; $\Delta P = P_{in} - P_{out}$ is the Laplace pressure across the interface. The gravitational deformation of the drop generates hydrostatic pressure (ΔP_{Hyd}),

$$\Delta P_{Hyd} = \Delta \rho g l \tag{4.2}$$

$\Delta\rho$ = ρ_d-ρ is the difference between the density of the drop phase and the surrounding phase, respectively. g is the gravitational acceleration and l is the vertical distance between the measuring point and the opening needle. The IFT was

calculated knowing the density difference of the fluids and by varying the shape parameter know as B-factor. The B-factor was varied within 0.4-0.6 for all tests. It accounts for the changes of the curvature of the drop vertically induced by gravity force. The oil drop was suspended via Drop Shape Analyser (DSA)-100 assembled with a J-shape syringe with inner diameter of 1.0047 mm. The crude oil drops were dosed at 2.67 μL/s until allowable volume was reached, then the IFT values measured every 20 seconds until stable value was reached.

For the spinning drop method, a SVT20N (Data Physics) spinning video tensiometer was used. Crude oil was injected dropwise into a capillary tube filled with designated fluid (water or nanofluid). The tube was rotated at speed varying from 6,000 to 8,000 rpm. The rotational speed elongates the oil drop along the axis of rotation resulting in increased surface area. When the equilibrium was reached, value of IFT was calculated using a model proposed by Than et al. (1988). The refractive index of the surrounding fluids was 1.338.

4.4 Flooding Experiments

4.4.1 Glass Micromodel

A glass micromodel is a simplified pore-throat network system, which can be used to study and visualise multi-phase flow at the micro-scale. The main advantage is that it uses small amounts of fluids and many experiments can be performed at relatively short time compared to conventional core flooding experiments. This was the main reason why micromodels were chosen to screen the nanoparticles in this work.

4.4.1.1 Micromodel Experimental Set-up

The micromodel holder was mounted horizontally on an Optika B-500 microscope with a mechanical adjustable stage. A UC90 camera attached to the microscope objective lens with a resolution of (3384x2708) pixels and (14.6x12.8) mm of effective area was used to capture the images, which were also viewed through a computer screen. The images were automatically analysed using Matlab code. The code counted the pixels in a certain colour range to calculate the relative change in crude oil saturation. A glass Hamilton syringe type with 5 ml capacity was assembled horizontally on the pump and connected to the micromodel through Polytetrafluoroethylene (PTFE) tubes lines. Figure 4.1 shows the schematic of the micromodel flooding used in this thesis. No pressure sensor was connected to the micromodel.

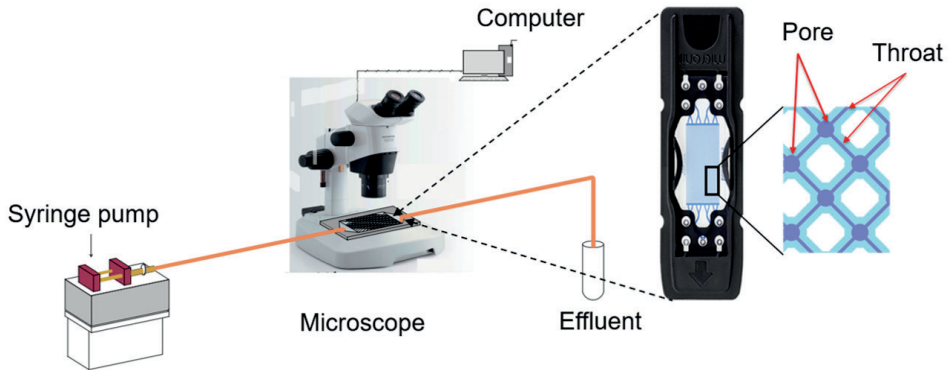

Figure 4.1: Schematic of the micromodel set-up used for fluid flow visualisation and screening of nanoparticles.

4.4.1.2 Micromodel Flooding Procedure

The nanoparticles were screened using water-wet glass micromodel with uniform pore network structure at ambient conditions. The nanofluids were injected following secondary oil recovery procedure:

1. The micromodel was vacuumed to reduce the air trapping effect. During this process, the down stream valves of the micromodel were kept opened while the upstream valve was closed. The micromodel was vacuumed until the pressure stabilised at 100 mbar. Then, the downstream valves were closed, and the vacuum pump turned off;

2. The lines were bled until the 3-way valve before saturating the micromodel with seawater at a flowrate of 0.1 ml/min for ≈2 minutes;

3. Crude oil was flowed until 3-way valve to minimise the dead volume. Then, the drainage was continued with crude oil displacing seawater in the micromodel at a constant rate of 0.01 ml/min until there was no water production, i.e. Initial water saturation (S_{wi}) was achieved. This process was conducted for ≈5 minutes. An image of the micromodel at S_{wi} was taken and named *"pre-flooded image"*;

4. Afterwards, the injection was continued with nanofluids at a constant flowrate of 0.01 ml/min until there was no change in crude oil saturation. This was achieved for about 400 minutes for all test. Here, the images or *"flooded image"* were taken stepwise (e.g. 5, 30 and 60 minutes, etc.) to determine the change in oil saturation. None of the injected fluids were artificially

coloured during the experiments. The remaining oil in the micromodel was automatically calculated by comparing the flooded and pre-flooded images. The results are reported as a function of time.

4.4.2 Core Flooding Experiments

This section introduces the main equipment and procedure adopted to perform flooding experiments with Berea sandstone cores. Materials used for flooding tests include core plugs, fluids, and flooding rig. The experiments were conducted to determine oil recovery factor as a function of pore volume PVs, permeability, the optimal injection scheme, and fluid pressure gradients. Unless otherwise specified, the flooding experiments were performed at room temperature. The obtained results and discussion are presented in Chapters 5 and 6, respectively.

4.4.2.1 Core Preparation Procedure

Prior to flooding experiments, the cores were prepared to be either water-wet or neutral-wet rocks. The following procedure was used:

1. **Core Cleaning:** The cores were received without having contact with crude oil. Therefore, the impurities were removed by Soxhlet extraction in methanol for ≈8 hours. After which, all cores were dried in the oven 60 °C temperature, for 2-3 days.

2. **Porosity and Permeability:** After cleaning and drying processes, porosity and permeability were measured. Porosity was measured via Helium porosimeter and weight difference between the dried and water saturated core. Air permeameter and core flooding methods were used to determine the permeability.

3. **Core Saturation:** The dried cores were 100% saturated with SSW using vacuum container. The cores were placed horizontally in a beaker and vacuumed for 2 hours under 100 mbar vacuum pressure before allowing the saturating fluid to enter the cores. This saturation process was run under vacuum for 2-3 hours. Then, the cores were removed and submerged in the same water for 10 days at ambient conditions to attain ionic equilibrium with the rock constituents.

4. **Establish Initial Water Saturation (S_{wi}):** Two methods were used to establish S_{wi} depending on the size of the cores. The first method consisted of pumping crude oil through the confined core in the core holder until no water production was observed. In the second method, the water saturated core plugs were centrifuged in crude oil at 5000 rpm and at 25 °C for 2 hours.

5. **Core Ageing:** The initial wettability of the core plugs was changed by ageing process in crude oil. That is because the wettability of a reservoir can change in pores invaded by crude oil. However, this process is highly dependent on water films stability, temperature and crude oil composition (Liu and Buckley 1999). To rupture the water films to allow the polar components of crude oil to adsorb onto the rock surface, the water-wet cores were submerged in the same crude oil used to establish S_{wi} inside metallic containers or ageing cells shown in Figure 4.2(a), and placed in the oven set at 80 °C (Figure 4.2(b)) for minimum of 6 weeks. The cores were weighed before and after ageing to ensure no water evaporation.

(a) **(b)**

Figure 4.2: (a) Ageing cells (b) Oven set at 80 °C during the ageing process.

4.4.2.2 Core Flooding Set-up

A schematic diagram of the core flooding rig with the main components labelled is presented in Figure 4.3. To flow the fluids through the core plug, the rig utilises an injection pump, three accumulators containing the designated fluids (crude oil, water and nanofluids) mounted vertically inside the convection oven. The rock core is loaded in the Hassler core-holder type with a Viton sleeve connected with pressure regulators at inlet and outlet. When the flooding experiments were conducted at elevated temperature, a check valve was mounted at core inlet and the back-pressure regulator (BPR) was assembled at core-holder outlet to prevent back-flow of the produced fluids and maintain constant pressure inside the core, respectively. The BPR was set to 5 bar pressure during the experiments. The flowing fluids were

transported via PTFE tubes with inner diameter of 1/16 inches.

The Swagelok® fittings and valves were used to direct the fluids. All the equipment carrying the fluids were place inside the temperature controlled oven. Teledyne ISCO 100DX Dual System Pump (0.01 μ/min to 50 ml/min;±0.3%) was used to pump the Exxol D60 toward the accumulator to push the designated fluid into the core plug. The pump was operated in constant flow mode throughout the duration of the experiments. The confined core was mounted horizontally in the core-holder during the experiments, that assumed negligible effect of gravity segregation of the fluids within the core. The sleeve pressure was held within 18-22 bar.

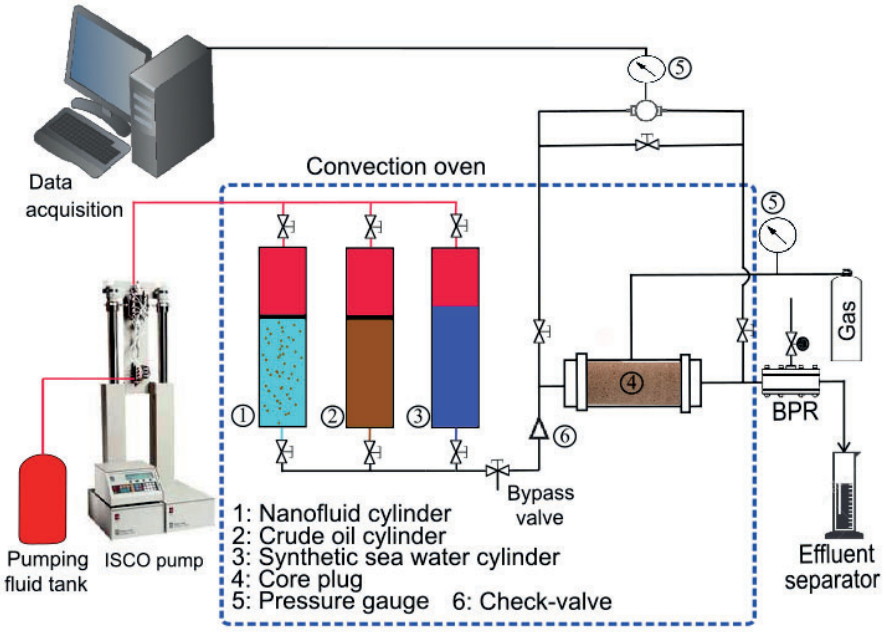

Figure 4.3: Schematic diagram of the core flooding apparatus.

The end-faces of the core-holder were specially designed with groove pattern to ensure even distribution of the fluids on entering and exiting the core plug. This pattern also intended to minimise the capillary end-effects during the flooding tests.

The differential pressure (dP) across the core was measured using Keller PD 33X pressure transmitter (0-30 bar; ±0.5%). The pressure was being transmitted by two pressure sensors connected at the inlet and outlet of the core-holder. The outlet sensor was kept opened to reflect the ambient conditions during the experiments.

The effluent was collected in test tubes with 0.1 ml graduation with ±0.5% accur-

acy. When oil production was delayed or produced at very low pace over time, a camera was used to capture oil produced in a graduated line, while the total production was being collected in a larger graduated tube.

4.4.2.3 Core Flooding Procedure

The text below describes the unsteady-state flooding procedure used to assess the oil recovery potential of nanoparticles obtained from micromodels experiments. The tests were performed on originally water-wet and on neutral-wet rocks. The terms neutral-wet, intermediate-wet and aged cores will be used interchangeably throughout this work. The detailed procedure is presented in Chapter 5 for the respective core flooding test.

1. **Secondary Nanofluid Flooding**

    - The 100% water saturated core was loaded in the core-holder and flowed with SSW to replace the soaking seawater for 1-2 PVs. Two different flowrates (1.0 and 1.5 ml/min) were used. Water absolute permeability was then measured using Darcy's equation 2.2.
    - **Crude Oil Injection:** The primary drainage was conducted by injecting crude oil at different flowrates (0.5, 1.5 and 3.0 ml/min) until no water production stopped. This procedure was conducted for a minimal of 8.5 PVs at ambient conditions. The flowrate was sequentially increased to reduce zones of capillary end-effects (Heaviside et al. 1983, Ramakrishnan and Cappiello 1991). Crude oil was injected on both core ends to even the distribution of the fluids. For the aged cores, about 2 PVs of fresh crude oil were re-injected. The effective permeability to oil was calculated using Darcy's equation. This procedure established S_{wi} and initial volume of oil (V_o) or original oil in place (OOIP).
    - **Nanofluid Flooding:** Then, nanofluid was injected to mimic the secondary EOR operation. The injection was conducted at a constant flowrate of 0.2 ml/min until there was no oil production for ≈3 PVs.

2. **Tertiary Nanofluid Flooding**

    Tertiary nanofluid flooding refers to the EOR operation in which the nanofluid is injected after water flood. After primary drainage, the procedure describe above is continued as follows:

    - **Water Flooding:** The core at S_{wi} was waterflooded at 0.2 ml/min until no oil production was observed for 2 PVs. For the tests conducted

at high temperature, after the low rate injection (0.2 ml/min), water flood was continued with the flowrate increased 2 ml/min. The tenfold increase in flowrate was intended to minimise the capillary end-effects Heaviside et al. (1983), Ramakrishnan and Cappiello (1991) and to make ensure that any additional oil recovery would be a result of nanofluid effect. The residual oil saturation (S_{or}) and effective permeability to water were calculated; oil recovery and differential pressure were recorded as function of PVs.

- **Nanofluid Flooding:** After water flood S_{or} was established, the injection was switched to nanofluid flood to simulate the tertiary oil recovery at the same constant flowrate of 0.2 ml/min until there was no oil production for ≈2 PVs. Then, the flowrate was increased tenfold and the injection continued with nanofluids for ≈ 2 PVs. This procedure was adopted for tests conducted at high temperature.

Oil production was collected for every 1/4 PV after the dead volume was produced during secondary EOR operations. Here, dead volume refers to the amount of oil present in the flood system, except that in the rock core. When the production was occurring at low pace, a camera with automated capturing was used to record the production in a graded line over time, while the total volume was being collected in a large effluent separator. The recorded pictures were then analysed to measure the amount of oil produced. This oil was compared to the total volume produced in the large effluent separator. The S_{or} was calculated for each step, and oil recovery factor and differential pressure recorded as function of pore volume. All flooding experiments were performed using two nearly identical core plugs to determine experimental repeatability and reduce experimental errors.

4.5 Evaluation of the Rock Wettability

Wettability of a reservoir strongly affect any oil recovery strategy. That is because it is a major factor controlling the location, flow, and distribution of fluids in porous medium (Anderson 1987, Abdallah et al. 1986).

In this work, wettability of the core plugs was measured before and after the injection of nanoparticles using Amott-Harvey method (Amott 1959). This method is one of the most acceptable for the characterisation of the wettability of reservoir cores in petroleum engineering; it combines spontaneous and forced displacements of the fluids to obtain the average wettability of a core (Anderson 1987, León-Pabón et al. 2014). The main problem with Amott-Harvey method is its insensitivity near neutral-wettability (Anderson 1987, León-Pabón et al. 2014). The Amott-Harvey method consists of four basic steps:

1. The core at S_{wi} is placed in an Amott-cell filled with water as shown in Figure 4.4. Water is allowed to imbibe naturally into the core displacing oil. The amount of oil produced is recorded over time until equilibrium is reached (no more oil production); the total volume of oil produced is denoted as V_{o_1};

2. The core is then centrifuged in water, or water is pumped through it to produce the remaining mobile oil down to residual oil saturation (S_{or}). The volume of oil produced is recorded as V_{o_2};

Figure 4.4: Water spontaneous imbibition and displacement of oil from top (left), and from all faces of the cores (right). Because *n*-decane was injected after nanofluid flood (at S_{or}), it dissolved/cleaned residual crude oil turning black.

3. The core at S_{or} is now placed in the Amott-cell filled with oil, as shown in Figure 4.5. The oil phase is allowed to imbibe spontaneously displacing water until equilibrium is reached in the core; the amount of water produced, V_{w_1}, is measured;

4. Finally, the remaining mobile water in the core is forcibly produced using the centrifuge or by core flooding method; the produced amount of water measured as V_{w_2}.

Figure 4.5: Displacement of water by oil spontaneous imbibition in the cores.

A schematic of core flooding rig and the centrifuge and its components used to perform forced displacements are shown by Figure 4.3 and Figure 4.6, respectively. Normal decane was used as oil phase. The Amott-Harvey wettability index (WI) is defined as the displacement by water ratio (I_w) minus the displacement by oil ratio (I_o), Equation 4.3.

$$\mathrm{WI} = I_W - I_0 = \frac{V_{o_1}}{V_{o_1} + V_{o_2}} - \frac{V_{w_1}}{V_{w_1} + V_{w_2}} \tag{4.3}$$

The difference is a number falling within -1.0 to +1.0. This number is used to infer the average wetting state of a reservoir rock. According to Cuiec (1984) a reservoir is water-wet when the WI falls within +0.3 and +1.0, slightly water-wet ($+0.1 \leq \mathrm{WI} \leq +0.3$), neutral/intermediate system ($-0.1 \leq \mathrm{WI} \leq +0.1$), slightly oil-wet ($-0.3 \leq \mathrm{WI} \leq -0.1$), and oil-wet ($-1.0 \leq \mathrm{WI} \leq -0.3$).

(a)

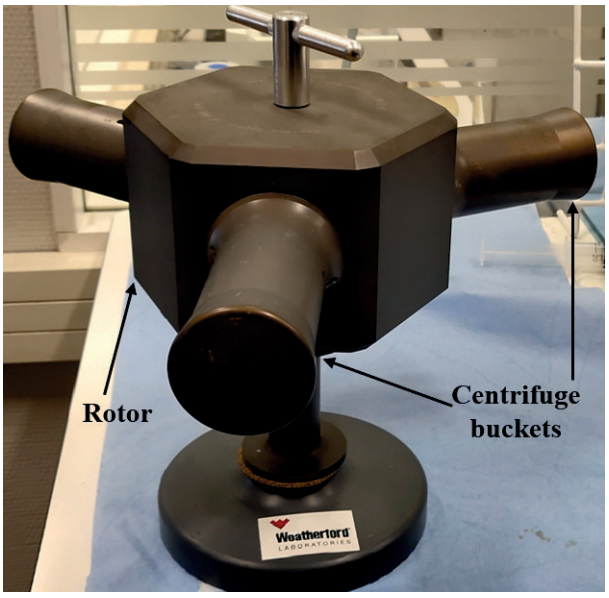

(b)

Figure 4.6: Ultracentrifuge with its main components: (a) Beckman Optima L-80 XP Ultracentrifuge; (b) Rotor assembled with centrifuge buckets .

CHAPTER 5

Results

5.1 Introduction

This chapter presents the main results obtained from our extensive flooding experiments with both the glass micromodels and Berea core plugs, including insight gained into the oil recovery mechanisms of the particles. The experimental results are divided into sections, in which each section presents the objectives, experimental results and the summary.

5.2 Nanoparticles Stability

5.2.1 Objectives

The nanoparticles' stability in SSW at 0.1 wt% was studied using PSD, zeta potential and sedimentation techniques. The tests aimed at evaluating whether the particles aggregated in SSW over time to predict their flow behaviour in porous media. The stability test was conducted for selected NPs presented in Table 3.2. Following Aurand (2017), sedimentation tests were carried out for a period of four months and the PSD was measured four months after the nanofluids were prepared; the measured size was then compared with the reference one (provided by the manufacturer). All the experiments were performed at room temperature (≈22 °C) and at the assumed reservoir temperature of 60 °C.

5.2.2 Results

The nanoparticles' average diameter size measured four months after the dispersion was prepared at room temperature are presented in Table 5.1. The diameter is an average of three measurements taken for each NP type. Table 5.1 shows that the

average size of NPs in SSW ($D_{avg.2}$) decreased slightly compared to the reference size ($D_{avg.1}$), except the size of samples NF02-4 and NF02-9. In these samples, the size increased when the NPs were mixed with SSW. Samples NF02-3, NF02-7 and NF02-13 show the largest reduction in size by 41, 57 and 43% relative to their corresponding primary size measured in distilled water using the same technique.

Table 5.1: Comparison of average diameter size of the NPs in distilled water ($D_{avg.1}$) and in SSW ($D_{avg.2}$).

Sample	**Basis**	**Ref. $D_{avg.1}$ (nm)**	**$D_{avg.2}$ (nm)**	**Differences** (%)
NF02-3	SiO_2 (sol-gel-cationic)	107	63	-41
NF02-4	SiO_2 (sol-gel-anionic)	32	38	19
NF02-6	SiO_2/Al_2O_3/MOX	218	154	-29
NF02-7	Silica - AE 200	376	163	-57
NF02-8	SiO_2/Al_2O_3/MOX	145	135	-7
NF02-9	Silica-AE200	157	195	24
NF02-13	Silica-AE200	229	131	-43
NF-18	SiO_2/Al_2O_3/MOX	112	109	-3
NF-23	Disp. W 1720 EPOMSI	112	109	-3

On the other hand, the largest increase in size relative to primary size is observed from samples NF02-4 and NF02-9 by 19 and 24%, respectively. As the primary size decreased in SSW and the observed increase in some particles is less than 50% compared with initial size, the results suggest that nanofluids were stable in SSW under the experimental conditions.

The sedimentation tests conducted at room temperature showed no particle aggregates for a period of four months in all samples. Measurement of zeta potential of the NPs gave unreliable results for unknown reasons.

Stability was further evaluated for samples NF02-3, NF02-4, NF02-6 and NF02-8 using the same techniques, but at high temperature. This is because the particle screening experiments conducted in sections 5.5.1 and 5.5.2 showed that the four samples had the most promising EOR potential. And, therefore, additional stability tests should be conducted at elevated temperature. At high temperature, the measured average diameter size in NF02-3 sample was 94 nm and 32 nm for sample NF02-4. These values are within the range claimed by manufacturer (i.e. 107 nm for NF02-3 and 32 nm for NF02-4), which suggest that NPs were stable in seawater solution. In contrast, the measurements of the size in NF02-6 and NF02-8 solutions resulted in large values of polydispersity index, suggesting that NPs were aggregating in SSW. Thus, it was not suitable to characterise the particle size with dynamic light scattering technique.

Sedimentation tests were then conducted to verify particle size measurement data. To this end, nanofluids were placed in the oven at 60 °Cand monitored daily. It was observed that samples NF02-6 and NF02-8 were rapidly rendered unstable, which is consistent with the size measurements. Large NPs structures were formed and deposited to the bottom of the glass vials within one-hour storage time (see Figure 5.1). The stability of nanofluids NF02-3 and NF02-4 was achieved for up to four days. After this storage-time, they also started to precipitate and gradually settling out of solution, forming large aggregates (Figure 5.1). The white colour in Figure 5.1 shows aggregate particles deposited at the bottom of the glass vials. In the glass vial labelled NF02-4, although difficult, during the test, we observed that some polymers were flocculating in the seawater solution due to the high temperature and the presence of divalent cations.

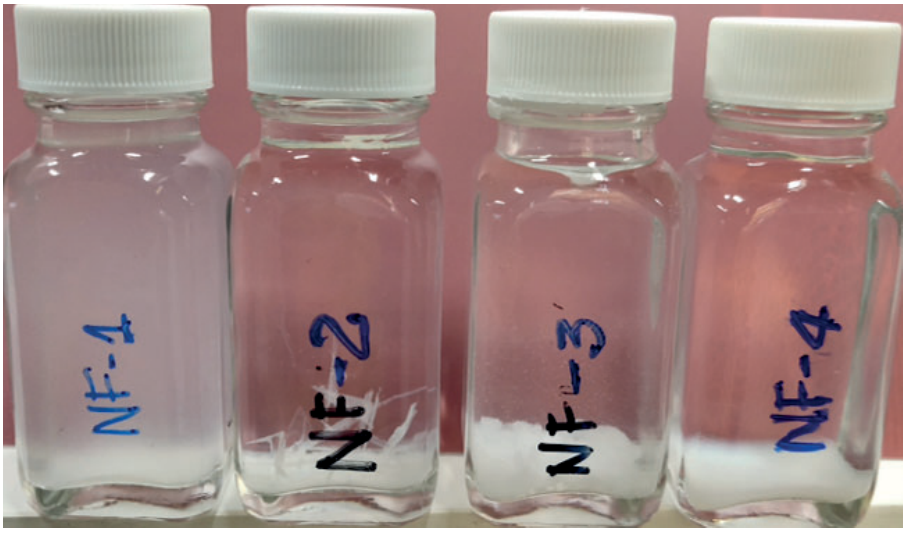

Figure 5.1: Visual analysis of NPs' stability in SSW at 60 °C. The white colour shows aggregated NPs. From left to right, labels refer to NF02-3, NF02-4, NF02-6 and NF02-8, respectively.

5.2.3 Summary of Results

Through systematic approaches, the stability of surface-functionalised silica NPs was examined over time. The main uncertainty was the limited input data for PSD measurements. Values such as absorbance factor were assumed, and refractive indexes were nearly the same for all samples. The aqueous suspensions of NPs at 0.1 wt% have shown remarkable stability for a period of four months at ambient conditions. However, by raising the temperature to 60 °C, the stability of all samples was

compromised; The aggregation of NPs in solution of samples NF02-3 and NF02-4 occurred after 96 hours, while samples NF02-6 and NF02-8 were readily rendered unstable. These findings have significant implications for the practical application of NPs in multiphase transport through porous media because the aggregates will reduce the particle mobility and surface functionality.

5.3 Interfacial Tension

5.3.1 Objectives

It is well-known that interfacial tension (IFT) reduction is one of the contributing mechanisms for oil recovery by silica nanoparticles injection. The IFT between the flowing aqueous phase and oil phase can be reduced by the presence of NPs. Accordingly, the capillary forces preventing the oil from moving are decreased, and the oil recovery can be improved. The main goal here was to evaluate to which extent the surface-functionalised silica NPs can reduce the IFT, and if the reduction could play a major role in the mobilisation of residual oil. The IFT was measured only for the selected nanofluid samples following the results of the particle screening process.

5.3.2 Results

Interfacial tension was measured using pendant drop and spinning drop techniques at ambient conditions and at elevated temperature. Crude oil B, SSW and nanofluids were used as fluid phases. All tests were conducted until stable value of IFT was reached. The measurements of IFT between crude oil and selected nanofluids using Pendant drop method at room temperature is shown in Figure 5.2.

At room temperature, it was observed that silica particles in injection seawater at a concentration of 0.1 wt% could decrease the tension between oil and water. Sample NF18 had the largest reduction of IFT, from 10.6 mN/m to a value of 2.53 mN/m. The lowest reduction was achieved with samples NF02-6 and NF02-7. Additional results are presented in Table 5.2.

At 60 °C, the IFT was measured between crude oil and selected samples (see sections 5.5.1 and 5.5.2), namely NF02-3, NF02-4, NF02-6 and NF02-8. Figure 5.3(a) shows a crude oil drop hanging from a needle within NF02-6 solution during the measurement of the IFT at room temperature with pendant drop method. When the temperature was increased to 60 °C, NPs in NF02-6 and NF02-8 solutions

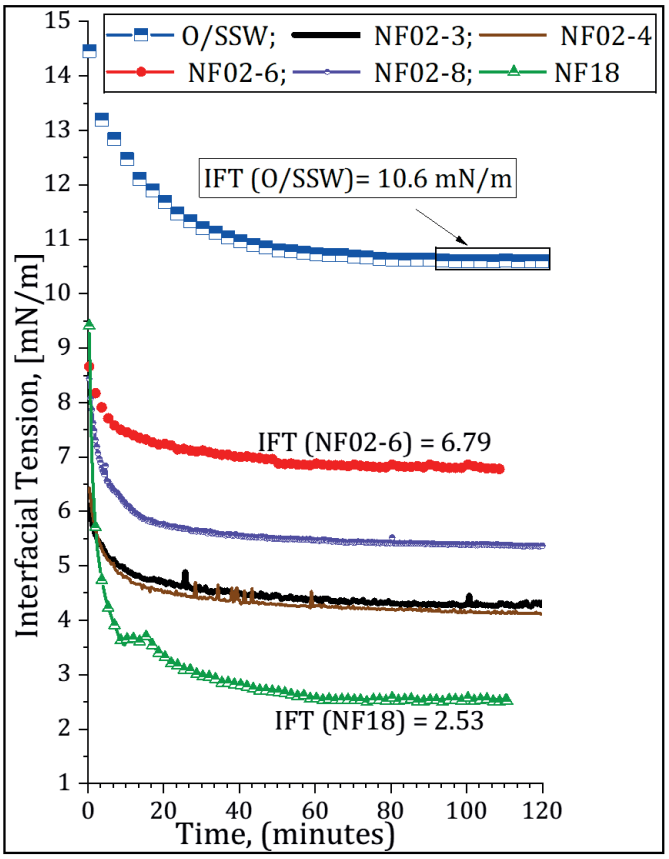

Figure 5.2: Dynamic measurement of IFT between crude oil and selected nanofluids at room temperature with Pendant drop method.

readily self-assembled at oil and water interface as shown by Figure 5.3(b). The solutions became opaque. Therefore, the pendant drop method was discarded as it failed to accurately measure the IFT. The spinning drop method was used instead. With a drop of oil immersed in the capillary tube filled with nanofluid solution and centrifuged at high rotational speed, no NP aggregates (see Figure 5.3(c)) were observed until the stable value was reached.

The main observation was that, the IFT was further reduced with increasing temperature, which is in line with previous work by Hendraningrat and Torsæter (2014). The smaller diameter NPs, NF02-3 and NF02-4, had a noticeable reduction in IFT from 10.28 mN/m to 3.12 mN/m, and to 2.90 mN/m, respectively.

Table 5.2: Variation of IFT between crude oil B and nanofluids at 0.1 wt%.

	at 22 °C		at 60 °C			
Fluid	γ^a (mN/m)	vol. (μL)	γ^a (mN/m)	vol. (μL)	γ^b (mN/m)	vol. (μL)
Water	10.6±0.33	16.04	11.15±0.23	12.50	10.28	5.2
NF02-3	4.33±0.30	6.75	3.46±0.28	4.77	3.12	1.15
NF02-4	4.12±0.33	6.30	3.27±0.16	4.87	2.90	1.05
NF02-6	6.79±0.32	13.15			6.54	6.35
NF02-7	7.12±0.21	12.64				
NF02-8	5.37±0.42	9.03			4.70	4.86
NF02-9	5.77±0.04	10.27				
NF02-13	5.80±0.29	9.96				
NF18	2.53±0.32	8.17				
NF23	8.73±0.95	11.44				

[a,b] IFT measured with pendant drop and with spinning drop methods, respectively.

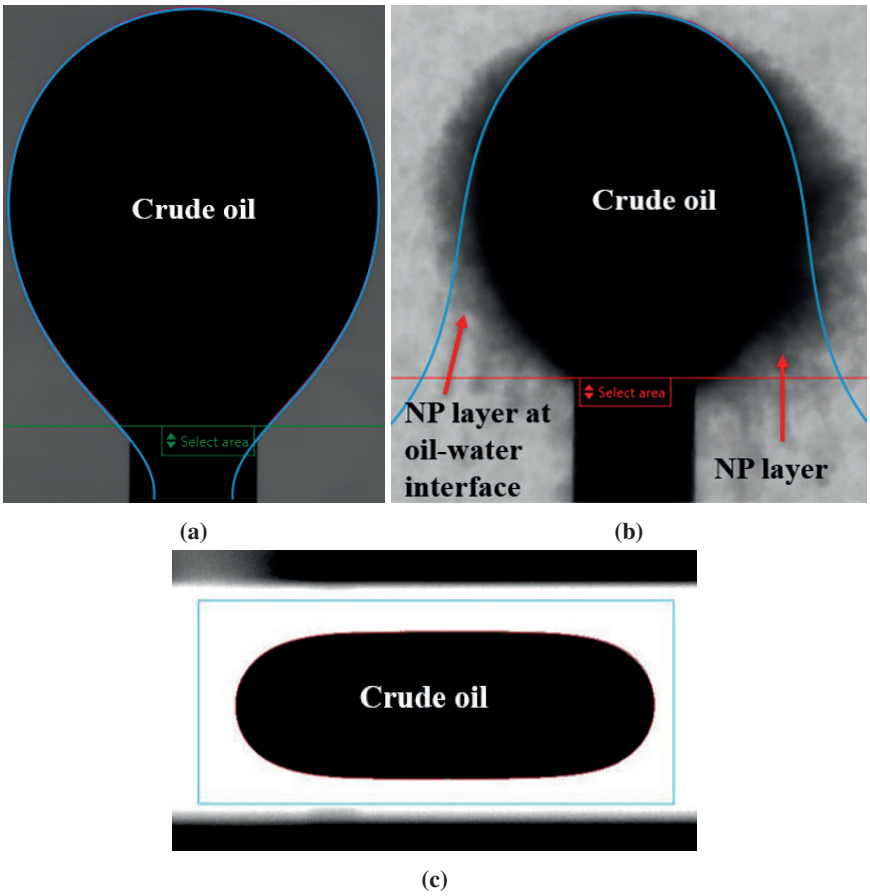

Figure 5.3: Exemplary of measurement of IFT between crude oil and nanofluids: (a) Shape of oil drop suspended from a needle in nanofluid "NF02-6" at 22 °C; (b) At 60 °C, the NPs readily self-assembled at oil/water interface and the solution became opaque; (c) Shape of crude oil drop immersed in a capillary tube filled with the same nanofluid and centrifuged at 7,000 rpm at 60 °C for IFT analysis.

5.3.3 Summary of Results

Interfacial tension between crude oil and water/nanofluids was measured with pendant drop and spinning drop techniques. Results show that IFT is reduced by surface-functionalised silica nanoparticles.

- Interfacial tension between crude oil and seawater was decreased by NPs at a concentration of 0.1 wt%. The reduction ranged from 8.73-2.53 mN/m compared to 10.6 mN/m of seawater and crude oil at ambient conditions. Sample NF18 had the largest reduction by 76%;

- Interfacial tension was further decreased with increasing temperature. At 60 °C, the largest reduction was achieved with NF02-3 and NF02-4 by a factor of 70% and 72%, respectively.

5.4 Screening of Nanoparticles using Glass Micromodel

5.4.1 Objectives

Glass micromodel tests were conducted with the main objective of rapidly obtaining oil recovery information and screen the NPs samples for further testing with Berea sandstone cores.

5.4.2 Micromodel Results

Micromodel injection experiments were performed after oil saturation and initial water saturation were established in the microchip. All twenty-thee nanofluid samples were prepared at a concentration of 0.1 wt% and injected directly through the microchip until no change in oil saturation was observed. To discriminate the nanofluid samples, a threshold value of 15% residual oil saturation (S_{or}) was used. This value was chosen because it may indicate a typical oil saturation after water flooding in a homogeneous unconsolidated sand system (Chatzis et al. 1983). If the S_{or} at the end of nanofluid flood is lower than 15%, the likelihood that the nanofluid sample will increase oil recovery in the consolidated rock system increases. Thus, the sample can be pre-selected for further testing with Berea sandstone. Otherwise, the sample is discarded.

Table A.1 in Appendix A shows secondary oil displacement efficiency for each sample in glass micromodels. The results are reported in terms of the amount of oil remaining in the microchip as a function of time. Based on these results, fifteen of the twenty-three nanofluid samples with S_{or} less than 15% passed the pre-selection stage. However, the nanoparticles' manufacturer decided to select 8 of the 15 nanofluids for an additional micromodel testing with physical rock pore systems to gain a more realistic information. The first four experimental tests using physical rocks gave similar results to those of uniform microchips. It was later realised that the injection pump was not delivering accurate flow due to malfunction. Then, it was decided to test all 8 pre-selected samples with water-wet Berea sandstone rocks instead. The performance of these samples with uniform micromodel is presented in Figure 5.4. Note that sample NF02-6 had the highest residual oil saturation (S_{or} = 27.34%). It was included here following the manufacturer suggestion. The manufacturer hypothesised that it would perform well with Berea cores compared to synthetic rock models. In Figure 5.4, the number identifies the sample type and the number in brackets is the amount of immobilised

oil after 400 minutes. Nanofluids NF02-3 and NF18 appear to have superior oil sweep efficiency in the micromodel. The two samples achieved the lowest residual oil saturation of 5.10 and 0.22%, respectively, unlike NF02-6 the lowest sweep efficiency.

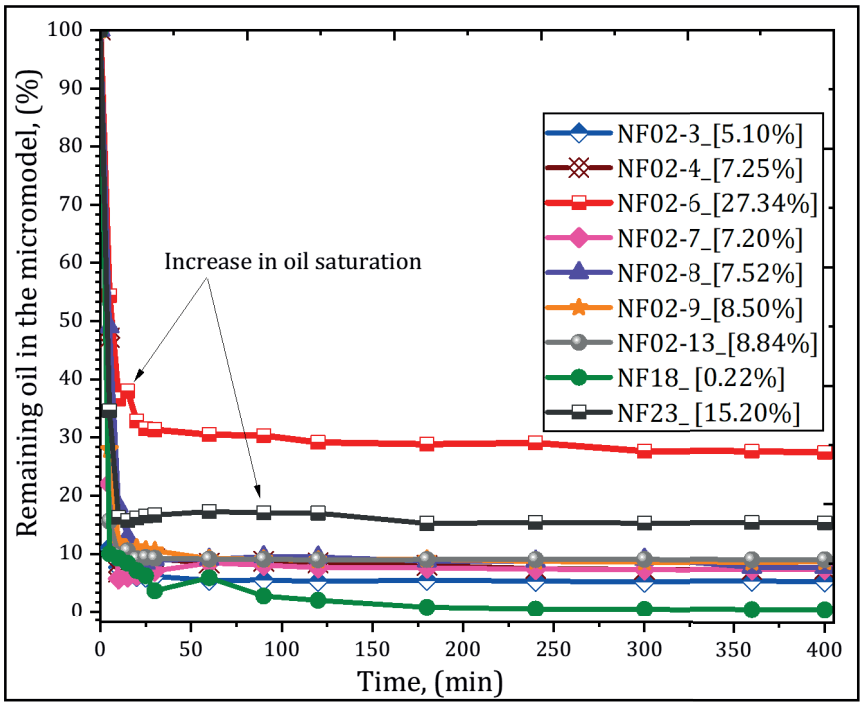

Figure 5.4: Percentage of oil remaining in the glass micromodel versus injection time.

The residual oil saturation was calculated using an automated image analysis. A pre-flooded image (taken at S_{wi}) was compared to the subsequent flooded images taken over time. The Matlab code counted the pixels appearing on the captured circular region of flooded and pre-flooded images to quantify the relative change in oil saturation. Figure 5.5 shows an example of processed images taken at different points in time during nanofluid injection until residual oil remained unchanged. Water phase is hidden in the microchip and could not be seen because it was not coloured. The brown colour is the crude oil phase.

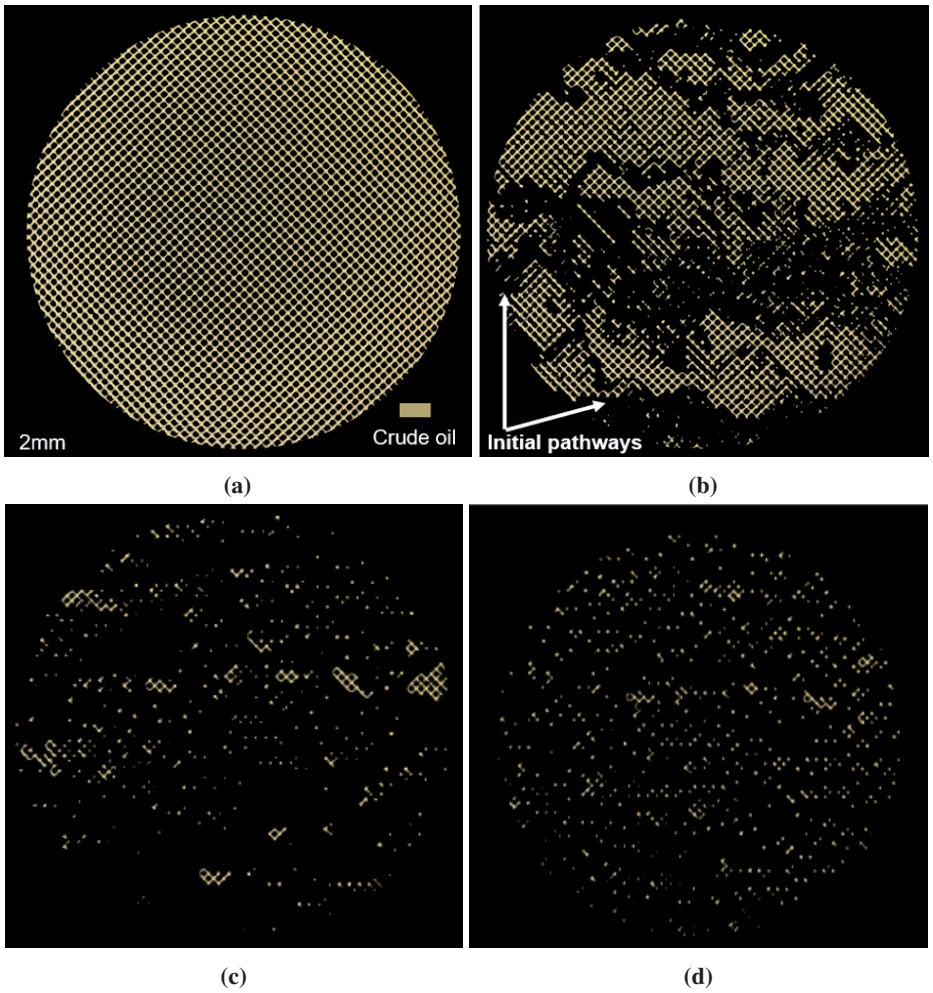

Figure 5.5: Microscopic view of crude oil within the pores of the glass micromodel; the oil appears in brown. (a) Pre-flooded image, t = 0 min at S_{wi}; (b) describes flooded image taken 5 min after nanofluid injection (S_{or} = 47.14%); (c) flooded image taken 10 min later, (S_{or} = 9.84%); and, (d) image taken 400 min (S_{or} = 7.25%).

5.4.3 Summary of Results

In this section, twenty-three different types of surface-modified silica NPs were screened for their EOR effect using water-wet glass micromodels with uniform pore network. Based on secondary nanofluids oil recovery results, the main observations are as follows:

- Fifteen of twenty-three NPs samples were pre-selected based on low residual

oil saturation (<15%) obtained at the end of the nanofluid injection. Nine of the pre-selected samples (see Figure 5.5) were suggested for further testing in Berea sandstone rocks.

- Visual observations through the micromodel showed that nanofluids tended to establish preferred pathways for sweeping oil from the start of the injection; At the end of the nanofluid injection, the residual oil was trapped as isolated oil droplets in the pore bodies. This behaviour was observed in all samples, which could be associated to displacement mechanism of NPs in water-wet systems.

5.5 Core Flooding Experiments

Flooding experiments were performed to evaluate the EOR potential of nanofluids with Berea core Plugs. Secondary and tertiary EOR operations were the injection procedures adopted. Parallel tests were performed for each nanofluid type. The most promising nanofluid samples at room temperature were further tested at high temperature as tertiary oil recovery agents. The differential pressure and oil recovery factor RF were recorded as a function of pore volumes PVs injected. The RF is expressed as the percentage of OOIP. When the nanofluid flood experiments were completed, the Amott-Harvey wettability index was determined on the cores; then the cores were cleaned and dried for permeability and porosity measurements.

5.5.1 Secondary Nanofluid Flooding with Water-wet cores

5.5.1.1 Objectives

Section 5.4 concluded that 9 of 15 nanofluids were promising candidates for oil recovery. This hypothesis was tested by conducting secondary core flooding tests using water-wet Berea sandstone cores, where the ultimate oil recovery was compared with that of "pure" water flood.

5.5.1.2 Flooding procedure

Eighteen flooding tests were conducted using core plugs (3.75 cm diameter and 4.5 cm length). The absolute permeability and porosity ranged from 247 to 407 mD and from 16.0 to 18.3%, respectively.

The primary oil drainage was conducted by injecting crude oil B at different flow rates until no SSW was produced. This procedure was performed for 8.5 to 10 PVs. This included injection at both core ends. The procedure established the oil in place and the residual water saturation presented in Table B.1 in Appendix B. The OOIP ranged between 5.4 to 6.7 ml and the S_{wi} from 19.6 to 39.8% of total PV. After primary drainage, the nanofluid was directly injected at 0.2 ml/min

constant flow rate until oil ceased production. The oil production and differential pressure across the core were recorded as function of PVs injected.

The post- nanofluid flooded cores were immersed in same nanofluid and placed in the oven at 40 °C for 10 days. The main objective was to assess the effect of long-term exposure of NPs on the rock surface, and whether this could benefit the oil recovery. The submerged cores were cooled-off and loaded in the Hassler core holder and injected with water at 0.5 ml/min. Finally, the cores were cleaned by toluene and methanol and dried for porosity and permeability measurements.

5.5.1.3 Nanofluid Flooding Results

Oil was produced under nanofluid flooding for all tests and was higher than reference water flood. All nanofluids delayed water breakthrough (BT) compared with "pure" water flood. At BT point, oil recovery of nanofluid was higher than pure water. Breakthrough points and corresponding recovery are given in Tables C.1-C.9 in Appendix C.1. Nanofluids were injected for 10 PVs on average. However, the ultimate recoveries were achieved between 4 to 7 PVs, as opposed to approximately 3 PVs in the case of reference water flooding (see Figure 5.6). This indicates the observed continuous oil production with nanofluid injection after BT point relative to pure water flooding. The average oil RF varied from 45.68% to 54.48% of OOIP compared with 39.67% of OOIP from reference water flood (WF). The nanofluids increased oil recovery by factors ranging from 6.0 to 14.8% points, on average. This is from 39.67% OOIP achieved by reference water flood to 45.68 to 54.48%OOIP by nanofluids. The oil RFs are presented in Figure 5.6 as a function of PVs injected to reach maximum oil production. Detailed core flooding results are presented in Tables C.1-C.9 and the corresponding plots in Figures C.1-C.5, respectively, in Appendix C.1.

Surprisingly, the low performing sample NF02-6 in micromodel experiments had the largest ultimate recovery in Berea sandstone cores. To this end, nanofluids NF02-3, NF02-4, NF02-6 and NF18 with oil recovery increase by 10% points relative to water flood were proposed for additional EOR testing. Water flood applied after soaking the cores at S_{or} had little effect on oil recovery (<1% oil recovery). The differential pressure increased during water injection and was higher than before soaking the cores. Probably, the nanofluids aggregated during the soaking period at 40 °C.

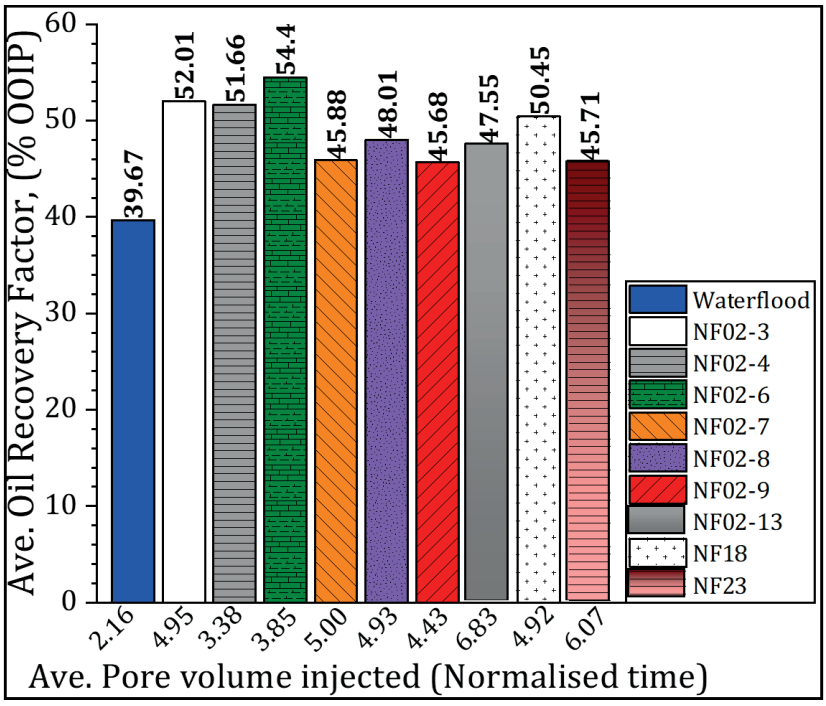

Figure 5.6: Comparison of the ultimate oil recoveries from secondary water flood and nanofluid flood. The X-axis shows the number of PVs injected to reach maximum oil recovery.

5.5.1.4 Differential Pressure

The differential pressure (dP) was recorded as a function of PVs to realise the migration behaviour of the NPs across the core plugs. The dP increased with nanofluid injection, and the maximum dP was greater than maximum pressure recorded during water flood (WF) process. The maximum dP ranged from 81 to 265 mbar compared with 76 mbar recorded during WF (in average). Additional plots of dP versus PVs are published in Appendix C.1, Figures C.1 through C.5. The oil recovery results did not suggest any correlation between the dP and the primary size of NPs, nor the recovery of oil with maximum differential pressure.

5.5.1.5 Wettability Evaluation Results

Two core plugs were used as the reference cores (original cores) and had an average wettability index (WI) of 0.86. The water spontaneous imbibition (SI) profile is described by Figure 5.7. Both results of the rate of SI and Amott WI indicated strongly water-wet condition of the core plugs. The core plugs used afterwards

were considered water-wet because they were obtained from the same block.

After nanofluid flood, wettability of the cores was evaluated. Figure 5.7(a) shows the SI behaviour determined using two core plugs injected with the same nanofluid type; the respective average WIs are presented in Figure 5.7(b). Each cycle of water or oil imbibition was conducted for 15 days. As can clearly be seen in Figure 5.7(a), the rate of water imbibition is as high as in original cores from the beginning of the test, producing significant amount of oil. However, this production declined after about 6 hours and no significant oil production occurred afterwards. Figures 5.7(a) and 5.7(b) show that the cumulative oil production and the wettability indexes (WIs) also decreased with nanofluids injection as compared to the original cores. This probably shows that NPs were retained on the pore spaces, thus reducing the permeability of the cores. The average WI of the cores was 0.57 and it varied from 0.52 to 0.60 (Figures 5.7(b)) indicating results of water-wet, as expected for the water-wet rock regime injected with hydrophilic silica nanoparticles. The overall data of natural and forced displacements used in the calculation of Wettability indexs (WIs) are presented in Table D.1 in Appendix D.

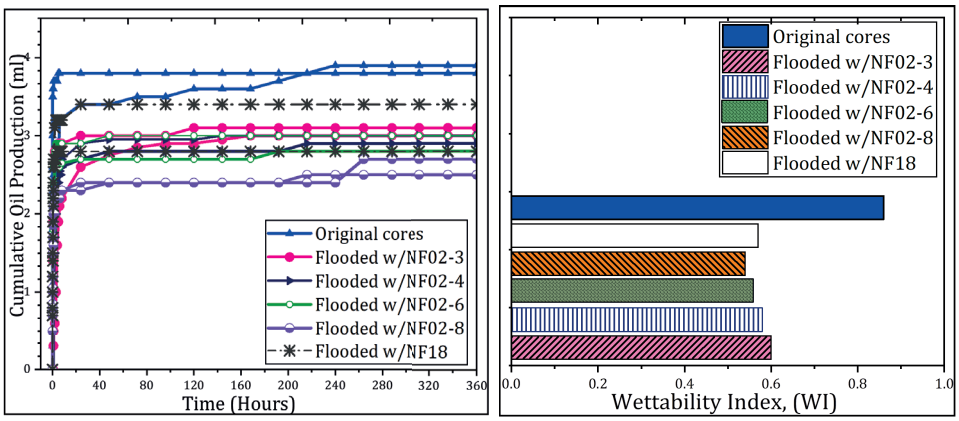

Figure 5.7: Wettability tests performed after soaking the cores (at S_{or}) in the same injected nanofluid for 10 days at 40 °C: (a) Water spontaneous imbibition curves; (b) Amott-Harvey wettability indexes.

5.5.1.6 Summary of Results

In this section, nine nanofluids samples prepared at 0.1 wt% concentration were injected in secondary recovery mode. All nanofluids resulted in higher ultimate oil recovery than reference water flood. The following summarises the main experimental findings:

- The nanofluids retarded the breakthrough of water (BT) with significant oil production recorded before breakthrough. However, after the BT oil saturation continued to decrease because oil was gradually produced at core outlet. As a result, oil recoveries by nanofluids were higher than the reference tests. On average, 4 to 7 PVs were needed for the nanofluid system to achieve the ultimate recovery compared to 2 in the case of reference tests.
- Four nanofluids samples (NF02-3, NF02-4, NF02-6 and NF18) with oil recovery greater by 10% points compared to average reference WF were selected for further testing;
- Soaking the cores (at residual oil saturation) in injected nanofluid followed by water injection did not mobilise residual oil;
- There was no clear correlation between the results obtained in water-wet glass micromodel and water-wet core floods experiments.
- Differential pressure increased with nanofluid injection and was higher than reference WF pressure. Possibly, pore plugging was occurring during nanofluid flooding in Berea sandstone rocks. However, no correlation was observed between the dP increase and the primary particle size.
- The clogging of the pores and structuring of the particles during nanofluid injection was likely responsible for the decreased rate of water SI and WIs. Nevertheless, the SI behaviour and measured WIs showed that the cores were in the range of water-wet condition, as expected. The hydrophilicity nature of NPs exposed to Berea cores would likely develop additional water-wet surfaces.

5.5.2 Secondary Nanofluid Flooding with Neutral-wet Cores

5.5.2.1 Objectives

The results obtained in Section 5.5.1 showed promising EOR effect of four NPs in water-wet Berea sandstone cores; it was hypothesised that the NPs would perform even better in aged cores. Therefore, the Berea sandstone core plugs were prepared to neutral-wet condition by ageing in crude oil. Two additional fluids #28 and #31, which are polymer-based with methacryl additives were tested. These fluids are free of NPs and were used to modify the surface of some of the nanoparticles. The purpose of the flood experiments was to evaluate the extent to which polymer-based fluids would affect oil recovery compared to nanoparticles.

5.5.2.2 Flooding procedure

Twelve core flooding tests were performed in this section. Core plugs with porosity and absolute permeability ranging from 15.4% to 18.2% and 256 to 355 mD, respectively, were used. All core plugs were aged in crude oil A at initial water saturation as described in Section 4.4.2.1. The primary drainage was performed using the centrifuge. The established initial water saturation (S_{wi}) varied from 10.2 to 18.7% of total pore volume of the core. The properties of the cores, oil in place and S_{wi} are given in Table B.2 in Appendix B.

The secondary nanofluid flooding was conducted according to the procedure presented in Section 4.4.2.3. After nanofluid flood ceased production, the injection was continued with water at 0.5 ml/min in one of the two core plugs. The second core was removed from the core holder and soaked in the injected nanofluid at 40 °C in the oven for 10 days. The purpose of soaking the cores was to evaluate the effect of prolonged interaction between the particles and the rock system compared to non-soaked cores, and if it would be beneficial for oil recovery. In the final step, both cores were submitted to wettability evaluation using Amott-Harvey test. The post-nanofluid flooding absolute permeability was determined after cleaning the cores with toluene and methanol to see whether permeability impairment had occurred as a result of the adsorption of NPs on the rock surface.

5.5.2.3 Nanofluid Flooding Results

The average oil recoveries due to nanofluid flooding varied from 59.3% to 71.5% of OOIP compared to 58.2% of reference WF; this is the nanofluids increased oil recovery by 1.1% to 13.3% points of OOIP. The recoveries from polymer-based fluids #28 and #31 were 66.4% and 60.4% of OOIP, respectively. Water flood applied after nanofluid flood incremented oil recovery from 0.6% to 3.5% of OOIP. An exemplary of oil recovery profiles are given in Figure 5.8 for NF02-6 and NF18. The remaining plots are presented in Figure C.6 through Figure C.7 in Appendix C.1. Table 5.3 summarises the most important data regarding nanofluid- and water flood results.

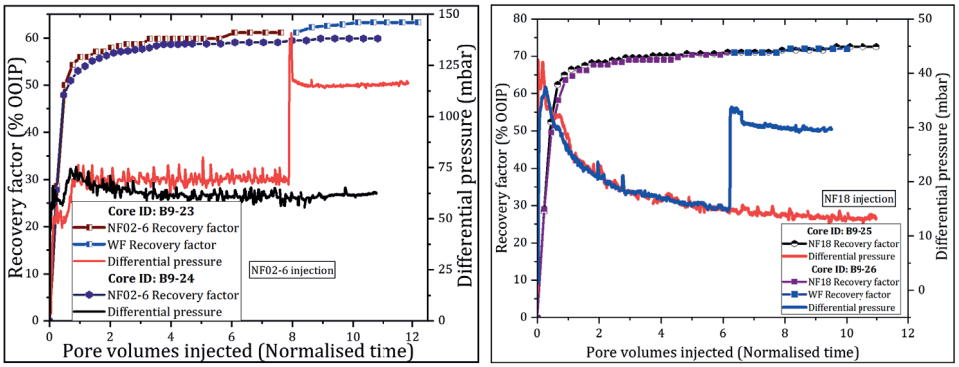

(a) **(b)**

Figure 5.8: Secondary oil recoveries and dP versus PVs injected. For each nanofluid type, two tests were conducted. Water flood was conducted only in replicate test at flow rate of 0.5 ml/min. (a) NF02-6 (dP= 65 mbar); (b) NF18 (dP= 14 mbar).

Flooding with nanofluids resulted in water BT as early as flooding with pure water. At the BT point, sample NF02-6 achieved the largest oil recovery from 47.2 to 50.0% of OOIP on both test #1 and #2, respectively. However, the highest ultimate oil recovery was achieved by NF18 with 71.5% of OOIP. Additional oil recovery was obtained after BT point during water or nanofluid flood. On average, ≈3 PVs were sufficient for water to reach ultimate recovery, unlike the nanofluid samples almost needed the twice as much to reach their maximum production. All nanofluid samples had higher oil recoveries than reference WF, and showed the ability to decrease injection pressure as shown by Figure 5.8(b).

Table 5.3: Summary of oil recovery factors and residual oil saturation achieved at the end of core flood (nanofluid- followed by water flood).

	Nanofluid flood						Water flood		
Fluid injected	PV @BT	RF @BT	PV @RF∗	RF (%)	S_{or} (%)	$\overline{RF}$ (%)	RF (%)	S_{or} (%)	RFt (%)
Water[1]	0.33	40.22	2.93	-	-	-	58.20	35.57	58.2
NF02-3	0.39	44.44	7.33	62.87	32.55	61.5	0.66	31.97	63.5
	0.35	40.52	7.05	60.13	35.83		-	-	60.1
NF02-4	0.33	40.79	4.42	59.50	35.86	59.3	1.42	34.58	60.9
	0.34	42.31	9.22	59.10	36.78		-	-	59.1
NF02-6	0.43	50.00	5.58	61.14	34.52	60.5	2.15	32.19	63.3
	0.36	47.22	8.93	59.89	33.92		-	-	59.9
NF18	0.34	41.89	5.00	70.41	24.89	71.5	1.62	23.52	72.0
	0.37	47.29	9.66	72.57	22.29		-	-	72.6
28†	0.31	36.10	4.61	66.83	29.03	66.4	2.32	27.19	68.9
	0.33	41.22	5.95	65.95	28.83		-	-	65.9
31†	0.32	36.36	4.27	56.10	38.02	60.40	3.51	34.99	59.6
	0.32	38.50	8.75	64.59	30.15		-	-	64.6

[1] Average values of thirteen water flooding tests in aged cores (see Table 5.10).
∗ Pore volumes injected to reach ultimate recovery
† Polymer-based fluids.

5.5.2.4 Differential Pressure

The differential pressure (dP) across the aged cores decreased during nanofluid injection compared to the reference WF pressure, except for nanofluid NF02-6. The nanofluids almost exhibited similar pressure behaviour at initial stage of injection; it was observed that the pressure increased until it reached water BT. Then, it declined and gradually stabilised. NF18 had the largest oil recovery while lowering the injection pressure relative to reference pressure (Figure 5.8(b)). The exception was observed during the injection of NF02-6; the pressure rose until ≈1.0 PV and then it levelled off (Figure 5.8(a)); however, the maximum dP at the end of the test was higher than reference water flood pressure. The reference water flood pressures were extracted from tests conducted in section 5.5.6, and the plots are shown in Figures C.9-C.11 in Appendix C.4. The average WF pressure was 33 mbar. The maximum pressure due to nanofluid injection varied from 14 to 65 mbar. Oil recovery and pressure profiles recorded throughout nanofluid injection are presented in Figures C.6 to C.7 in Appendix C.1. All core plugs showed absolute permeability reduction up to 22% of the initial values. However, no correlation was observed between permeability reduction and pressure or oil recovery.

5.5.2.5 Wettability Evaluation Results

Six core plugs were aged in crude oil A. The average wettability index was -0.1 and varied from -0.07 to -0.17, indicating neutral-wet condition.

After nanofluid flooding was completed, one of the two cores was removed from the core holder and soaked in the injected nanofluid for 10 days at 40 °C, while the second core was immediately submitted to wettability evaluation. Figure 5.9 presents the SI curves. As can be clearly seen, significant amount of oil was produced in the early stages of 15-days water imbibition cycle on both soaked and non-soaked cores; After this period, the imbibition reached stability, which indicated that wettability alteration took place during nanofluid flooding process in most pores of the rock. The variation in the rate of water imbibition observed in Figure 5.9 can be attributed to differences in core properties, the retained NPs in the cores and the accuracy of the measurements. The average Amott-Harvey WI was 0.69 for soaked cores, while for non-soaked cores it was 0.59. The results of spontaneous and forced displacements used to calculate the WIs are presented in Table D.2 in Appendix D.

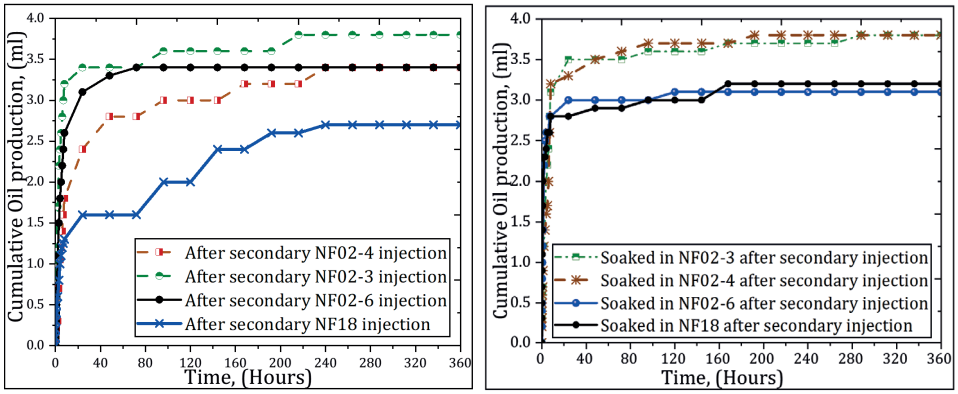

(a) **(b)**

Figure 5.9: Spontaneous imbibition (SI) curves of the cores after: (a) nanofluid flood; (b) nanofluid flood plus soaking in injected nanofluid for 10 days at 40 °C.

5.5.2.6 Effect of Nanoparticles on Core Permeability

After core flood and wettability tests, the cores were cleaned and dried. Then the core absolute permeability was measured. The results are summarised in Table 5.4. The NF02-6 and NF18 had the largest average absolute permeability reduction ranging from 22 to 11%, respectively. No correlation was found between the permeability reduction with the particle size. It is likely that the results were af-

fected by using the centrifuge to perform forced displacement of fluids. In this course, the rock fines may be released and NPs desorbed from the rock surface due to high centrifugal forces. This can improve the permeability of the rocks to some extent. In fact, some grains of sand were observed glued to the walls of the glass vials when measuring the amount of fluid produced by the centrifuge.

Table 5.4: Core absolute permeability measured before and after nanofluid flooding.

Core	Sample	**Absolute permeability (mD)**		% difference
		Before	After	
B9-19	NF02-3	321	285	-11
B9-20		391	388	-1
B9-21	NF02-4	238	207	-13
B9-22		368	343	-7
B9-23	NF02-6	248	195	-21
B9-24		304	236	-22
B9-25	NF18	347	299	-14
B9-26		301	281	-7

5.5.2.7 Summary of Results

In this section, secondary EOR experiments were performed in aged cores or neutral-wet cores. The experimental results revealed that all nanofluid samples have potential for recovery of oil; the following conclusions were obtained:

- Secondary nanofluids resulted in early water breakthrough and significant oil was produced after breakthrough;
- The nanofluids increased oil recovery by factors of 1.1 to 13.3% points of OOIP compared with reference WF. The largest ultimate oil recovery was achieved by sample NF18, which was not coated/modified by any of the polymers-based fluids #28 and #31 samples.
- The polymer-based fluids #28 and #31 had comparable oil recoveries with respect to the NPs samples, except for NF18;
- Additional oil recovery was produced after the injection was switched to water flood. It is possible that part of the produced oil had accumulated at the core outlet and was produced due to increased flow rate.
- Differential pressure decreased with nanofluid injection and was lower than reference water flood pressure. The exception was NF02-6, which increased

the pressure. The pressure profile suggested that the NPs were easily propagating through the aged Berea sandstone rocks without causing significant damage to the rock permeability;

- Wettability of the cores was changed from neutral- to more water-wet condition during nanoparticles injection.

5.5.3 Water Flooding

5.5.3.1 Objectives

Water flooding was conducted to simulate secondary oil recovery. All experiments were conducted with initial water saturation established in core plugs. The main objective of WF was to determine the oil recovery factor and establish residual oil saturation. The WF oil recovery was used as a benchmark to assess the performance of the secondary nanofluid flooding. Tertiary nanofluid flooding was performed to assess the extent to which nanofluids could re-mobilise residual oil and thereby increase oil recovery.

5.5.3.2 Water Flood Procedure

All flooding tests were conducted at a constant flow rate of 0.2 ml/min as described in Section 4.4.2.3(2). The number of PVs of water injected varied with core length, core's initial wettability and the intrinsic core properties. To help negate the trapping of oil due to capillary effects at the end of WF, the flow rate was increased ten-fold (2 ml/min) and the injection performed for 1 PVs. The total oil produced during low and high rate injections was measured as ultimate oil recovery. This procedure was later applied in tests conducted at 60 °C (see Sections 5.5.8 and 5.5.9).

5.5.3.3 Water Flooding Results

The initial water saturation (S_{wi}), WF oil recovery factors, residual oil saturation and the end-point relative permeability to water (k_{rw}) are all given in their corresponding core flooding sections. Table 5.5 summarises the S_{wi} values established in the core plugs according to the section in which they were used. The average S_{wi} was 19% (±5.8%) and ranged from 8 to 34% of total pore volume. The S_{wi} while established by the centrifuge (Section 5.5.6) was the lowest.

Table 5.5: Variation of initial water saturation established in the core plugs.

	Initial water saturation (%)				
	A	B	C	D	All tests
Maximum	33.93	24.29	32.24	24.67	34
Minimum	18.41	8.00	10.53	14.00	8
Average	24.25	16.58	18.47	18.06	19
Standard deviation	4.94	5.14	7.22	3.40	6
# of flood tests	08	13	08	08	37

[A,B,C and D] For tests conducted in Section 5.5.5, Section 5.5.6, Section 5.5.8 and Section 5.5.9, respectively.

A summary of the ultimate oil recoveries achieved by water flood is given in Table 5.6. For the flood tests conducted with water-wet core plugs at room temperature (≈22 °C), the average oil recovery was 39.67% (± 2.30) and varied from 35.08% to 43.07% of OOIP. For the tests conducted at 60 °C, the average recovery was 52.39% (±3.11) with a variation from 47.20% to 56.11%.

Table 5.6: Variation of ultimate oil recovery from water flood.

Water flood oil recovery	Water-wet core plugs		Neutral-wet core plugs	
	RF[1] at 22 °C	RF[2] at 60 °C	RF[1] at 22 °C	RF[2] at 60 °C
Maximum	43.07	56.11	63.75	66.75
Minimum	35.08	47.20	49.59	46.17
Average	39.67	52.39	58.21	56.00
Standard deviation	2.30	3.11	3.90	5.91
# of flood tests	08	08	13	08

[1] Section 5.5.5 and Section 5.5.6.
[2] Section 5.5.8 and Section 5.5.9

In neutral-wet cores, the average recovery was 58.21% (±3.90) and varied from to 49.59% to 63.75% of OOIP at room temperature. At high temperature, the average was 56.00% and it ranged from 46.17 to 66.75% of OOIP. The tests conducted with neutral-wet rocks at 60 °C, in Section 5.5.9, showed the largest variation with 5.91% of OOIP compared with 2.3, 3.1 and 3.9% of OOIP observed in Sections 5.5.5, 5.5.6 and 5.5.8, respectively. This variation is probably due to the accuracy of measurements experimental. The flood system was interrupted to correct some leaks and, at the end of the flood, the core plug in question had recovered the lowest oil of 46.17% of OOIP. This test is responsible for the large variation ob-

served in the tests conducted in Section 5.5.9. The other tests gave comparable and consistent oil recoveries values. The flood results show that water flood achieved maximum oil recovery under neutral-wet conditions. This is because little or no oil production occurred after water breakthrough point in water-wet core plugs, while the neutral-wet rocks continued to produce more oil after breakthrough point.

The end-point relative permeability to water (k_{rw}), where applicable, was calculated with air (absolute) permeability as the base permeability. All measurements are summarised in Table 5.7. The largest variation in k_{rw} was observed in neutral-wet rocks.

Table 5.7: Variation of relative permeability to water.

	Water-wet core plugs	Neutral-wet core plugs
Maximum	0.24	0.86
Minimum	0.04	0.04
Average	0.10	0.20
Standard deviation	0.05	0.16
# of flood tests	16	21

The following plots describe the oil recovery profiles as a function of initial water saturation (Figure 5.10), permeability (Figures 5.11(a) and 5.11(c)) and porosity (Figures 5.11(b) and 5.11(d)).

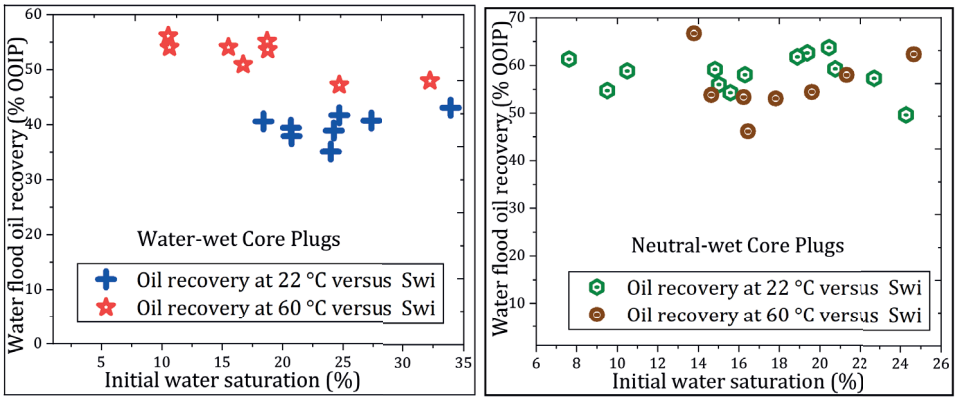

(a) **(b)**

Figure 5.10: Effect of initial water saturation on water flood oil recovery: (a) Flood tests conducted with water-wet core plugs at 22 °C and at 60 °C; (b) Flood tests conducted with neutral-wet core plugs at 22 °C and at 60 °C.

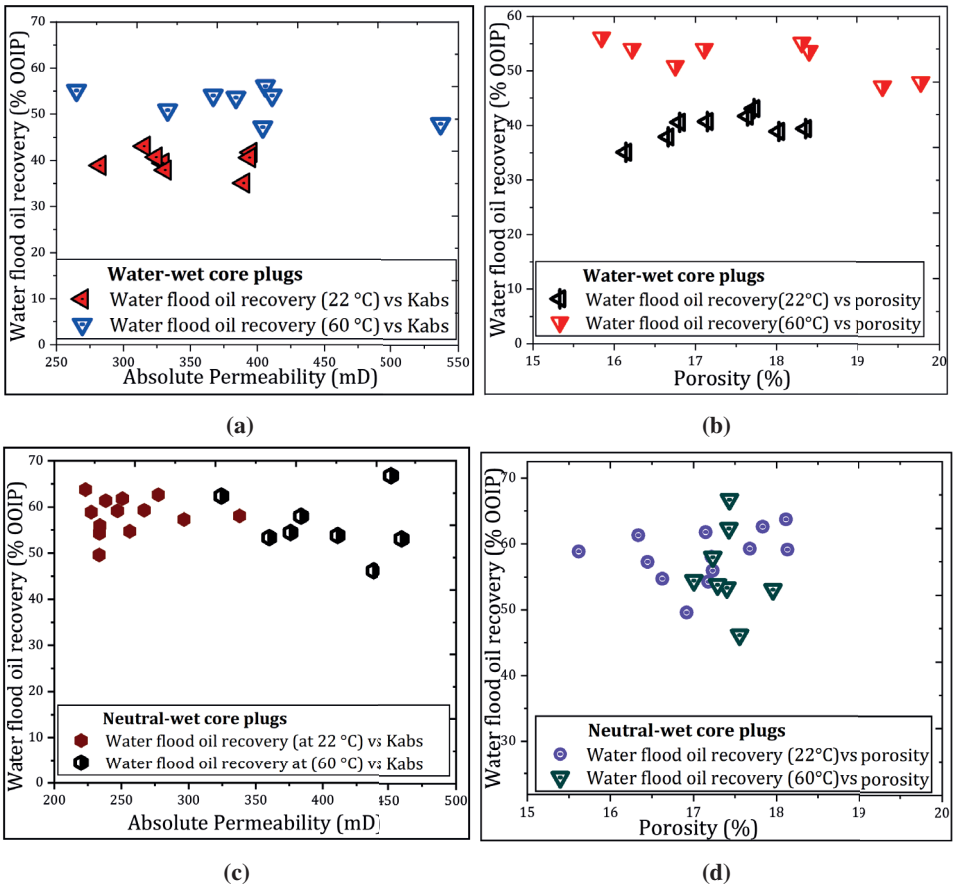

Figure 5.11: Water flood oil recovery versus: (a) permeability for water-wet core plugs used in Sections 5.5.5 and 5.5.8; (b) porosity for neutral-wet cores plugs used in Section 5.5.5 and 5.5.8; (c) permeability for neutral-wet cores used in Sections 5.5.6 and 5.5.9; and, (d) porosity for water-wet cores used in Sections 5.5.6 and 5.5.9.

5.5.3.4 Summary of Results

- The average initial water saturation established in the core plugs was 19% and it ranged from 8 to 34% of total pore volume; The tests conducted with centrifuge gave the lowest initial water saturation values;

- Water flood conducted with water-wet core plugs resulted in average oil recovery of ≈ 40% and varied from 35 to 43% of OOIP at room temperature. At high temperature, the average was 52% and ranged from 47 to 56% of OOIP. With neutral-wet cores, the average recovery was 58% and varied from 50 to 64% of OOIP at room conditions, while at high temperature the

average was 56% and it varied from 46 to 67% of OOIP;

- Overall results suggest that maximum oil recovery is achieved with neutral-wet rocks.
- There was no correlation between water flood oil recovery with permeability, and with porosity.

5.5.4 Tertiary Nanofluid Flooding Tests

5.5.4.1 Objectives

Flood experiments conducted in Section 5.5.1 resulted in the selection of four nanofluid samples based on the oil recovery potential. These samples are NF02-3, NF02-4, NF02-6, and NF18. They were therefore proposed for additional testing in tertiary recovery mode using water-wet and aged cores or neutral-wet cores. It is noteworthy that the nanoparticle screening process was based on water-wet systems; Thus, no correlation was expected when testing the same samples with aged cores. The manufacturer of NPs suggested excluding nanofluid NF18 from this section onward. That was because they were unable to determine the exact composition of surface additive materials attached to it. Nanofluid NF02-8 was therefore proposed to replace NF18 sample because it was composed of the same material and composition, and the particle surface was modified with the same additive materials used for the NF02-6 sample. The main difference was the primary particle size and particle concentration in distilled water (as received from the manufacturer). Therefore, it was believed that it would give results as good as the NF02-6 sample.

5.5.5 Nanofluid Flooding with Water-wet Cores

Eight core flood tests were performed using water-wet cores at room temperature. The cores were prepared to have similar dimensions: 3.76 cm in diameter and 6 cm in length. The measured absolute permeability and porosity of the cores ranged between 283-395 mD and 16.1 to 18.4%, respectively. Overall core properties including oil-in-place and initial water saturation obtained after primary oil drainage are presented in Table B.3 in Appendix B. The average OOIP was 8.8 ml and varied from 7.8 to 9.7 ml. The S_{wi} varied from 18.4% to 33.9% of total PV and the average was 24.3%. In this section S_{wi} was established by core flooding method.

Nanofluid flood was carried out after water flood to simulate tertiary oil recovery (procedure described in Section 4.4.2.3(2)). After nanofluid flood, the cores were injected with decane down to residual nanofluid saturation before being immersed in Amott cells for wettability evaluation. Finally, the cores were cleaned with

toluene and methanol to determine absolute permeability and porosity.

5.5.5.1 Nanofluid Flooding Results

Oil recovery factors from water- and nanofluid-flood are summarised in Table 5.8. The average oil recovery at the end of WF was 39.67% (± 2.30) of OOIP and varied from 35.08 to 43.08%. The main oil recovery occurred before water breakthrough point, with no significant oil production occurring afterwards. Water flood residual oil saturation was 45.75% (± 3.79), on average, and varied from 37.61% to 49.35%. All nanofluids could mobilise residual oil and the incremental oil recovery averaged 7.6% (± 1.57) and it varied from 4.6% to 9.8% of OOIP. The highest incremental recovery was achieved by samples NF02-6 and NF02-8. For these samples, oil recovery profile is presented in Figure 5.12. Additional plots are presented in Appendix C.3 including details of flooding tests in Table C.14 for the remaining experimental tests.

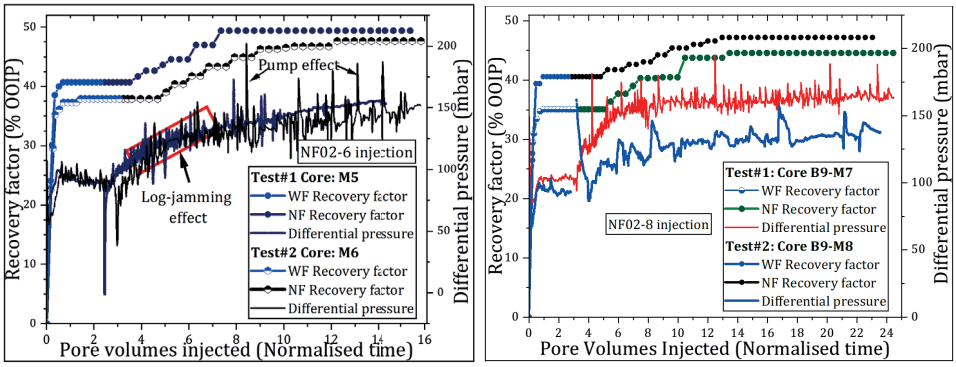

(a) **(b)**

Figure 5.12: Oil recovery factors and dP recorded as function of PVs throughout the injection of nanofluid as tertiary EOR in water-wet cores. Both flooding schemes were conducted at 0.2 ml/min. Two tests were conducted for each nanofluid type. (a) NF02-6 flooding: In test#1, the first oil appeared at after 1.75 PVs resulting in oil RF of 0.96%. Test#2, produced the first oil at 2.16 PV with recovery of about 1.14% of OOIP; (b) NF02-8 flooding: In test#1, the first oil appeared after 1.99 PV of nanofluid injection resulting in oil RF of 1.31%. Test#2, the first oil appeared after 2.39 PV and resulting in recovery of 1.18% of OOIP.

The occurrence of first oil due to nanofluid flood varied with NP type, core properties and it was affected by water flood stage. The first oil due to nanofluid was observed within 0.50 to 2.39 PVs were injected and reached the production lines in the form of dispersed oil droplets that merged upwards in the effluent separator. As shown in Table 5.8 most nanofluids could mobilise residual oil and form an oil

bank after 1 PV was injected. The main parameters used to determine the viability of tertiary nanofluid flood are summarised in Table 5.8.

Table 5.8: Summary of oil recovery factors (expressed as percentage of OOIP) and residual oil saturation achieved at the end of core flooding in water-wet cores.

	Water flood		Nanofluid flood					Total
NF type	RF (%)	S_{or} (%)	PV‡ @1^{st} oil	RF⋆ (%)	RF (%)	S_{or} (%)	E_D (%)	RF (%)
NF02-3	43.07	37.61	0.50	1.33	4.61	35.55	8.11	47.69
	38.91	46.29	1.33	1.10	7.25	40.83	11.87	46.15
NF02-4	41.70	43.91	0.51	0.60	7.39	38.36	12.67	49.09
	39.42	48.05	1.79	1.03	7.01	42.52	11.57	46.43
NF02-6	40.72	43.07	1.75	0.96	8.67	36.78	14.63	49.39
	37.91	49.22	1.98	1.14	9.77	41.47	15.74	47.68
NF02-8	35.08	49.35	1.99	1.31	9.51	42.14	20.71	44.59
	40.58	48.48	2.39	1.18	6.62	43.09	11.14	47.20
Average	**39.67**	**45.75**	-	-	**7.61**	**40.00**	-	**47.28**

‡ number of PVs injected for the nanofluid to produce the first oil at the outlet core.
⋆ First oil produced at core outlet due to nanofluid.

5.5.5.2 Differential Pressure

The differential pressure (dP) was observed to increase with NPs injection, and it was higher than reference water flood pressure in water-wet cores (Figure 5.12, and Figure C.8 in Appendix C.3). The dP response during nanofluid flood showed that NPs were blocking and being retained within the pores. A correlation was found between particle size and pressure increase. As a result, the largest permeability reduction was observed in the cores flooded with particles of large size (see Table 5.9). Nanofluid N02-4 with the smallest particle size and NF02-6 with the largest particle size showed, respectively, the lowest and largest effect in reference water flood pressure.

5.5.5.3 Wettability Evaluation Results

Because the cores were relatively long than those used in previous sections, a prolonged spontaneous imbibition period was allowed. The rate of spontaneous water imbibition during the 30-day test showed variable behaviour among the samples. It may have been affected by NPs retention in the pores and differences in core properties. Figure 5.13 shows that oil production rate is as high as in the original core from the start of imbibition test; then it declined and seemed to stabilise over time. Meanwhile, we see points of a sudden increase in oil recovery, which indicated

dynamic change in wettability due to the exposure of nanoparticles on the rock surface. After spontaneous imbibition, full Amott test was conducted. There was no oil imbibition in the second cycle of the spontaneous imbibition test, implying that Amott oil index is zero, $I_o = 0$. Therefore, the Amott-test was not completed, and the obtained water indexes were used to assess the effect of NPs on the rock surface. The Amott water indexes, I_w, varied from 0.53 to 0.79. While similar to the results achieved in section 5.5.1.5, the actual results also indicated that the rock surface was continuously altered towards more water-wet condition.

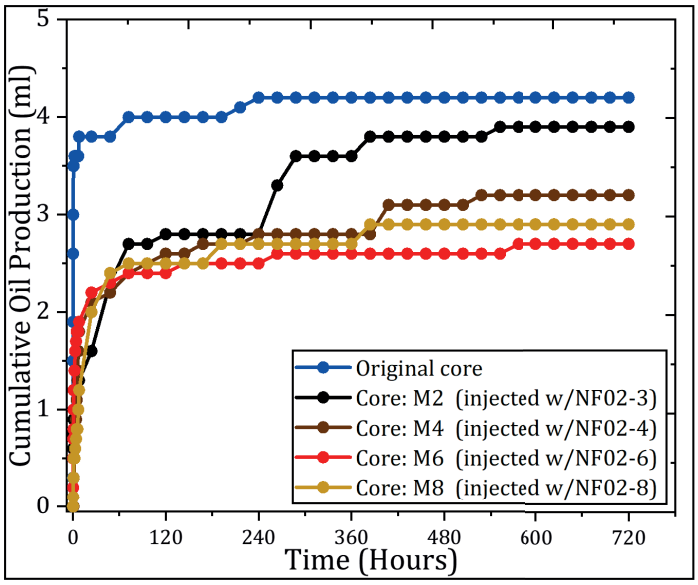

Figure 5.13: Oil production from water spontaneous imbibition in cores before and after NPs flooding.

5.5.5.4 Effect of nanoparticles on permeability

Experimental results showed that NPs reduced the core absolute permeability. The reduction varied 5 to 24% of initial values. The inspection of the results presented in Table 5.9 shows a large permeability reduction in the cores injected with large primary size nanoparticles. In summary, the permeability reduction reported in Table 5.9 is low. This may be associated with the role played by surface modification on the primary particle to improve NPs fluidity and low retention through the cores. Additionally, the measurement may have been affected by core preparation steps and the accuracy of the measurements.

Table 5.9: Variation in core absolute permeability due to nanofluid injection.

Core	Sample	Gas Permeability (mD)		% difference
		Before	After	
M1	NF02-3	315	278	-12
M2		283	252	-11
M3	NF02-4	395	369	-7
M4		329	311	-5
M5	NF02-6	324	245	-24
M6		331	266	-20
M7	NF18	390	335	-14
M8		394	340	-14

5.5.5.5 Summary of Results

Flooding experiments revealed oil recovery enhancement with silica nanoparticles in water-wet Berea sandstone at room temperature.

- The nanofluids (0.1 wt%) increased oil recovery in the range of 4.62% to 9.77% of OOIP. The oil production was delayed compared to breakthrough of water; no significant oil was recovered within the first pore volume (>5% of OOIP). The nanofluids could mobilise residual oil and form an oil bank after significant volumes of nanofluid were injected; Samples NF02-6 and NF02-8 showed better oil sweep efficiency while increasing pressure across the core;
- Despite high incremental oil recoveries due to nanofluids, the ultimate recoveries in the tertiary mode are lower than secondary ultimate oil recoveries obtained Section 5.5.1, Figure 5.6;
- There is, somewhat, a positive correlation between oil recovery and primary size of NPs and interfacial tension reduction; As with secondary nanofluid injection, the pressure increased with NPs injection when the NPs were injected after water flood. In both cases, the pressure response indicated that microscopic flow diversion played a role for oil recovery;
- The wettability tests indicated that silica nanoparticles gradually change the rock wettability to a more water-wet condition;
- The surface modified NPs resulted in low permeability reduction.

5.5.6 Nanofluid Flooding with Neutral-wet Cores

Nanofluid samples tested in Section 5.5.5, with water-wet cores, were also investigated in neutral-wet cores. Three additional samples, the polymers-based fluids #28 and #31 and NF18, were included in this section. All tests were conducted in tertiary recovery mode at room temperature. Here, the NF18 sample test was motivated by the high secondary recovery obtained with neutral-wet cores in Section 5.5.2.3; the manufacturer was no longer interested in testing NF18 sample due to the reasons mentioned in Section 5.5.4. The polymer-based fluids were tested to assess their effect on oil recovery compared to nanoparticles.

For this purpose, fourteen core flooding experiments were conducted in the present section. The core absolute permeability and porosity varied from 223 to 278 mD and 15.6 to 18.1%, respectively. The primary oil drainage was performed using the centrifuge. The established OOIP and S_{wi} varied from 6.4 to 7.5 ml and 10.49 to 24.29% of total PV, respectively. The properties of all cores are presented in Table B.4 in Appendix B.

5.5.6.1 Nanofluid Flooding Results

The average water flooding oil recovery obtained in neutral-wet cores was 58.20% (±3.90) and varied from to 49.59% to 63.75% of OOIP. The average residual oil saturation, at the end of WF, was 34.82% (±3.53) and ranged from 28.84 to 40.96% of total PV.

The nanofluids increased oil recovery from 2.57% to 5.21% of OOIP; the average was 3.54% (±1.07) of OOIP. The oil recoveries (water-, and nanofluid-flooding) and the main parameters used to assess the viability of NPs in EOR are given in Table 5.10. The NF02-6 and NF02-8 samples showed relatively better displacement efficiency. Polymer-based fluid recoveries were lower than those obtained by NPs samples. Selected RFs and dP profiles as a function of PVs are presented in Figure 5.14. The remaining plots are shown in Appendix C.4 (Figures C.9-C.12).

Table 5.10 shows the variation in production of first oil at core outlet between nanofluid samples. As with water-wet cores, no significant oil recovery was observed during the first injected PVs for all samples; the recovery at 1 PV was less than 5% of OOIP. The first oil recovered at core outlet due to nanofluid occurred from 0.5 to 1.63 PVs with recovery ranging from 0.41 to 1.56% of OOIP. Despite large volumes injected, the nanofluids hardly achieved recovery factor greater than 5% of OOIP in aged cores.

No clear correlation was observed between the primary particle size and oil recovery. The twin cores used for each nanofluid flood gave small variations in oil

recoveries (<5% of OOIP), indicating reproducibility of experimental results.

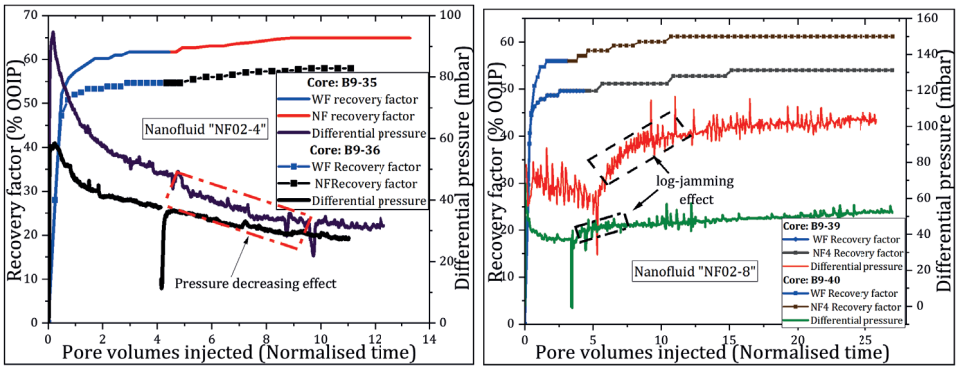

(a) **(b)**

Figure 5.14: Oil RFs and dP recorded as function of PVs oil recover tests in neutral-wet cores. (a) NF02-4 flood: in test#1, the first oil production was observed at 0.74 PV and the RF was 1.10% OOIP; Test#2, the RF was 1.33% OOIP at ≈ 1.30 PVs; (b) NF02-8 flood: Test#1 and #2 produced the first oil at 1.5 and 0.7 PVs. The recovery was 5% OOIP.

Table 5.10: Oil recovery factors (water-, and nanofluid-flooding), expressed as % of OOIP, and residual oil saturation achieved at the end of core-flooding in neutral-wet cores.

	Water flood		Nanofluid flood					Total
NF type	RF (%)	S_{or} (%)	PV @1^{st} oil	RF⋆ (%)	RF (%)	S_{or} (%)	E_D (%)	RF (%)
NF02-3[1]	58.86	36.83	0.50	0.71	2.71	34.39	6.6	61.57
NF02-4	61.33	35.72	0.74	1.10	3.33	32.64	8.6	64.67
	54.70	40.96	1.30	1.33	3.36	37.98	7.3	58.03
NF02-6	59.29	32.26	1.40	1.14	3.29	29.66	8.1	62.57
	58.05	35.10	1.63	0.41	4.17	31.62	9.9	62.22
NF02-8	49.59	38.16	1.50	1.56	4.44	34.80	8.8	54.03
	55.97	37.41	0.70	0.00	5.21	32.99	11.8	61.17
NF18	57.29	36.38	0.50	0.90	2.85	33.94	6.7	60.14
	59.14	31.57	0.88	0.85	2.57	29.58	6.3	61.71
28[†]	62.64	30.12	-	-	1.81	28.67	4.81	64.44
	63.75	28.84	-	-	2.78	26.63	7.66	66.53
31[†]	61.81	32.24	-	-	0.83	31.54	2.17	62.64
	54.28	37.09	-	-	2.75	34.86	6.01	57.03
Average	**58.20**	**34.82**	-	-	-	-	-	-

[1] The replicate test failed. [†] Polymer-based fluids. ⋆ First oil recovered at core outlet due to nanofluid.

5.5.6.2 Differential Pressure

As shown in Figure 5.14, the injection pressure shows two patterns; the decrease and increase when the nanofluid were flooded through aged cores. The differential pressure (dP) across the core decreased with the injection of small nano-sized particles (NF02-3, NF02-4 and NF18) and was lower than that obtained during reference water flood. This pressure behaviour is associated to a good propagation of NPs with little retention through neutral-wet cores. Furthermore, the dP suggested that emulsions were generating in-situ during flooding experiments (Adil et al. 2018). By contrast, dP increased with large nano-sized particles (NF02-6 and NF02-8) and it was higher than reference water flood pressure. In this case, the pressure increase indicated clogging of the pores due to NPs and restricting normal flow of the injected fluids. Possible zones of log-jamming events that occurred during nanofluid flood process are highlighted in Figure 5.14(b). The oil recovery from samples NF02-6 and NF02-8 showed some positive correlation with dP profile, (i.e. increase in oil recovery with increasing pressure); the reduction in core permeability ranged from 15% to 21% and was the largest (see Table 5.11 in Section 5.5.6.4). The small diameter particles did not show any correlation between oil recovery with pressure.

5.5.6.3 Wettability Evaluation Results

To investigate the effect of NPs on the rock surface and on oil recovery during flooding experiments, the core plugs were prepared to simulate short and prolonged exposure of NPs to rock surface. One of the two cores injected with the same nanofluid type was immediately prepared for wettability evaluation, while the second one was removed from the core holder and soaked in nanofluid for 10 days at 40 °C.

The results of spontaneous imbibition tests carried out for fifteen days showed a huge contribution of NPs on wettability alteration process. The rate of water imbibition was dramatically increased on both soaked and non-soaked cores. The reference wettability index of the cores was increased from -0.1 to a range of 0.51 to 0.71, for soaked cores (Figure 5.15(a)), and from 0.46 to 0.66 for non-soaked cores (Figure 5.15(b)). The spontaneous imbibition and WIs results suggest that the wettability was altered from neutral-wet to water-wet condition during nanofluid flooding process, which is consistent with the results obtained in Section 5.5.2.5.

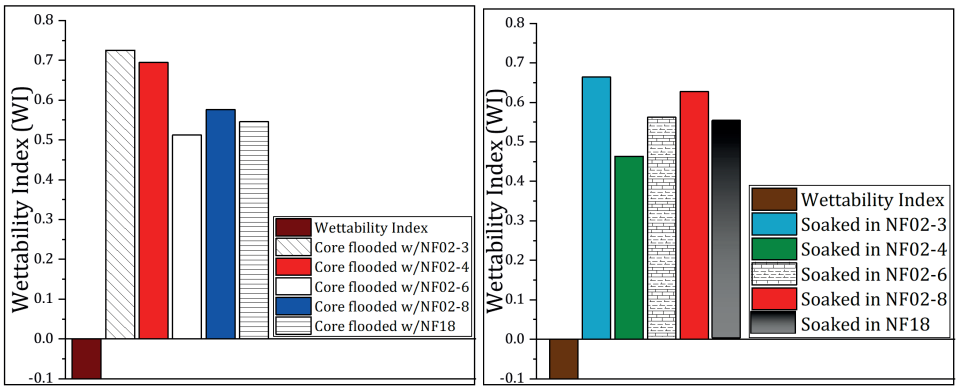

(a) **(b)**

Figure 5.15: Amott wettability indexes measured on reference "aged" cores, and on cores after: (a) nanofluid flooding; (b) nanofluid flooding plus soaking the cores in nanofluid.

5.5.6.4 Permeability

Results of core permeability determined after nanofluid flooding are presented in Table 5.11. There was some permeability reduction (negative values) and permeability improvement (positive values). However, the change in the initial values of permeability is not significant. Again, the results may have been affected by several factors, from the core preparations steps to wettability testing, core handling during cleaning and drying, and experimental measurements.

Table 5.11: Variation of absolute permeability before and after nanofluid core flooding.

Core	Sample	Gas Permeability (mD)		% difference
		Before	After	
B9-33	NF02-3	228	282	23
B9-35	NF02-4	238	207	-13
B9-36		256	284	11
B9-37	NF02-6	248	195	-21
B9-38		270	220	-19
B9-39	NF02-8	233	190	-18
B9-40		234	200	-15
B9-41	NF18	230	245	6
B9-42		247	220	-11

5.5.6.5 Summary of Results

In this section, nanofluids were injected in tertiary recovery mode in aged cores. Results showed an increase in oil recovery for all samples.

- The incremental oil recoveries varied from 2.57 to 5.2% of OOIP; Nanofluids NF02-6 and NF02-8 showed better sweep efficiency. Nevertheless, the recovery was less than 5% of OOIP before 1 PV; even with the injection of large amounts of PVs, the nanofluids could hardly recover more than 5% of OOIP;
- Flooding tests gave very small variations in oil recovery, making it difficult to conclude on the effect of polymer-based fluids on oil recovery over nanoparticles.
- Small size nanoparticles (NF02-3, NF02-4 and NF18) showed pressure decreasing effect, which could be associated with generation in-situ emulsions. Large size nanoparticles (NF02-6 and NF02-8) increased the pressure, which is associated with clogging of the rock pores and flow diversion mechanism on oil recovery;
- The Amott tests indicated a dramatic contribution of NPs on wettability alteration of neutral-wet rocks to a more water-wet condition.

5.5.7 Nanofluid Flooding at Elevated Temperature

5.5.7.1 Objectives

Previous sections have revealed EOR potential of samples NF02-3, NF02-4, NF02-6 and NF02-8 at room temperature. This section aimed to evaluate oil recovery of the samples at a high temperature. The lowest threshold reservoir temperature of 60 °C (Aurand 2017) was used and is referred to high temperature hereinafter. The nanofluids were tested with both water-wet and neutral-wet Berea sandstone cores. "Long" core plugs (3.8 cm in diameter and 10 cm in length) were used. The average porosity of the cores was 17.4% (±0.94) and varied from 15.8% to 19.7%. The absolute permeability ranged from 156 to 603 mD. After primary drainage, the established initial water saturation varied from 11 to 32% of total pore volume. Additional properties of the cores are presented in Tables B.5-B.6 in Appendix B.

5.5.8 Core flooding with water-wet core plugs

After primary drainage, the core at S_{wi} loaded in the Hassler core holder under confining pressure was heated while injecting crude oil at low flow rate of 0.02

ml/min until the temperature stabilised at 60 °C. Then, water (SSW) was injected at a constant flow rate 0.2 ml/min. This procedure was conducted until no oil production was occurring for 2 PVs. After that, the flow rate was increased ten-fold (bump rate) for ≈1 PV to overcome capillary end-effects. In the following step, the injection was continued with nanofluid at 0.2 ml/min until there was no more oil production for 2 to 4 PVs. Again, the flowrate was bumped for ≈1 PV. After nanofluid flooding was completed, the cores were cleaned with toluene and methanol and dried at 60 °C to determine core permeability and porosity.

5.5.8.1 Flooding Results

Eight flood tests were conducted using water-wet cores. The main findings from tertiary flooding process are given in Table 5.12. The RF_1 and RF_2 represent oil recovery factors achieved at the end of water- or nanofluid flood at low rate and high rate, respectively; The RF is total oil recovery. The average oil recovery achieved by WF was 52.39% OOIP (±3.10) and it varied from 47.20 to 56.12% of OOIP. On average 13 PVs of nanofluid were injected. This resulted in incremental oil recovery from 4.67% to 11.56% of OOIP during the low rate injection. When the flow rate was bumped, additional oil was produced; it ranged from 0.91 to 4.05% of OOIP. Thus, the ultimate recovery reached 7.0% to 14.1% OOIP; the average ultimate recovery was 10% (±1.9). Residual oil saturation calculated at the end of high rate varied from 28% to 35% of total PV.

An example of oil recovery profile (water- and nanofluid-flood) during low- and bump-rates is given in Figure 5.16. Additional plots showing oil recovery profiles are given in Appendix C.5, Figure C.12 through Figure C.13. The segment line shows the connection between two points, where the rate has been increased to the point at which it was stopped; otherwise it is the recovery during low rate injection. As it can be seen in Table 5.12 and Figure 5.16, it was with the increased number of pore volumes of NPs that significant oil recovery was recovered.

The core flood effluent collected at the end of the injection of samples NF02-3 and NF02-4 showed that oil was produced as oil-in-water emulsions, especially when the flow rate was increased. These samples had the smallest particle size. The yellowish colour in Figure 5.17 shows that some interaction between the NPs and crude oil system was occurring during the flood experiments, which led to the emulsification of oil in the aqueous phase. Little to no formation of emulsions were observed during the injection of samples with large particle size (NF02-6 and NF02-8), even when the flow rate was increased flow rate.

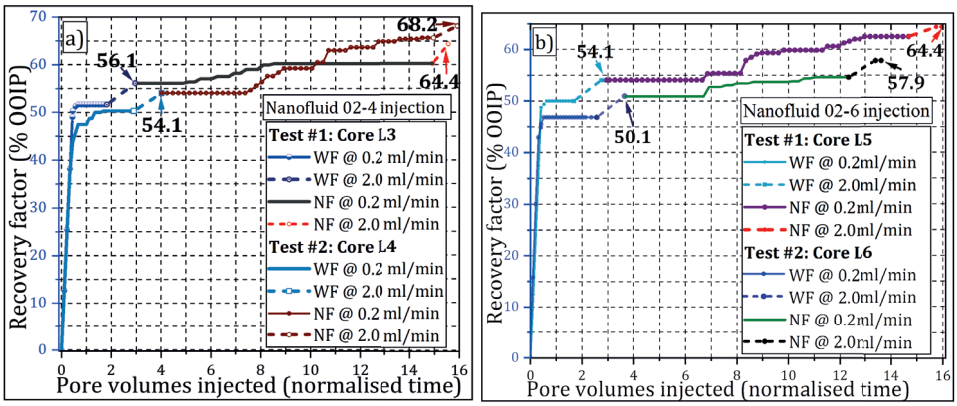

(a) **(b)**

Figure 5.16: Oil recovery factor versus pore volumes: (a) Nanofluid "02-4" injection, Test#1 produced first oil at 2.2 PVs and Test#2 after 3.6 PVs were injected; (b) Nanofluid "02-6" injection, the first production occurred after 4.4 PVs in Test#1, and after 3.8 PVs in Test#2.

Table 5.12: Summary of oil recovery factors (expressed as percentage of OOIP) achieved at the end of low rate (RF_1) and high rate (RF_2) for both water- and nanofluid-flooding.

	Water flood				**Nanofluid flood**					
Sample	RF_1	RF_2	RF	S_{or1}	RF_1	RF_2	RF	S_{or2}	E_D	RF
NF02-3	44.72	2.48	47.20	39.77	8.57	1.37	9.94	33.59	16	57.1
	43.92	4.05	47.97	35.25	7.03	4.05	11.08	27.75	21	59.1
NF02-4	51.66	4.46	56.12	39.27	5.22	3.18	8.40	31.86	18	64.4
	50.31	3.75	54.06	41.05	11.56	2.50	14.06	28.48	31	68.2
NF02-6	50.00	4.06	54.06	38.81	8.44	1.88	10.31	30.10	23	64.4
	46.75	4.16	50.91	44.34	4.67	2.34	7.00	35.09	21	57.9
NF02-8	49.39	4.24	53.64	37.67	8.18	0.91	9.09	30.03	20	62.7
	52.42	2.73	55.15	36.46	7.27	3.03	10.30	28.08	23	65.5
Average	-	-	**52.39**	**39.08**	-	-	**10.00**	**30.62**	-	**62.4**

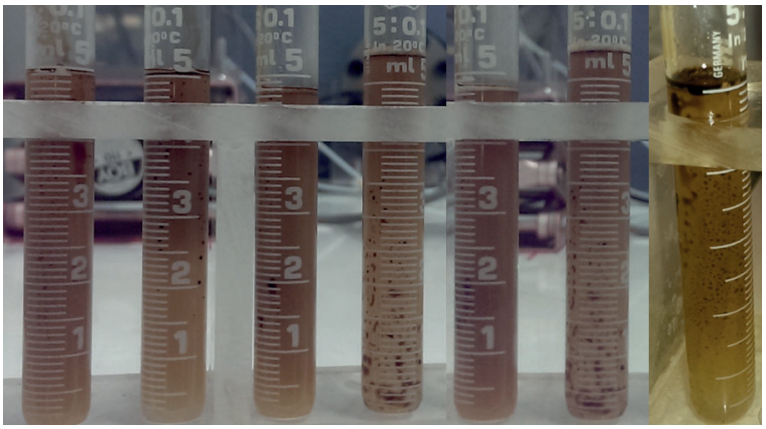

Figure 5.17: Core flooding effluent collected during nanofluids "NF02-3" and "NF02-4" high rate injection.

5.5.8.2 Differential Pressure

Nanoparticles of small size, NF02-3 and NF02-4, had no significant influence in water flood pressure. As it can be seen in Figure 5.18(a), the pressure shows a slight increase for ≈ 1 PV, then it decreased and seemed to level off to the reference water flood pressure. This implied an improved particle propagation through water-wet Berea sandstone and emulsification of oil into aqueous phase as result of reduced interfacial tension, flow dynamics and high temperature.

On the other hand, the larger diameter nanoparticles had a noticeable influence on the reference injection pressure. These samples are NF02-6 and NF02-8. As illustrated in Figure 5.18(b), the differential pressure gradually increased until it reached a zone where it was spiky. This profile was observed until the tests were stopped, and at the end of the tests a nanoparticle "cake" was formed at core inlet (see Figure 5.19). This indicated the occurrence of crossflow filtration and clogging of the pores throughout the duration of the flooding. The formed "cake" and clogging of small pores at core inlet were likely the primary reasons for pressure increase. This was expected because tested nanoparticles had limited stability at 60 °C. The pressure behaviour shows that filtered particles penetrated the core and probably further aggregated in-situ blocking inner pores, resulting in the diversion of injection water and entrainment of by-passed oil to the production lines.

Additional plots showing pressure profiles for other samples are given in Appendix C.5, Figure C.12 through Figure C.13.

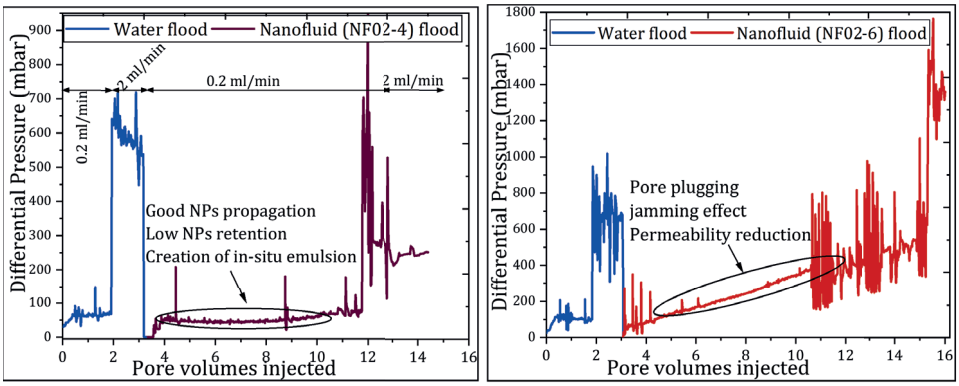

Figure 5.18: Differential pressure versus pore volumes injected: (a) Core flooding "02-4", the pressure profile shows good NP propagation and low retention on the cores; (b) Core flooding "02-6", the pressure shows that pores were gradually plugged and reached zones of maximum blockage; then, the dP was redistributed to the adjacent pores (zones of log jamming events).

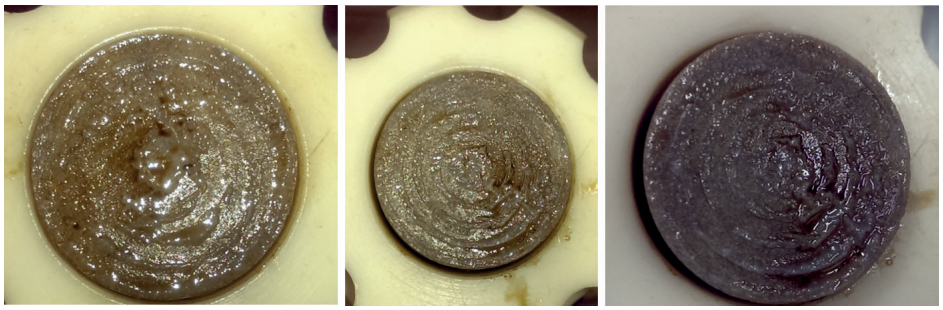

Figure 5.19: Filter cake build-up at core inlet during the nanofluid (NF02-6 and NF02-8) injection.

5.5.8.3 Wettability Evaluation Results

After nanofluid flooding was completed, one of the two cores (at S_{or}) was flooded with decane at high flow rates (1 to 3 ml/min) until residual nanofluid saturation was achieved. Then, each core was dipped into the Amott cells following the procedure described in section 4.5. Figure 5.20 shows SSW spontaneous imbibition behaviour during a 30-days test. It was observed that the rate of SSW imbibition and oil recovery slightly decreased in nanofluid flooded cores compared to the original cores. Small droplets of oil were produced from top and lateral faces of the cores at the beginning of the test. This oil merged upwards in the Amott glasses.

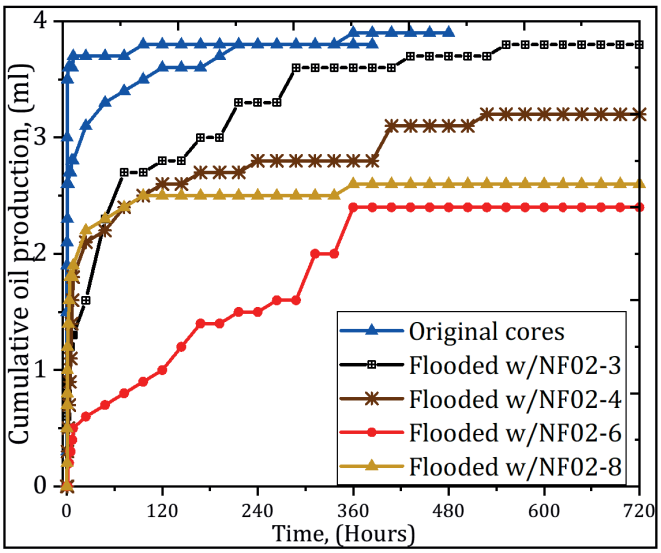

Figure 5.20: Spontaneous imbibition behaviour of the nanofluid flooded cores compared with original cores.

After 2 to 3 days, the rate of oil production declined; Most of oil droplets were being produced from the top of the cores. The produced oil droplets detached from the rock surface after several days or by gently shaking the Amott cells. The measured Amott water indexes, I_w, varied from 0.5 to 0.89. In the second SI cycle, oil did not imbibe into the core or displace water; thus, the Amott oil index, I_o, was zero.

5.5.8.4 Porosity and Permeability

After nanofluid flood and wettability tests, the cores were cleaned with toluene and methanol for several days using Soxhlet extractor; then they were dried at 60 °C. The permeability and porosity were measured. The results are presented in Table 5.13. Negative values indicate permeability or porosity impairments. As expected, the larger particles had huge permeability impairment induced by particle aggregation during oil displacement process.

Table 5.13: Porosity and permeability of cores measured before and after nanofluid flooding.

		Porosity (%)			Permeability (mD)		
Core	Sample	Before	After	% difference	Before	After	% difference
L1	NF02-3	19	17	-11	404	350	-13
L2		20	16	-20	537	452	-16
L3	NF02-4	17	15	-12	460	446	-3
L4		18	16	-11	411	370	-10
L5	NF02-6	18	13	-28	367	232	-37
L6		18	14	-22	331	246	-26
L7	NF02-8	18	15	-17	384	292	-24
L8		20	17	-15	265	193	-27

5.5.8.5 Summary of Results

All nanofluids mobilised residual oil and increased oil recovery in water-wet cores at high temperature;

- Nanofluids incremented oil recovery from 7 to 14% of OOIP. None of the nanofluids could increase oil recovery by 5% of OOIP at 1 PV. the reported oil recovery was achieved at the expense of large pore volumes injection;
- Small diameter NP size had the greatest oil recoveries while having no significant influence on the reference water flood pressure. This is associated to the improved particle propagation through the cores and emulsification of oil into water phase during oil displacement.
- Large diameter NP had noticeable influence on reference pressure. The pressure behaviour indicated the occurrence of pore blockage at core entrance and inside of it. Accordingly, the reduction in permeability was greater.
- The recoveries were higher than at room temperature, indicating an improved sweep efficiency of NPs with the increased temperature.
- The nanoparticles could affect wetting properties of Berea cores to increasingly water-wet condition.

5.5.9 Core flooding with neutral-wet core plugs

Eight naturally water-wet cores were prepared to neutral-wet condition. The cores were aged the longest in crude oil B to allow the asphaltenes to adsorb strongly on

the rock surface. They were aged for about 7 months at 80 °C. Then, each core was cooled off before loading it in the Hassler core holder under confining pressure held within 18-22 bars. To mimic secondary and tertiary oil recovery processes, water was injected until there was no oil production; then nanofluid flood followed at the same constant rate of 0.2 ml/min. The flooding procedure is described in Section 5.5.8. All tests were conducted at 60 °C.

5.5.9.1 Flooding Results

Oil recoveries from secondary water flood varied from 46.18 to 66.75% of OOIP. Additional oil was produced with nanofluid injection. On average, about 10 PVs were injected during low flow rate; as a result, oil recovery increased from 1.20 to 4.29% of OOIP. Then, the flow rate was increased for 1 PV and resulted in additional oil recovery from null to 2.07% of OOIP. The total incremental oil varied from 1.51 to 6.13% of OOIP. Overall core flooding results are presented in Table 5.14. An example of oil recovery profile as a function of PVs is given by Figure 5.21 for samples NF02-4 and NF02-6 with relatively higher average oil recoveries. Similar plots are presented in Figure C.14 in Appendix C.

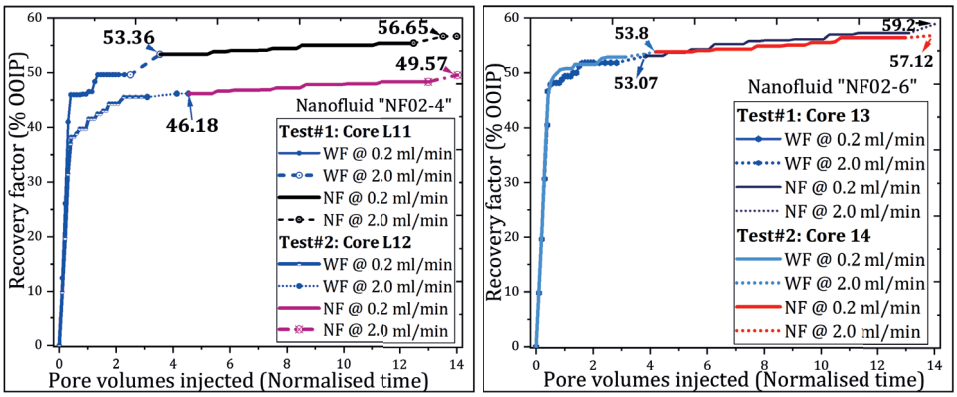

Figure 5.21: Effect of nanofluid injection on oil recovery during low rate and bump rate injections: (a) Sample NF02-4: In test#1, the first oil occurred at ≈1.8 PVs and RF ≈0.5% of OOIP; Test#2 produced ≈ 0.5% of OOIP at 1 PV. (b) Sample NF02-6: Test #1 the oil production occurred at ≈2.2 PVs and the RF ≈2.3% of OOIP; In test #2 the first production occurred at ≈1.3 PV and the RF ≈0.3% of OOIP.

Table 5.14: Oil recovery factors (water- and nanofluid flooding), expressed as % of OOIP, and residual oil saturation achieved at the end of core flooding in neutral-wet cores.

	Water flood				**Nanofluid flood**					
Sample	RF_1	RF_2	RF	S_{or1}	RF_1	RF_2	RF	S_{or2}	E_D	RF
NF02-3	59.45	2.90	62.35	28.37	2.76	2.07	4.83	24.47	14	67.52
	57.33	0.67	58.00	33.05	1.73	0.00	1.73	31.68	4	59.73
NF02-4	49.63	3.73	53.36	39.07	2.05	1.24	3.29	36.32	7	56.65
	45.56	0.62	46.18	44.97	2.16	1.23	3.39	42.14	6	49.57
NF02-6	51.84	1.23	53.07	38.57	4.29	1.84	6.13	33.63	13	59.20
	52.88	0.92	53.80	39.43	2.82	0.50	3.32	36.61	7	57.12
NF02-8	66.45	0.31	66.75	28.67	1.20	0.30	1.51	27.37	5	68.25
	53.64	0.80	54.44	37.27	3.05	0.93	3.98	34.08	9	58.41

5.5.9.2 Differential Pressure

As with water-wet core plugs (see Section 5.5.8), small diameter particles did not significantly affect flooding pressure of reference water in neutral-wet cores. The recorded pressure profile during the injection of NF02-3 and NF02-4 samples is presented in Figures 5.22(a) and 5.22(b); it shows slight increase from the start of low injection rate and at some point, is spiked. The increase in pressure is noticeable at later injections, but is not very significant compared to water flood pressure. When the flow rate was tenfold increased, the pressure dropped compared to water flood pressure at same flow rate. Nanoparticles of large diameter (NF02-6 and NF02-8) recorded the largest pressure increase throughout the duration of flooding as shown in Figures 5.22(c) and 5.22(d). Like in water-wet core plugs, nanofluids NF02-6 and NF02-8 aggregated at the core inlet, resulting in nanoparticle "cake". The formed "nano-cake" appeared to be more noticeable in water-wet rocks (see Figure 5.19) than in neutral-wet core plugs (Figure 5.23). The primary nanoparticle size appeared to correlate positively with differential pressure, but it does not exhibit a clear correlation with oil recovery.

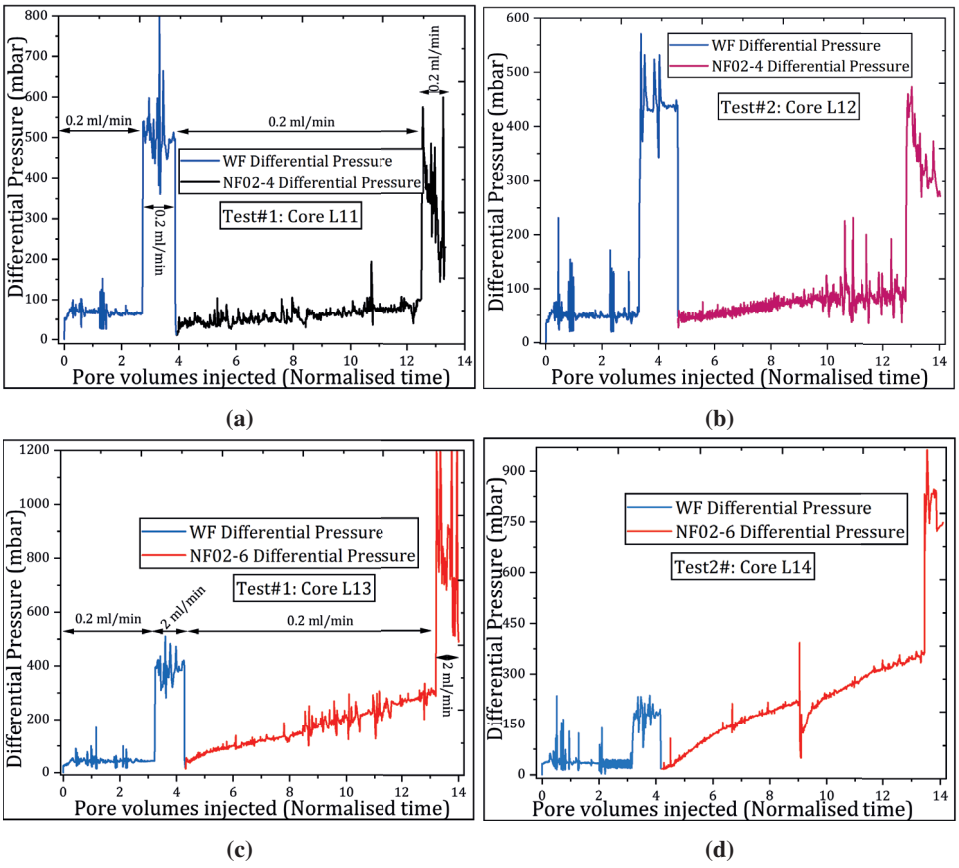

Figure 5.22: Pressure profile recorded during water and nanofluid flood: (a) Test #1: Nanofluid "NF02-4" injection shows little effect on water flood pressure; (b) Test #2 shows a slight increase in pressure compared to WF injection pressure; (c) Test #1, the pressure gradually increased upon injection of nanofluid "NF02-6"; and, (d) In Test #2 also shows the log-jamming effect with NF02-6 injection.

Figure 5.23: Physical filtration and formation of nanoparticle "cake" at neutral-wet core inlet during nanofluid (NF02-6 and NF02-8) flooding.

5.5.9.3 Visualisation of Emulsion System

The differential pressure profiles obtained in Sections 5.5.6 and 5.5.8 above, as well as in this section, Figures 5.22(a)-5.22(b), suggested that samples NF02-3 and NF02-4 were able to generate in-situ emulsions during flooding experiments. This hypothesis was confirmed by direct visualisation of core flooding effluent through microscope. The core flood effluent was collected at the end of high rate injection and immediately placed under a microscope with objective lenses varying from 10 to 50 magnifications. Figure 5.24 shows the obtained images of oil droplets dispersed in aqueous phase. The emulsion droplets appeared to be stable in aqueous phase due to the presence of nanoparticles at the interface. The phase separation of water and oil occurred about one hour after the effluent was collected; the separated volumes were measured after two days. The core flood effluent from samples NF02-6 and NF02-8 showed little to no emulsification of oil in aqueous phase.

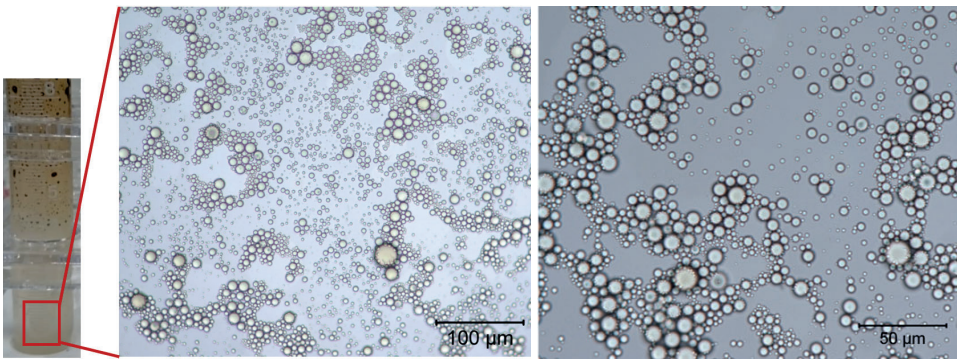

(a) **(b)**

Figure 5.24: Magnified visualisation of oil-in-water emulsion from nanofluid flood (NF02-4) effluent: (a) 20x magnification; and (b) 50x magnification.

5.5.9.4 Wettability Evaluation Results

Figure 5.25 shows water spontaneous imbibition profile on the reference aged core plug and on the nanofluid flooded cores. The brown curve shows water imbibition on the aged core. After conducting full Amott test, the wettability index was -0.08 indicating neutral-wet condition of the aged core. The cores used for EOR experiments in this section were assumed neutral-wet. Following nanofluid flooding experiments, the rocks were injected with decane and immersed in Amott cells to assess whether the initial change in rock wettability was occurring with nanoparticle injection. Results showed a significant improvement in water capillary in-take due to nanoparticles exposure on the rock surface. As can be seen in Figure 5.25, rate of oil production by water imbibition is higher than in the reference core. Core L10 injected with sample NF02-3 indicated greater particle ability to reverse the wettability at shorter exposure times as witnessed by significant oil recovery within 24 hours. Amott water indexes were then determined after 360 hours and varied from 0.67 to 0.77. These results proved the capability of surface-functionalised silica NPs to alter the wettability of the rock surface towards water-wet condition, which could be the main mechanisms of oil recovery in aged-cores.

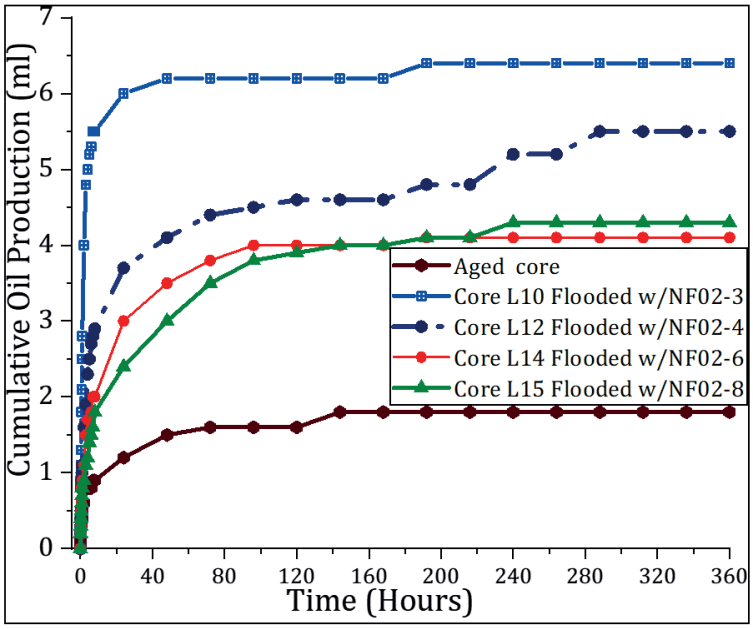

Figure 5.25: Improved water imbibition rate due to NPs injection; Brown curve shows water imbibition behaviour on aged core free of nanoparticles.

5.5.9.5 Summary of Results

Nanofluid flooding experiments have revealed that silica-based nanofluids can increase oil recovery in aged cores, but the incremental recoveries are lower than in water-wet cores at the same temperature.

- The incremental oil recoveries varied 1.5 to 6.1% of OOIP. No recovery greater than 5% of OOIP was obtained at 1 PV; again, the experiments showed that large pore volumes were needed to increase the production;
- Small particles size (NF02-3 and NF02-4) did not affect water flood pressure; In contrast, the large particles size (NF02-6 and NF02-8) resulted in larger differential pressure through the cores than water flood pressure;
- Small particles size, NF02-3 and NF02-4, generated in-situ emulsion during oil displacement process;
- All surface-functionalised silica NPs altered the wettability of the rock surface towards more water-wet conditions, which could be the main mechanism of oil recovery.

CHAPTER 6

Discussion of the Results

6.1 Nanoparticle's stability

The screening process carried out throughout this work ended up selecting four type of silica nanoparticles with potential for oil recovery. The primary surface of these nanoparticles was modified/coated with polymer molecules, resulting in *polymer-coated silica nanoparticles*. All nanoparticles were investigated for stability; however, the discussion of the results focus only on the four selected samples with the highest EOR potential.

Most oil fields are characterised by high temperature, high pressure, high salinity and uneven reservoir properties (Miranda et al. 2012, ShamsiJazeyi et al. 2014, Khalil et al. 2017). Hence, nanoparticles injection must withstand reservoir conditions, and remain stable while travelling through porous media during oil recovery process. The stability of four polymer-coated silica nanoparticles (NF02-3, NF02-4, NF02-6 and NF02-8) at 0.1 wt% concentration in SSW was not an issue at room conditions. Particle size distribution and sedimentation tests proved that polymer chains coating on the particles surface could provide steric repulsive forces, thus keeping NPs dispersed in SSW for more than four months testing period at 22 °C. With the increased temperature, the solution of NPs behaved differently. The behaviour of NPs in solution depended on the type, composition and polymer coating materials. Nanofluids NF02-3 and NF02-4 remained stable for up to 96 hours storage-time at 60 °C in synthetic seawater. After that, they precipitated and gradually settled out of solution, forming large aggregates of NPs. This was not an issue for laboratory scale oil recovery tests because the flood tests conducted in this work did not last longer than 96 hours. Unlike, samples NF02-6 and NF02-8 were im-

mediately rendered unstable at 60 °C. This induced high injection pressure during EOR process. The effect of high temperature on the hydrodynamic interactions and the coating materials adsorbed on the particle surface are likely responsible for aggregation of silica particles. The precipitation of polymer molecules and aggregation of NPs can be induced by divalent cations in aqueous solution (Seright et al. 2009, Gbadamosi et al. 2018). The high temperature increases the likelihood of particle collision and aggregations, likewise high ionic strength compresses the electrical double layer surrounding the NPs (Yu et al. 2017). As a result, the desired repulsive forces between the NPs can be diminished in solution.

This study illustrates that producing highly stable NPs, especially for high salinity and temperature environment, continues to be a major challenge. Despite the stability issues, the NPs produced additional oil recovery at laboratory scale, which is in line with others studies (Hendraningrat and Torsæter 2015, Mohammadi 2013, Choi et al. 2017). However, the limited stability of NPs will greatly affect their practical applications because the NPs must travel long distances in harsh environments that characterise most of oil fields; the NPs aggregates will likely deposit near the well-bore and damage the formation (Kuang et al. 2018), resulting in increase in oil production costs. Hence, further research efforts are needed to investigate the conditions needed to achieve long-term stability of NPs dispersion under various of oil fields. The particles studied in this work have shown remarkable EOR potential, but the surface modification needs to be improved and optimised. Sedimentation tests showed that polymers were fluctuating in solution probably due to poor compatibility with seawater or the polymers were weakly attached to the surface of the particles. The stability also should to be verified at lower particle concentration, as high concentration decreases the distance between adjacent particles, leading to reduced repulsive forces (Yu et al. 2017).

6.2 Oil Recovery and Uncertainties

Evaluation of oil recovery at laboratory scale is always subject to many experimental errors, which introduce many uncertainties in the results. In an attempt to mitigate these errors, parallel tests were carried out using nearly identical core plugs (matching porosity and permeability). Due to the complex nature of the rocks and the randomly dispersed pores, the composition and the paths that injected fluids choose to follow during the oil recovery process, it is difficult to reproduce the results.

In present work, an oil recovery test is reproducible if the results given by duplicate experiments (i.e. separate tests using nearly two identical core plugs) is within 5% of OOIP.

6.2.1 Screening of nanoparticles with glass micromodels

All nanoparticles tested using glass micromodels produced additional oil. The nanofluids pre-selected based on low residual oil saturation achieved in the micromodel are presented in Figure 5.4. Typically, after water flood in a homogeneous unconsolidated porous media, residual oil saturation can be 15% of pore volume (Chatzis et al. 1983). This was chosen as a benchmark value for the categorisation of the samples. Due to the very uniform pore size distribution of the glass micromodels and improved particle properties, lower residual oil saturation values were expected than the reference at the end of nanofluid flooding.

In the first screening step, 15 of the 23 samples with residual oil saturation lower than 15% were pre-selected. Nanofluid NF02-3 and NF18 with residual oil saturation of 5.10 and 0.22% were the most promising samples, respectively. The glass micromodels of uniform porous structure gave very high oil recoveries, in contrast to those typically obtained by core flooding method in Berea sandstone under the same injection procedure. The uniform pore-throat geometry and limited observation area through the glass micromodel for oil saturation analysis introduced the main uncertainties in ranging of the samples based on oil recovery. The camera could only view the more central region of the microchip, and captured a circular shape of it and not the entire chip. The effect is visible in the oil displacement profile shown in Figure 5.4, where oil saturation increases at some point. That was because the oil that was not visualised by the camera in the micromodel, was subsequently pushed into the main camera area and counted in the following images. Despite these limitations, the pre-selected fluid samples from the water-wet glass micromodel tests are believed to be representative fluids for further testing in water-wet rocks. The low viscosity induced the nanofluids to preferentially channel through the pores of the micromodel and leave the oil trapped during the displacement process. At the end, the residual was trapped in the large pore bodies showing a large trapping effect of capillary forces.

It is worth to mention that the screening of nanoparticles using water-wet rocks was not expected to correlate with the results obtained with aged cores due to the wettability contrast. Future studies are therefore recommended to use the corresponding rock wetting system when screening EOR fluids and verify possible correlation of the results.

6.2.2 Water flooding oil recovery

The displacement efficiency of water flood is controlled by many factors, some of which include initial water saturation, core wettability, permeability, residual oil saturation and flowrate, pore volumes injected, etc. Selected factors are discussed

below in an attempt to improve our understanding on water flood oil recovery effiency prior to EOR tests with nanoparticles.

Initial water saturation (S_{wi}): The S_{wi} was established using water with the same salinity content as that used in flooding experiments; this was mitigate the swelling of clays and/or detachment of fine particles and core permeability, which may adversely affect the injectivity (Shepherd 2009, Alagic et al. 2011). Initial water saturation is typically greater than 20% in water-wet reservoirs (Craig 1971). In this work, the established S_{wi} varied from 8 to 33.9% of total pore volume. The lowest values of S_{wi} were achieved by the centrifuge method. The S_{wi} values established by the core flood method fell within the range predicted by Craig's rule of thumb for water-wet rocks. The high centrifugal forces are likely responsible for producing low values of S_{wi} compared to core flood method. Additionally, the variations resulted from differences in number of pore volumes, capillary end-effects, core heterogeneity and the accuracy of the measurements.

Oil recovery from water flooding water-wet cores at high temperature showed somewhat a negative correlation with S_{wi} (i.e. the lower the S_{wi} the higher the recovery); however, the same trend was not observed for the tests conducted at room temperature using similar rock wettability (see Section 5.5.5, Figure 5.10(a)). Probably the temperature was the main impact factor; low-rate flooding with high viscosity ratios (μ_o/μ_w = 34), as it is at low temperature, is more affected by the capillarity trapping effect than the flooding at high temperature, which decreases fluid viscosity ratio.

Oil recovery results from aged cores did not correlate with S_{wi}, see Figure 5.10(b). That is because neutral-wet reservoirs tend to exhibit long periods of oil production, despite early water breakthrough (Abdallah et al. 1986, Anderson 1987, Alagic et al. 2011). This trend was observed in this work for all aged cores, which confirmed neutral-wet condition and the efficacy of ageing process. Unlike, water-wet cores exhibited later breakthrough of water, with no significant oil production occurring afterwards.

Core Permeability: There was no clear correlation between water flood oil recovery and core porosity and permeability in this thesis. The effective permeability to oil determined at S_{wi} yielded values larger than core absolute permeability in water-wet cores, which is consistent with the fact that strongly water-wet rock water acts as lubricant promoting the flow of oil through the pores (McPhee and Arthur 1994). Furthermore, the calculated end-point relative permeabilities to water (k_{rw}) varied from 0.04 to 0.24, showing typical characteristics of water-wet media according to Craig's rule. The aged cores produced the largest variation in k_{rw} from 0.04 to 0.86. This indicated that some pore spaces were still water-wet

dominated.

Effect of flood rate on water flood oil recovery: Low rate flood would allow capillary forces to continue to dominate after breakthrough; thus promoting water imbibition into oil-filled pores, resulting in low residual oil saturation (McPhee and Arthur 1994). In this work, the low rate injection was chosen to mimic typical flow velocity of 1 ft/day.

Oil recovery from water flood was greatest at low residual oil saturation as shown in Figure 6.1(a). However, the tests conducted with water-wet cores at 60 °C showed much deviation despite using nearly identical cores. The residual oil saturation was found to decrease with increasing initial water saturation (Figure 6.1(b)). The cores whose S_{wi} was established using centrifuge shows scattered data probably owing to the difficulties encountered in measuring the produced fluids during the tests. The water-wet cores exhibited high values of residual oil saturation in the range of 37.6 to 49.4% of the pore spaces, which is within the range predicted by Chatzis et al. (1983) for water-wet systems.

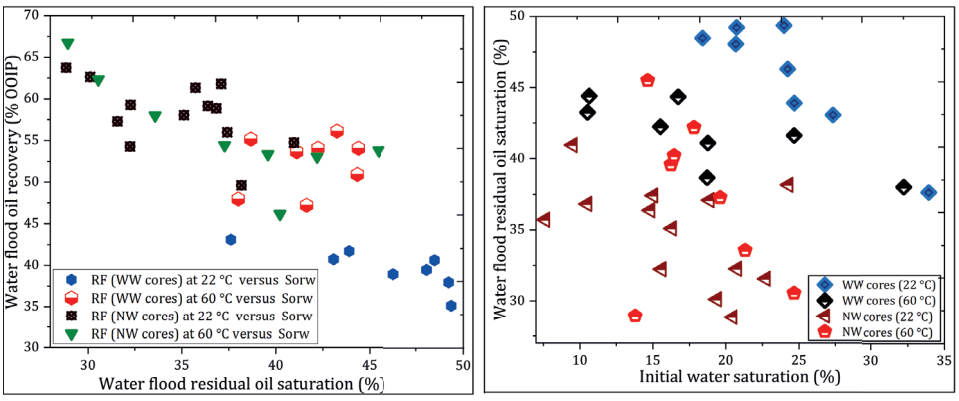

(a) **(b)**

Figure 6.1: (a) Water flood oil recovery versus residual oil saturation and; (b) the effect of initial oil saturation on water flood oil recovery.

Flood tests conducted in Sections 5.5.8 and 5.5.9 resulted in additional oil recovery during bump flood stage. This was an adverse effect and was not expected. In a standard water flood, water films grow on water-wet pores snapping off and trapping oil within the pores where capillary forces are high (Abdallah et al. 1986, Muggeridge et al. 2014). The trapped oil will resist mobilisation even if it is then flooded at much higher capillary numbers than those present at trapping (McPhee and Arthur 1994). The oil produced on a bump flood presumably indicated that

capillary stability was not achieved prior to bump rate. The produced oil is probably that trapped within the small gap between the core plug and the end-plug, this phenomenon is known as capillary end-effects. In aged cores, the amount of oil produced on a bump flood was negligible, showing that capillary end-effects is not an issue in less water-wet cores (Eide et al. 2014).

In summary, the most notable feature in this section is that maximum oil recovery from water flood was achieved at neutral-wet condition; these results are in agreement with previous results reported inn the literature (Anderson 1987, Morrow 1990, Zhou et al. 2000, Alagic et al. 2011). Therefore, this allows water to displace most oil located within large pores.

6.2.3 Nanofluid oil recovery

In this thesis, flooding experiments were conducted to evaluated oil recovery using silica-based nanofluids in water-wet and neutral-wet core plugs. The following text discusses the results obtained following the injection scheme applied in both water-wet (un-aged cores) and neutral-wet cores (aged cores).

Secondary oil recovery with water-wet cores: All pre-selected nanofluid samples from micromodel experiments produced additional oil in water-wet Berea sandstone cores. The nanofluid retarded the breakthrough of water and gave higher oil recoveries than reference water flood. On average, the water breakthrough was observed at 0.25 PV and the recovery was about 31.4% of OOIP in the case of reference water flood tests. While the injection of water with added NPs, the breakthrough occurred at 0.45 PV and the average oil recovery was 46.83% of OOIP. The nanofluid continued oil production after breakthrough point compared to reference tests. As a result, more pore volumes were injected for the nanofluids to achieve ultimate recovery compared with water flood.

The nanofluids increased oil recovery by factors ranging from 6.01 to 14.81% point compared to 39.67% of OOIP from reference test (average values). The nanofluids NF02-3, NF02-4, NF02-6 and NF18 increased oil recovery by factors ≥ 10% point compared to water flood. These samples were proposed for additional EOR testing. Micromodel and core flood experiments produced variable results due to difference in pore structures. No clear correlation was found between the two screening procedures. For example, sample NF02-6 did not perform well in micromodel tests but appeared to perform better on Berea cores than either samples. The variable results can be attributed to high permeability and high porosity, and homogeneous pore structure of the micromodel compared to Berea sandstone cores, as well as the preferred pathways the nanofluids chose to displace oil from the start of the injection. Additionally, the composition of NPs and surface coating materials, and

rock mineralogy can yield different interactions and variations in oil recovery performance.

The water flood conducted after soaking the cores (at S_{or}) did not mobilise residual oil; instead, it increased the injection pressure, suggesting that the NPs aggregated within the core during the soaking time at 40 °C. Therefore, the on-set period of aggregation of NPs should be determined in advance, followed by an evaluation oil recovery.

The oil recovery from nanofluid injection did not show any correlation with porosity or with permeability (see Figure 6.2). The duplicate set of core plugs gave small variations in ultimate oil recovery (≤ 5% of OOIP).

No correlation was found between ultimate oil recovery from nanofluid injection in water-wet cores and initial water saturation (see Figure 6.3(a)). Most of NP samples showed negative correlation with primary particle size; the oil recovery decreased with increasing primary particle size (see Figure 6.3(b)). Accordingly, the maximum differential pressure was greatest from large particle size (see Figure 6.3(b)). These results suggested a contribution of mechanical oil displacement mechanism, such as log-jamming of the nanoparticles within the pore-throats.

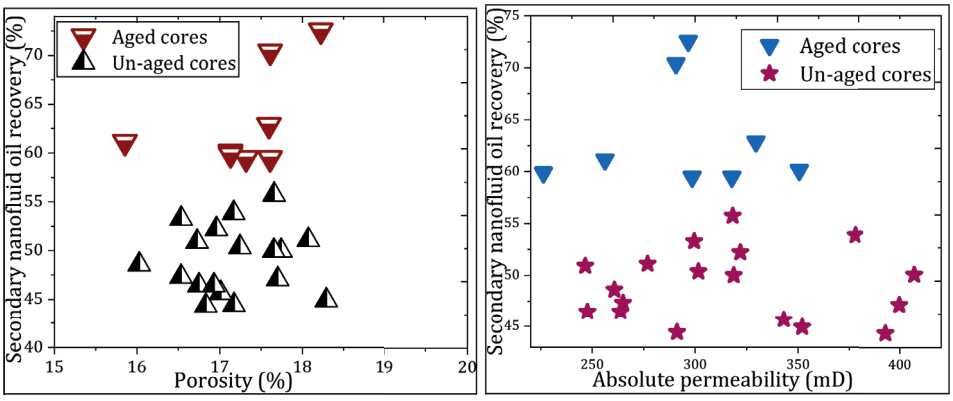

(a) **(b)**

Figure 6.2: Nanofluid oil recovery factor versus porosity and permeability: (a) Porosity was measured prior to nanofluid flooding by saturation method; (b) Absolute permeability was determined before nanofluid flooding.

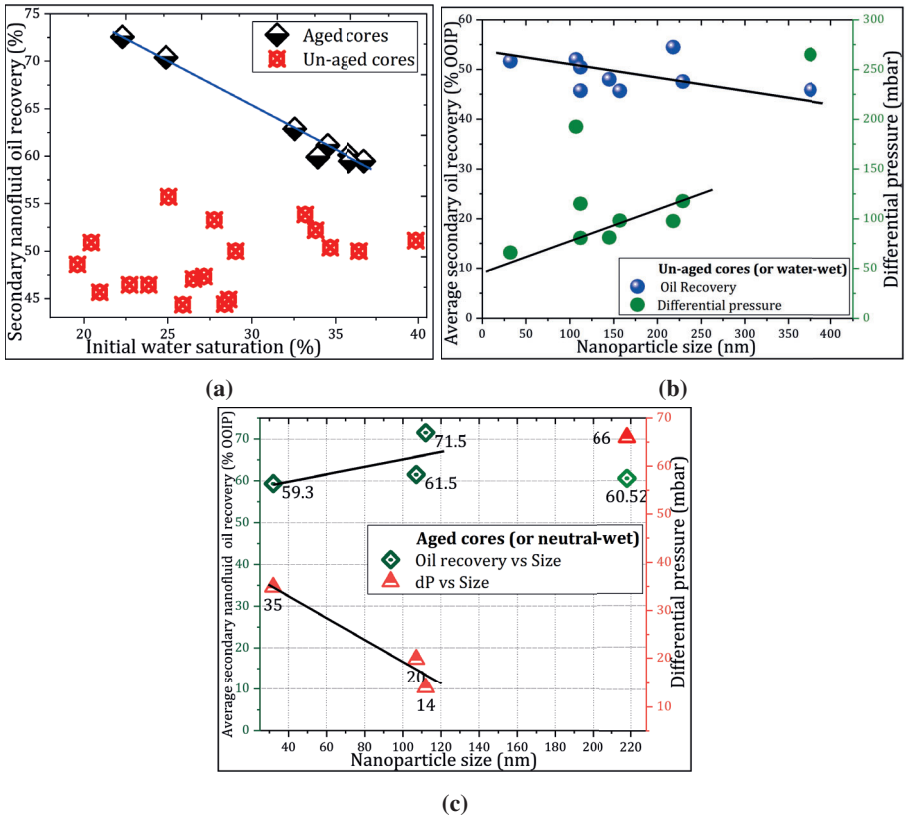

Figure 6.3: (a) Influence of initial water saturation on oil recovery; (b) Oil recovery and differential pressure vs. nanoparticle size (un-aged cores), and (c) the effect of nanoparticle size on oil recovery and differential pressure on aged cores.

Secondary oil recovery with aged cores: Flooding tests conducted with samples NF02-3, NF02-4, NF02-6 and NF18 including polymer-based samples #28 and #31 with aged cores, in Section 5.5.6, resulted in greater oil recovery than reference water flood. There was no noticeable difference in water breakthrough points (BT) during floods of water and nanofluids. On average, the BT point was detected from 0.34 to 0.4 PV; the oil recovery varied from 41.55 to 48.61% of OOIP for nanofluid system. In the case of water flood, the BT occurred at 0.33 PV and the recovery was 40.22% of OOIP. Sample NF02-6 had the highest recovery at BT point, but the highest ultimate recovery was obtained with sample NF18. The slow but prolonged period of oil production after water BT allowed nanofluids to increase oil recovery by factors ranging from 1.1 to 13.3% point over the reference water flood.

An additional oil was produced by water flood applied at the end of nanofluid flood, and it was from 0.66 to 3.51% of OOIP. It is likely that some of this oil was produced due to the increased flowrate. The high rate would also assist the production of accumulated oil at the core outlet due to the capillary end-effects. Therefore, the oil produced at this stage was counted separately.

The Water breakthrough occurred earlier in aged cores than in water-wet cores regardless injected fluid. This behaviour mirrors water flood characteristics in neutral-wet rocks; while it suggested that modified silica NPs propagated with easiness through and with little retention on aged cores. This implied that the surface modification with polymer molecules played a role in improving NPs fluidity through the aged rock surface.

Similar to water-wet cores, there was no correlation between porosity (Figure 6.2(a)), absolute permeability (Figure 6.2(b)) and ultimate oil recovery in aged cores. As expected, oil recovery demonstrated negative correlation with increasing initial water saturation (see Figure 6.3(a)). Oil recovery seemed to increase with increasing particle size (Figure 6.3(c)), but this trend can not be argued for the largest particle size ($\geq$ 200 nm). All nanofluids exhibited low differential pressures throughout the duration of oil recovery process, which confirmed improved transport properties of NPs through the pores.

The ultimate oil recoveries of nanofluids NF02-3, NF02-4 and NF02-6 were 61.5, 59.3 and 60.52% of OOIP, respectively. This oil recovery is quite comparable to polymer-based fluids #28 and #31 of about 66.4 and 60.4% of OOIP, respectively. These results can no provide a conclusive statement as to which polymer-based fluid is suitable for modifying the surface of the particles. Additional studies are needed to verify our findings and investigate different concentrations of NP for oil recovery.

Tertiary oil recovery with water-wet cores: Nanofluids NF02-3, NF02-4, NF02-6 and NF02-8 were evaluated in secondary recovery mode in Section 5.5.1; to determine the best injection scheme, all samples were then tested in Section 5.5.5 in tertiary recovery mode using water-wet cores. At the end of WF, the average oil recovery was 39.67% of OOIP. After that, an average of 10 pore volumes of nanofluids were injected at a low rate. The oil recovery increased from 5.93 to 9.22% of OOIP. The nanofluids NF02-3 and NF02-4 produced the first oil slightly earlier than the larger particle size samples NF02-6 and NF02-8. On overage, the additional oil recoveries were about 1.3% and 0.57% of OOIP and occurred nearly at 0.5 and at 0.34 PVs for NF02-3 and NF02-4, respectively. Nanofluids NF02-6 and NF02-8 mobilised the first oil after $\approx$2 PVs. Despite delayed oil production, samples NF02-6 and NF02-8 recorded the highest average incremental oil recov-

eries.

The results presented in Figure 6.4(a) show that oil recovery is high with larger diameter NPs, which is consistent with Aurand (2017), but also different from other findings (Hendraningrat et al. 2013c, Adil et al. 2018). The dependence of oil recovery on particle size shows that log-jamming may have played a significant role in the mobilisation of residual oil. This is consistent with earlier results where the large diameter particles had little effect on the oil/water interfacial tension (see Figure 6.4(b)). Thus, the displacement mechanisms can be through pore plugging and diversion of injected water to the adjacent pores. Despite high incremental recoveries, the ultimate recoveries are low compared to those obtained in secondary recovery mode, at ambient conditions. Similar observations have been reported in the literature (Torsater et al. 2012). The choice for the EOR scheme may be tied to the prices oil and acquisition of nanomaterials, bearing in mind that in most cases water flood would be preferable due to its low price.

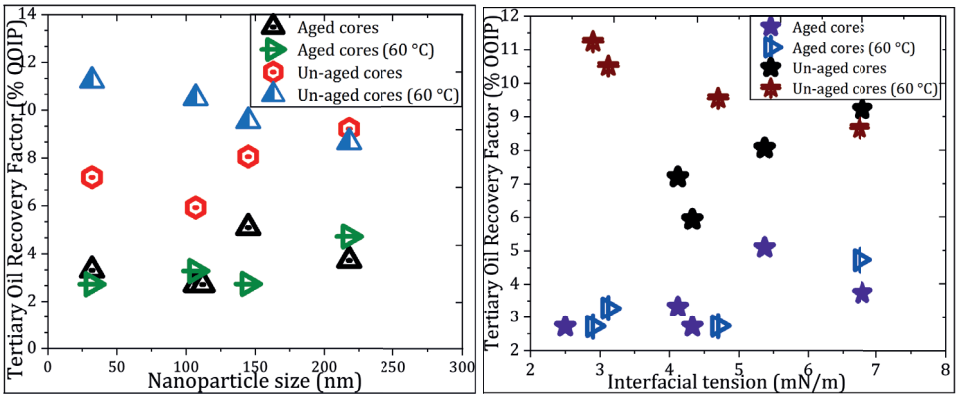

(a) **(b)**

Figure 6.4: (a) Effect of NP size on oil recovery: in un-aged cores, oil recovery decreases with NP size for tests conducted at 60 °C, unlike those conducted at room temperature. In neutral-wet cores (aged cores) there was no visible trend between oil recovery with particle size at room temperature, while the RF appeared to increase with size for tests conducted at 60 °C, and (b) In water-wet cores, oil recovery show a negative correlation with the IFT reduction for tests conducted at 60 °C; the opposite trend was observed at room temperature. Neutral-wet cores, the data is very scatted with no visible correlation.

Flood tests conducted in Section 5.5.5 were successful at room temperature. The tests were repeated in Section 5.5.7, but at high temperature. The procedure was also improved to mitigate capillary end-effects. A bump flood was applied after low rate flood. A minimal of 10 PVs were injected during low rate through each

10 cm core plug. The average recovery factors of nanofluid varied from 6.55% to 8.22% of OOIP. When the rate was increased for 1 PV, additional oil was produced. The average incremental oil recovery reached 8.66% to 11.23% of OOIP. The amount of oil produced during low and high rates are presented in Table 5.12.

All tested nanofluid samples showed positive effect on oil recovery in water-wet Berea core plugs, especially at high temperature. None of the NPs could increase oil recovery by 5% of OOIP within 1 PV. This factor was achieved with increased pore volumes injected. This can partly be attributed to viscosity contrast between the fluids. In addition, tertiary recovery is affected by water flooding stage and variations in core properties. After water flood, most oil is located or trapped within tiny pore spaces, its mobilisation is determined by the time-dependent physicochemical interactions between NPs and rock system (Hendraningrat et al. 2013b;c, Adil et al. 2018). These findings also support the notion that the longer the time NPs are in contact with the rock system, the better the oil recovery (Zhang et al. 2016).

Core flood effluent from samples NF02-3 and NF02-4 was produced as oil-in-water emulsion, especially at high flow rate. Contrary to the results obtained at room conditions, the flood tests conducted at high temperature demonstrated that incremental oil recovery was high with the smallest particles (Figure 6.4(a)). This observation ties very well with the reduction of IFT determined at 60 °C. As shown in Figure 6.4(b), small diameter particles were likely more efficient at binding to the oil/water interface than large ones, resulting in low tension. All findings showed an outstanding oil recovery potential of nanoparticles in water-wet Berea sandstone rocks. The results also proved that NPs injection respond differently to specific reservoir conditions.

Tertiary oil recovery with aged cores: For the flood tests performed in Section 5.5.6, no oil was produced before 1 PV during low rate (Table 5.10), except, for the cores flooded with samples NF02-3 and NF02-4. Each core produced 0.71 and 1.1% of OOIP, respectively, but the replicate tests failed to reproduce the results. The average oil recovery with NPs varied from 2.71 to 4.83% of OOIP. Flooding results gave small variations in oil recovery. Samples NF02-6 and NF02-8 had slightly high oil recovery performance. Surprisingly, the best performing sample NF18 in secondary recovery mode (Section 5.5.2) had an incremental oil recovery of 2.71% of OOIP, and ranked below other samples. No further studies were performed with this sample as it was no longer in the manufacturer's interest.

Tests conducted with polymer-based samples #28 and #31 increased oil recovery by 2.3 and 0.65% of OOIP, respectively. The recoveries are low compared to those obtained with NPs injection, but the difference is minimal. Therefore, it

is not clear whether the polymer additives played any role on oil displacement efficiency. Further studies are encouraged to investigate concentration of polymer additives, the surface reactivity and the effect of polymer binding on the particle surface to predict the effect on oil recovery.

There was no clear relationship between tertiary recovery with particle size (see Figure 6.4(a)) nor with IFT reduction (see Figure 6.4(b)). The results showed that other parameters, besides the reduction of the IFT reduction and log-jamming effect, may have played fundamental role in the mobilisation of residual oil.

Flood tests performed in Section 5.5.9 at high temperature also resulted in an additional oil recovery. The main results are summarised in Table 5.14. At the end of low injection rate, the average incremental oil recovery varied from 2.1 to 3.6% of OOIP. When the nanofluid injection rate was increased (for 1 PV), the average incremental recoveries reached 2.7% to 4.7% of OOIP. As with water-wet cores, crude oil was produced as oil-in-water emulsions during the injection of samples NF02-3 and NF02-4, especially at high flowrate. This confirmed the earlier observations on the ability of samples NF02-3 and NF02-4 to generate in-situ emulsions. The emulsions were probably stabilised by NPs as suggested by Figure 5.17 and Figure 5.24. The formed emulsion separated within an hour in the effluent separator.

The oil recovery appeared to increase with increased particle size (see Figure 6.4(a)). An unexpected increased oil recovery with increased IFT was observed for all samples as seen in Figure 6.4(b). This probably indicated that microscopic sweep efficiency was controlled by the wettability of the cores.

The nanofluids hardly increased oil recovery by factor greater than 5% of OOIP when injected through aged cores, even after large injection of pore volumes. This is because oil adheres to the surfaces and increases the likelihood of continuous production during water flood stage, resulting in low residual oil saturation (Abdallah et al. 1986, Muggeridge et al. 2014). This oil is located in tiny pore spaces and for its mobilisation requires a significant reduction of the IFT. The oil recoveries due to nanofluids in neutral-wet cores were quite comparable at both room and high temperatures. In the latter, the aggregation of NPs could be the main hindrance factor for the mobilisation of residual oil. It becomes apparent that future studies should investigate oil recovery at optimal concentration of nanofluids.

6.2.4 Evaluation of nanofluid oil recovery

After an extensive core flooding tests, the average oil recovery results obtained in the present thesis are presented in Figure 6.5 through Figure 6.7 for comparison purposes. As noted in previous chapters, the screening process has shortlisted four

samples, namely NF02-3, NF02-4, NF02-6 and NF02-8, with the largest potential for oil recovery in water-wet and neutral-wet reservoirs. Interestingly, all selected nanoparticles were modified with polymer-based fluids. This section will focus on these samples with the main objective of proposing the best injection scheme and the most suitable reservoir formation wettability for its injection for oil recovery.

In secondary recovery mode, an extra amount of oil produced by nanofluid relative to reference water flood is denoted by % point increase in oil recovery. The comparison of oil recoveries due to nanofluids relative to water flood is presented in Figure 6.5. This is the difference between ultimate oil recoveries from nanofluid flood and from water flood (WF).

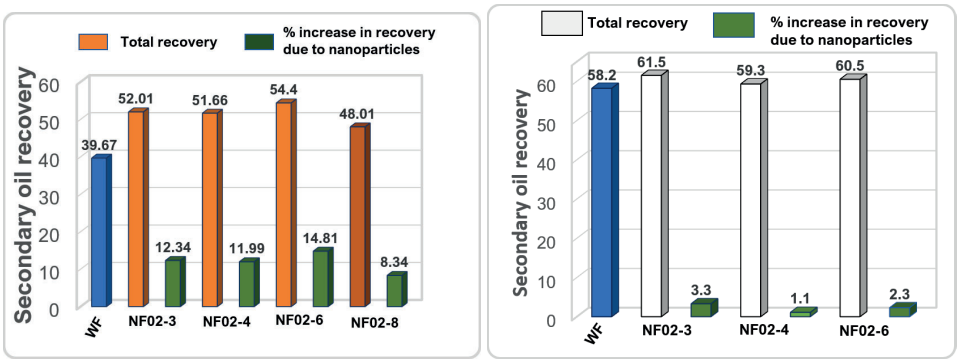

Figure 6.5: Comparison of secondary oil recoveries from various nanofluid flood: (a) Oil recovery due to nanofluids versus reference water flood obtained in water-wet core plugs, and (b) Oil recovery due to nanofluids versus reference water flood obtained in neutral-wet cores.

In tertiary mode, the incremental recovery factor is expressed as a percentage of OOIP. The comparison of the average results obtained in water-wet cores is shown in Figure 6.6. The average values were calculated from Table 5.8 and Table 5.12.

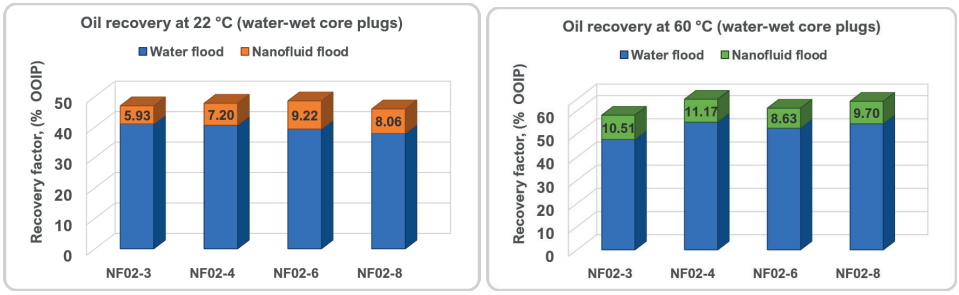

(a) **(b)**

Figure 6.6: Comparison of oil recoveries from different nanofluids in water-wet Berea sandstone core plugs: (a) Water- and nanofluid-flood oil recovery at room temperature, and (b) Water- and nanofluid-flood oil recovery at high temperature (60 °C).

Figure 6.7 presents a comparison of the oil recovery results obtained in neutral-wet cores. The results are average values from Table 5.10 and Table 5.14.

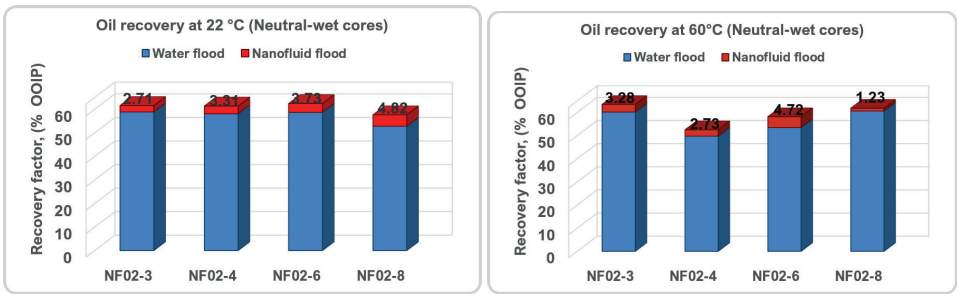

(a) **(b)**

Figure 6.7: Comparison of oil recoveries from various nanofluid flood in neutral-wet Berea sandstone core plugs: (a) Water- and nanofluid-flood oil recovery at room temperature, and (b) Water- and nanofluid-flood oil recovery at high temperature (60 °C).

It is well-known that water flood is the most preferred secondary recovery technique for most reservoirs because of availability of water, high recovery rates and low capital and operating costs involved for its execution (Muggeridge et al. 2014, Satter and Iqbal 2016, Youssif et al. 2018). However, under some circumstances, an EOR process can be applied after primary production stage, i.e., as a secondary recovery process; in this case, the displacement process must be better than water flood (Green and Willhite 1998). This trend was observed in this thesis. Additionally, all nanofluids produced an extra oil in tertiary recovery mode.

For tests performed in water-wet cores, secondary ultimate recoveries were higher

than those obtained in tertiary recovery mode at room temperature (see Figure 6.5(a) and Table 6.6(a)). Conversely, the tests conducted at high temperature gave high incremental recoveries compared to those performed at room temperature (see Figure 6.7) . At glance, the results appeared to favour the application of nanofluid as tertiary EOR fluid at least at 60 °C in water-wet Berea reservoirs. More importantly, the results are consistent with the fact that, in most cases, water flooding would be preferable due to its low price. Then, nanofluids would be injected as tertiary recovery agents to exploit the ability of silica particles to alter reservoir properties to benefit oil recovery.

In neutral-wet cores, the ultimate recoveries due to nanofluids were slightly higher than those achieved by reference water flood. As shown in Figure 6.5(b), the oil recovery was increased by factors ranging from 1.1 to 3.3% point of OOIP. While in tertiary recovery mode, the incremental oil recoveries of the nanofluids were nearly the same at both room and high temperatures as illustrated in Figure 6.7. The results may indicate that tertiary recovery could be the choice over secondary scheme.

In summary, the polymer-coated silica nanoparticles were more efficient in enhancing oil recovery from water-wet Berea sandstone rocks in tertiary recovery mode than in neutral-wet cores. The explanation could be that during water flood of a water-wet reservoir, water fill in the smaller pores and oil is displaced and immobilised in the center of larger pores (Abdallah et al. 1986, Anderson 1986). Continued water injection causes the growth of water films and water to flow through the already established paths. In this course, huge amount of oil is bypassed and trapped due to high capillary forces. This oil is target for EOR fluid injection. The nanoparticles could therefore improve the microscopic sweep efficiency of water flood through modification of properties of the rock, resulting in greater oil recovery than in neutral-wet cores, where oil is left trapped in the smaller pores after water flood. The recovery potential of nanofluids was revealed at the expense of large amount of pore volumes of nanofluid injected. This raises a question on how many pore volumes must be injected at core scale to make the nanoparticle technology profitable at field scale? Upscaling core flood results for application in large oil fields was beyond the scope of this thesis. This has not been fully addressed in the literature. Khanamiri and Torsæter (2017) bring some insights about the problem. The authors believe that a significant number of pore volumes must be injected into a single core at laboratory scale to better simulate the injections at large-scales. Readers are directed to the work by Khanamiri and Torsæter (2017) for more details.

6.3 Evaluation of EOR Mechanisms of Nanoparticles

Previous sections detailed the main experimental findings with respect to oil recovery. It was observed that oil recovery occurred through synergistic effect or combination of various EOR parameters, such as IFT reduction, generation and stabilisation of oil emulsions, microscopic flow diversion due to plugging of the pore, increase in structural disjoining pressure and wettability alteration. The following sections attempt to propose the underlying mechanisms of silica nanoparticles.

6.3.1 Visual observations through the micromodel

The micromodel was also used to provide visualisation of the flowing fluids. Although, the wetting phase movement could not be tracked in the micromodel, it was visually possible to observe a piston-like displacement of water by crude oil due homogeneous porous network system, viscosity contrast between crude oil and water, and low injection velocity. In contrast, the nanofluids tended to establish preferred pathways for sweeping oil from the start, which was used to obtain an insight flow behaviour of the same fluids in Berea sandstone cores. Water breakthrough occurred rapidly through the chosen paths. Meanwhile, oil was bypassed and snapped-off in the micromodel and trapped. It was swept gradually produced as the injection progressed (post- breakthrough). In this course, some of oil droplets were reconnected and produced until residual oil was remained unchanged over time. At the end, residual oil remained trapped as isolated oil droplets in the pore bodies of the micromodel (see Figure 5.5(d)). The trapping of oil droplets was likely due to the high capillary forces caused by an increase in oil droplet curvature. This entrapment mechanism of oil is commonly observed in water-wet porous structures (Ryles 1988, Xu et al. 2015).

6.3.2 Effect of nanoparticles on viscosity of injection seawater

The viscosity of the injection water is affected by the size and concentration of nanoparticles (ShamsiJazeyi et al. 2014, Afolabi and Yusuf 2019). The increase in the viscosity of water due to NPs is reflected in the mobility of adjacent fluid molecules around the nanoparticles. For instance, highly concentrated nanofluid gives an even displacement front (Ponnapati et al. 2011, Afolabi and Yusuf 2019), which is favourable for increasing oil sweep efficiency.

In the present thesis, the results showed that NPs at a concentration of 0.1 wt% do not affect the viscosity of injection synthetic seawater, neither at room temperature nor at elevated temperature. This result ties well with previous studies in which low concentrations ($\leq$5 wt%) of NPs have been shown not to affect aqueous viscosity (Metin et al. 2013). Therefore, it is concluded that oil recovery is significantly influenced by factors other than viscosity.

6.3.3 Effect of nanoparticles on interfacial tension

The interfacial tension IFT) decreases during partitioning of nanoparticles at the oil-water interface from the aqueous solution; the affinity of the NPs to partition at the interface is size and wettability dependent (Chevalier and Bolzinger 2013, Tangparitkul et al. 2018).

The surface-functionalised silica NPs studied in present work decreased the tension between oil and water under the experimental conditions. The reduction of the IFT showed dependence with the size of nanoparticles. Small diameter NPs were more efficient at attaching to the oil-water interface and decrease the IFT than the large ones. Moreover, the wetting and adsorption properties of NPs to the oil-water interface were enhanced with increased temperature, resulting in lower tension than that obtained at room temperature (see Figure 6.8). Nevertheless, the overall conclusion was the NPs were not surface active enough to cause a dramatic reduction of IFT if compared to properly chosen surfactants.

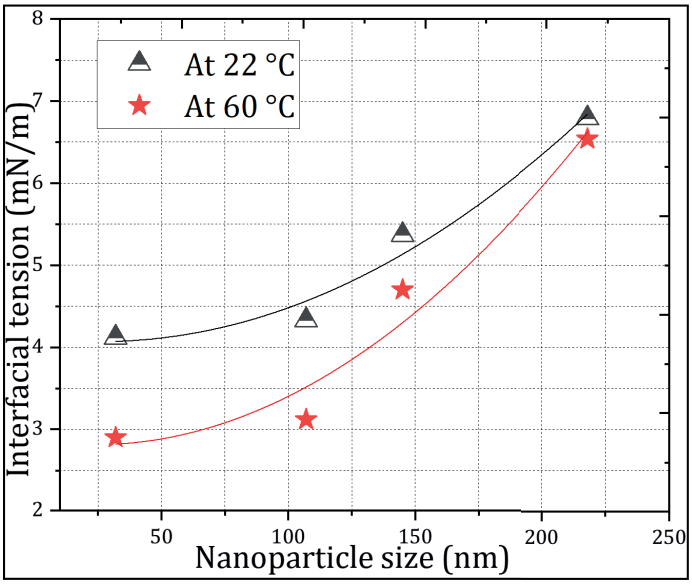

Figure 6.8: Variation of IFT between crude oil and aqueous solution of NPs at 0.1 wt% with size and temperature.

The reasons for the small reduction in IFT may be the aggregation and structuring of NPs at the oil-water interface, especially at high temperature (see Figure 5.3(b)). The surface modification can also add surface functionalities to the fluid interface; The accumulation of the coating materials or surface additive materials such as

polymer molecules on the particle surface can prevent or reduce the amount of NPs that can move toward the interface between oil and water phases (Zhang et al. 2012, Kuang et al. 2018). This can decrease the adsorption/surface activity of the NPs even under favourable adsorption energy (Paunov et al. 2002). Nevertheless, the amount of NPs that migrate and adsorb at interface still play a predominant role for stabilisation of oil droplet emulsions (ShamsiJazeyi et al. 2014, Hua et al. 2018). In addition, changes in the microscopic distribution of the oil within the pores can still occur at IFT below critical value for mobilisation of oil (Chatzis et al. 1988).

In summary, IFT reduction played a role in the mobilisation of residual oil, but is probably not the primary oil drive mechanism of surface modified silica NPs. Similar conclusion was reported by other studies (ShamsiJazeyi et al. 2014, Choi et al. 2017, Behzadi and Mohammadi 2016, Aurand 2017) that investigated the effect silica nanoparticles on oil displacement.

The NPs tested in this work are promising for oil recovery, but are likely not optimal for the crude oil/rock/water systems used in this work. Future studies are recommended to investigate IFT reduction at optimal concentration of NPs in injection water. Moreover, the key factors affecting IFT behaviour, such as surface coating materials, NP size and type, temperature, composition of base fluid, and concentration of both coating and nanoparticle materials need to be characterised.

6.3.4 Generation of emulsion

Adsorption of NPs can decrease the IFT of fluids interface and lead to stabilisation of emulsion. This hypothesis was studied via:

(i) an analysis of flooding pressure behaviour. The decrease in the pressure during nanofluid injection can provide an indication of the occurrence on in-situ emulsion (Adil et al. 2018);

(ii) increasing flowrate can provide an extra energy necessary to break up oil phase and allow for NPs to adsorb at the fluid interface (Kim et al. 2016) and generate emulsions; and

(iii) microscope visualisation of the core nanofluid flooding effluent.

The lowest pressure was recorded during the injection of nanofluids NF02-3 and NF02-4 compared with water flood pressure; this suggested an improvement in oil relative permeability to oil and a reduction in residual oil saturation due to NPs. This probably occurred through destabilisation of oil/water interface, i.e. reduction of IFT in the presence of NPs, which promoted easy flow of oil droplets within

aqueous phase. The formation of emulsion was verified by increasing flow rate. Moreover, the microscopic images of effluent production showed droplets of crude oil in the aqueous phase. The oil droplets appeared to be stable in the presence of NPs (see Figure 5.24).

The present findings led to a conclusion that NF02-3 and NF02-4 can improve microscopic sweep efficiency of water flood by creating stabilised emulsions. These samples had the smallest diameter particles and were the most efficient at reducing IFT. This oil recovery mechanism was reported by authors (Zhang et al. 2010, Suleimanov et al. 2011, ShamsiJazeyi et al. 2014). These studies showed that polymer-coated silica NPs, such as NF02-3 and NF02-4, can stabilise oil droplets in aqueous solution; the stable oil droplet emulsions can easily flow through the pores, resulting in increased oil recovery. Nanofluids NF02-6 and NF02-8 did not produce noticeable emulsion droplets; This was likely due to their aggregation state in aqueous phase.

Further studies are recommended to determine the size distribution of oil droplet emulsions at optimal NP concentration. This can help grasping the contribution of oil emulsification in lowering injection pressure while improving oil recovery.

6.3.5 Effect of nanofluid flooding on differential pressure

Several studies have relied on the differential pressure (dP) behaviour across the core to understand the process of oil displacement by NPs injection. It has been shown that NPs can pass through and/ or block the pores of a reservoir, which may result in the mobilisation oil trapped in the pores due to increased pressure.

In a typical oil displacement process by water flood, the dP across the core increases steadily as water pushes forward the oil phase in a piston-like displacement process until water breaks through (maximum dP). Then, the pressure decreases and stabilises as there is no more oil production at core outlet. If water flood is continued at high flowrate, the dP is expected to increase due to increased flowing velocity. Considering the flooding sequence described in section 4.4.2.3, the pressure pattern observed during the injection of nanofluids is shown in Figure 6.9. Under the same operating conditions, some nanofluids showed stable fluctuation of differential pressure without a noticeable effect on the reference water flood pressure (Figure 6.9(a)). This is, the pressure due to nanofluid injection remained almost at the same level as that of reference water. On the other side, Figure 6.9(b) shows that after water flood ceased production, other type of nanofluids gradually increased the pressure because the nanoparticles were clogging the pores and reducing the mobility of the fluids. The most notable feature is that all nanofluids mobilised residual oil and increased oil recovery regardless the pressure behaviour.

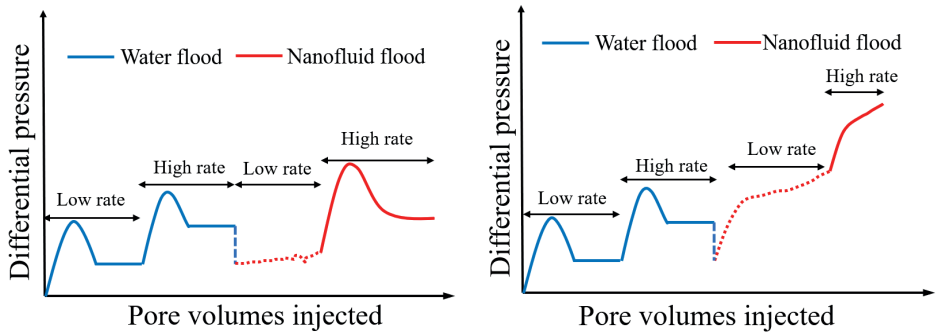

Figure 6.9: Schematic of dP behaviour observed during oil displacement process (a) The nanofluids injected after water has ceased production did not show a noticeable effect on reference water flood pressure; (b) The nanofluids did increase the injection pressure during both low and high rate injections and the pressure was higher than reference water flood pressure.

ThedP was affected by injection flowrate, fluid viscosity, oil saturation, nanoparticle type and size, pore size distribution, and retention of nanoparticles on the surface. The mobilisation of oil at low injection pressures provided an indication of low particle retention on the rock surface and an improved particle mobility through the pores. This could due to chemical interaction between the nanoparticles and the rock system, which enhanced microscopic sweep efficiency of water flood by creation of oil emulsion droplets in water phase. On the other hand, the rise in pressure through the core suggested that physical displacement of oil due to nanoparticles blocking the pores, possibly through log-jamming effect, took place during EOR process.

The injection scheme and wettability of the cores also influenced the pressure. To analyse the pressure behaviour during oil recovery process, the focus is placed on four samples NF02-3, NF02-4, NF02-6 and NF02-8 because of their outstanding oil recovery potential compared to others.

Pressure behaviour through water-wet cores: For tests conducted in Section 5.5.1 following secondary recovery mode, the dP increased and it was higher than the maximum dP recorded during water flood. Upon the nanofluid injection, the pressure rose sharply until it reached breakthrough point; after that, it appeared to gradually stabilise, however some periods of spiky pressure were observed until the end of the experiments. At times, the rise and fall in pressure was accompanied by the production of oil droplets. This was notable during the injection of nanofluids NF02-3 and NF02-4 (Figure C.1 in Appendix C). A notable increase

in pressure compared with reference water flood pressure was recorded during the injection of samples NF02-6 (Figure C.2(a)) and NF02-8 (Figure C.3(a)). The presence of viscous oil phase occupying most of the pores, coupled with particle size and differences in pore sizes can be the primary reasons for pressure increase.

In Section (5.5.5), the nanofluids were injected after water flood to simulate tertiary EOR process. The nanofluids raised the dP for approximately 0.5 PV (samples NF02-3 and NF02-4), then it levelled to water flood pressure (Figure C.8 in Appendix C.3). The endpoints dP (extracted at the end of the injection) were lower than those achieved in secondary mode for the same nanofluid samples. Samples NF02-6 and NF02-8 showed the largest increase in pressure and fluctuations, as shown in Figure 5.12. This indicated confinement and/or aggregation of NPs within the pores. Oil recovery appeared to increase with endpoint pressure for the tests conducted at ambient conditions (see Figure 6.10(a)), which may indicate contribution of physical mechanisms such as log-jamming in mobilisation of residual oil.

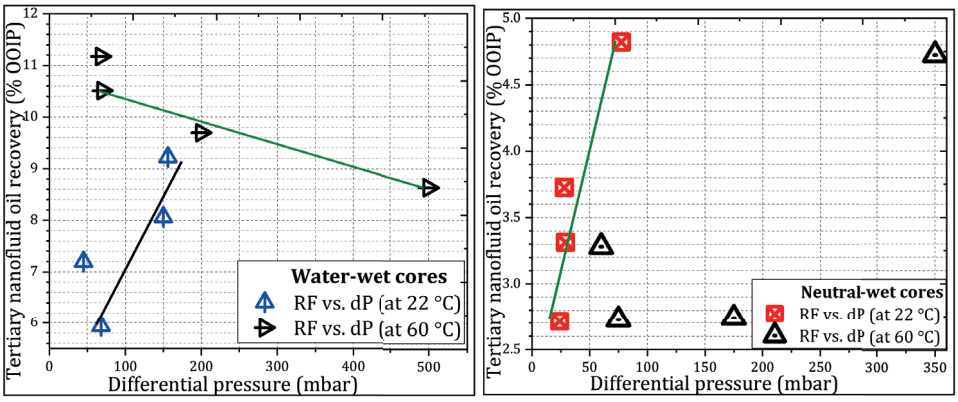

(a) **(b)**

Figure 6.10: Oil recovery vs. maximum dP recorded at the end of nanofluid flood in: (a) water-wet cores; (b) neutral-wet cores.

The tests conducted in Section 5.5.8 (at 60 °C) gave an indication of improved particle mobility for samples NF02-3 and NF02-4. The temperature could be the catalyse for the crude oil/rock/nanofluid interactions and promoted emulsification of oil into aqueous phase. The injection of NF02-3 and NF02-4 nanofluids (see Figure 5.18(a) and Figure C.12(b) in Appendix C.5) slightly lowered the pressure relative to injection pressure of "pure" water. The pressure patterns demonstrated that NPs were easily propagating through water-wet Berea cores with little retention, while increasing microscopic sweep efficiency of water. The mechanistic

involving the interactions between NPs and rock system might be associated with NP type, composition and surface modification.

Nanofluids NF02-6 and NF02-8 were agglomerating at 60 °C, consequently the flood experiments gave the largest increase in differential pressure. Soon after the injection, the pressure increased sharply and then reached a zone where largely fluctuated (see Figure 5.18(b) and Figure C.13(a) in Appendix C.5). The early pressure rise can be attributed to the structuring of NPs and blocking of the small pores at core inlet. Moreover, the externally applied pressure forced the filtration of larger particles and formation of filtered cake at core entrance. Meanwhile, the weakly attached NPs to the pore walls were removed, causing pressure to drop and fluctuate. The accumulated layer of NPs at the core inlet (see Figure 5.19) suggested the occurrence of straining or crossflow filtration and clogging of the pores during nanofluid flooding. The fluctuation of dP predicts maximum pore plugging and redistribution of pressures on a microscopic level and possibly the diversion of flow to the adjacent unswept pores, which helps pushing the oil towards the production lines (Spildo et al. 2009, Skauge et al. 2010). Therefore, it is believed that, the microscopic flow diversion played a primary role in oil displacement of nanofluids NF02-6 and NF02-8. There is a negative correlation between tertiary oil recovery and particle size (see Figure 6.4(a)). The endpoint pressure also shows a negative correlation with oil recovery (Figure 6.10(a)); This means that the largest incremental oil was found with the smallest particles, which opposes the results obtained at ambient conditions. This shows, among other factors, the dependence of oil displacement on temperature and NP type (composition, surface modification, etc.).

Pressure behaviour through neutral-wet cores: The tests conducted with neutral-wet cores exhibited the lowest pressure. This may be because the oil films attached to the pores prevented the NPs from accessing the clay minerals on rock surface. Hence, the particles were less adsorbed/attached to the rock surface. There was somewhat a positive correlation between tertiary oil recovery and endpoint pressure (maximum dP) for the tests conducted in Section (5.5.6) at ambient conditions (see Figure 6.10(b)). Notable oil recoveries were obtained from large particles, but at the expense of increasing pressure. This led to similar conclusion for tests conducted at room temperature in the case of water-wet cores, showing a contribution of physical oil displacement mechanism rather than chemical interactions.

Unlike at ambient conditions, the flood tests conducted at high temperature spurred surface interactions and resulted in different pressure profiles. This leads to similar observations made in the case of water-wet cores, where nanofluids NF02-3 and NF02-4 had little influence on the injection pressure, while NF02-6 and NF02-8 showed a noticeable increase in pressure. The pressure due to nanofluids NF02-

3 and NF02-4 injection remained stable throughout the duration of experiments. Again, this could be an indication of the role the surface modification/coating played to prevent the NPs from adsorbing on clay minerals. Thus, the particles could to travel through and assist oil recovery even in the smallest pores. The main hypothesis is the formation of stable emulsion droplets that enhanced oil mobility as discussed in Section 6.3.4. The surface modification acted as to eliminate electrostatic interactions between the NPs and neutral-wet rock pores (Rodriguez et al. 2009, Zhang et al. 2015), resulting in good propagation of nanoparticles. Nanofluids NF02-6 and NF02-8 were aggregating throughout the duration of oil recovery process at high temperature. As expected, the pressure to increased, but it was smaller than in water-wet cores under the same injection conditions. At the end of the floods, the particle filter "cake" formed at core entrance appeared to be thinner than that formed in water-wet rocks (see Figure 5.19 and Figure 5.23) for the same injected nanofluids.

The most important observation is that all four NPs types can travel through neutral-wet pores with little retention. The surface modification appeared to play a major role in improving particle fluidity through neutral-wet pores than in water-wet pores. However, there is no relationship between oil recovery and maximum dP (Figure 6.10(b)), and particle size. This leads to a conclusion that neither nanoparticle-stabilised emulsion droplets nor microscopic diversion due to pore clogging played a major role in oil recovery in neutral-wet systems.

6.3.6 Effect of nanoparticles flooding on wettability alteration

Wettability of a reservoir plays an important role in oil recovery mechanisms and productivity of the reservoir (Ali et al. 2018). It can be changed during various stages of oil recovery; hence its evaluation is important to understand oil recovery by designated fluid injection. In this work, wettability was evaluated before ad after oil recovery process. After nanofluid flooding, the cores were flooded with *n*-decane to set S_{wi}. A set of spontaneous imbibition (15 to 30 days) and full Amott-Harvey tests were then conducted to investigate the effect of NPs on the rock wetting properties. Oil production by water imbibition is plotted against time to describe the amount of oil produced over time as well as the rate of imbibition. Based on this information, the efficiency of nanofluids in modifying fluid-rock properties leading to oil are interpreted.

Originally water-wet core plugs: The average wettability index (WI) of reference core plugs (i.e. before NPs injection) was 0.86 and water spontaneous imbibition (SI) profile is presented in Figure 5.7. This indicated strongly water-wet cores before nanofluid flood. |

The nanofluids were injected in secondary and tertiary modes at room and high temperatures. After each flood scheme, the wettability of the cores was evaluated. The results showed an enhancement of capillary imbibition intake due to nanoparticles. All tests exhibited remarkably high rates of oil production by water imbibition, with oil production occurring from all core faces (see Figure 4.4 in Section 4.5). This showed a contribution both gravity and capillary forces during wettability alteration (Mohammed and Babadagli 2015). After this period, the rate of water imbibition declined; however, periods of sudden of oil production were observed over time. This provided an indication of the ability of NPs to change the wettability over time. At this stage, most oil production was occurring from top of the cores due to gravity forces (Høgnesen et al. 2006, Mohammed and Babadagli 2015). Full Amott wettability indexes (WIs) were determined for test conducted in Section 5.5.1, and varied from 0.5 to 0.63. In Sections 5.5.5 and 5.5.8, there was no spontaneous imbibition of oil into the cores, thus the Amott water indexes were used to interpret the results. The Amott water index values, I_w, varied from 0.50 to 0.89. The amount of oil produced by water imbibition as well as values of WIs decreased on nanofluid flooded cores compared to those determined initially. This may be attribute to the aggregation and retention of NPs within the pore spaces and variation in core properties, as well as the accuracy of the measurements.

Extensive wettability results showed that NPs can progressively affect wetting properties of Berea sandstone to a water-wet condition. These results were expected because of the hydrophilic nature of the silica NPs exposed to the hydrophilic surface of Berea sandstone. As asserted by Wasan and Nikolov (2003), NPs tend to confine themselves in pre-existing wedge-like formed between the three-phase water-oil-rock contact line during nanofluid flood process. The particle confinement results in well-ordered structures and the development of additional surface roughness responsible for altering wettability.

The small variations in the wettability of the cores (before and after nanoparticle injection) showed that fluid-rock interactions may not be the first order parameter affecting oil recovery in water-wet Berea sandstone.

Neutral-wet core plugs: The core plugs used in Sections 5.5.2 and 5.5.6 were aged in crude oil B for a minimal of four weeks. Because crude oil B was consumed, the cores used in Sections 5.5.9 were aged the longest in crude oil A (7 months). The average Amott's WI was -0.1 and -0.08 for cores aged in crude oils B and A, respectively. This indicated neutral-wet condition of the reference aged cores. New core plugs were prepared for EOR tests assuming that ageing process would yield similar results.

After nanofluid flood testing, the effect of NPs on the neutral-wet surface was

investigated. The results of water imbibition tests revealed a dramatic increase in oil recovery rate. Significant amount of oil was produced within 24 hours-test with little production occurring over time (See Figure 5.9 and Figure 5.25). The WIs measured on reference cores was noticeably increased to a range from 0.46 to 0.77, on average. The behaviour of water imbibition suggested that the NPs can modify wetting properties of oil-wet surfaces at shorter exposure times and benefit oil recovery.

The mechanism of wettability alteration in oil-wet pores due to NPs is complex. Sofla et al. (2019) investigated the wettability alteration in oil-wet rocks and concluded that NPs cannot diffuse into oil-rock interface in the same manner as in water-wet rocks, and change the wettability. On the other hand, when hydrophilic NPs flow in oil-wet porous media, some of the NPs may adsorb onto the rock surface while others adhere to the oil-water interface due to the attractive forces originating from dipole-dipole interactions (Khilar and Fogler 1998, Ju et al. 2006, Roustaei et al. 2012, Li 2016, Afolabi and Yusuf 2019) and from physical interactions due to the applied injection pressure. These interactions result in the development of new surface roughness (Dai et al. 2017), decrease the interfacial energy between the rock surface and water (Afolabi and Yusuf 2019), and destabilise oil films coating on the surface. Furthermore, at the oil-water interface, NPs can form hydrogen bonds with water molecules, thereby increasing IFT between oil and water (Mohammadi 2013). This work-flow process allows for the creation of water-wet surfaces on the pore walls and greater capillary pressure, which ensures greater imbibition of water and increased oil recovery efficiency. These findings highlight the wettability alteration from neutral-wet to more water-wet condition as the main EOR mechanism of the nanoparticles investigated in this thesis.

CHAPTER 7

Conclusions and Recommendations for Further Work

7.1 Summary and Conclusions

Twenty-three fluid samples with different types of nanoparticles were provided by Evonik as additives to injection water for use in oil reservoirs. Additionally, two polymer-based fluid samples used in the modification of the nanoparticles were made available. Earlier literature has shown that nanoparticles in the injection water may increase oil recovery compared to water injection alone. The present nanoparticles are surface-modified with different additives (e.g. silane, polymers, etc.) to get even better oil recovery than earlier reported. In the present thesis, experiments were conducted to evaluate NPs stability, to evaluate oil recovery potential of the NPs and identify the underlying oil recovery mechanisms. The main goal was to identify the most promising NPs candidates for oil recovery and provide fundamental knowledge on how the NPs can improve microscopic sweep efficiency of water flooding in water-wet and neutral-wet reservoirs.

The following investigations were performed to verify oil recovery potential of the NPs: 1) Initial screening based on secondary nanofluid flooding (start at S_{wi}) in water-wet glass micromodels; 2) Screening of the NPs from micromodel tests using secondary recovery mode in Berea sandstone cores; and 3) Testing of the selected NPs from 2) in tertiary recovery mode at room and at elevated temperatures. In the core flooding experiments, the pressure difference across the core sample was

measured to relate it to the migration behaviour of NPs in porous media. The influence of NPs on the crude oil-water interface was studied by measuring the IFT, while the rock-fluid interactions were investigated by Amott wettability test. From the extensive flooding experiments, the following conclusions were obtained:

7.1.1 Nanofluid stability

Stability tests showed that the surface-modified silica nanoparticles were stable in SSW for a period of four months at ambient conditions. However, at the assumed minimal reservoir temperature of 60 °C the NPs were unstable. Nanofluids NF02-3 and NF02-4 were stable for up to four days, after that the particles flocculated and aggregated in solutions of SSW. Nanofluids NF02-6 and NF02-8 immediately aggregated at high temperature. This was a negative outcome because the NPs were modified targeting stability in seawater. This results highlight the challenges to achieve highly stable nanofluids especially, within a high salinity and high temperature environment. Therefore, more studies are needed to improve the surface modification/optimisation of the particles. At present, these NPs may not be suitable for practical field-scale injections despite their oil recovery potential at core scale.

7.1.2 Screening of nanoparticles

7.1.2.1 Glass micromodel flooding

Nanofluid flooding in glass micromodels have the potential of being a quick and easy way for screening of NP suspensions for EOR application. In this work, water-wet glass micromodels with regular pore network were used. The micromodel experiments revealed that the surface-modified silica NPs have the potential to increase oil recovery. The nanofluid flooding tests resulted in very high oil recoveries and small variations between the recoveries obtained with different NPs samples. From this procedure 15 of 23 NPs samples were pre-selected based on low residual oil saturation ($\leq$15%) achieved at the end of the secondary micromodel injection. Based on manufacture's recommendations, nine of the fifteen samples were further tested (screened) with Berea sandstone cores. Visual observations through the micromodel showed that nanofluids tend to establish preferred pathways for sweeping oil at initial stages of the injection, and residual oil was trapped as isolated oil droplets in the pores.

7.1.2.2 Core flooding

Flooding tests with Berea sandstone cores also showed that surface-modified silica NPs could be promising additives to the water flood for EOR applications. There was no clear correlation between the results obtained in the micromodel and the

flooding results with Berea core plugs. A stepwise core flood procedure provided the following conclusions:

- Nanofluid flooding from start (at S_{wi}) in water-wet cores resulted in the selection of 4 of 9 nanofluid samples for further testing. The average oil recovery of the selected samples varied from 48.01% to 54.48% or 8.3% to 14.81% points increase compared to water flood recoveries. The best performing nanofluid sample was NF02-6;
- Tertiary nanofluid flooding in water-wet cores gave an average additional oil recovery of 4.6% to 9.8% of OOIP. The highest incremental recovery was achieved by nanofluid samples NF02-6 and NF02-8;
- Tertiary nanofluid flooding in water-wet cores, at the assumed threshold reservoir temperature of 60 °C, gave better oil recoveries than at room temperature. The average additional oil recovery varied from 8.66% to 11.23% of OOIP; The relatively best performing nanofluids samples were NF02-3 and NF02-4;
- Nanofluid flooding from start (at S_{wi}) in neutral-wet cores resulted in an average oil recovery from 59.3% to 61.5% of OOIP, which corresponds to increase in oil recovery by 1.1% to 3.3% points of OOIP relative to reference water flood. The relatively best performing samples were NF02-3 and NF02-6;
- Nanofluid flood following water flood in neutral-wet cores resulted in average additional oil recovery from 2.71% to 4.80% of OOIP. The best performing nanofluid samples were NF02-6 and NF02-8;
- Tertiary nanofluid flooding in neutral-wet cores, at 60 °C, incremented oil recovery in the range of 2.75% to 4.73% of OOIP, on average. The best performing nanofluid samples were NF02-3 and NF02-6.

The overall conclusions regarding core flood oil recovery are that samples NF02-3, NF02-4, NF02-6 and NF02-8 all give additional oil recovery, both when injected initially and after water flood in water- and neutral-wet cores. However, none of the NPs samples increased significantly oil recovery (i.e. ≥5% of OOIP) within the first pore volumes injected. This implied that NPs could mobilise significant quantities of residual oil at the expense of large volumes of NPs injected. Moreover, core flood experiments showed that all four NPs are more effective as tertiary oil recovery agents in water-wet Berea sandstone cores than in neutral-wet cores, and oil displacement efficiency improved with temperature.

7.1.3 Proposed EOR mechanisms of surface-functionalised silica NPs

Oil displacement studies showed that various recovery mechanisms may be operating during the injection of nanoparticles. Therefore, there is still a need for additional studies specifically investigating the mechanisms of surface-functionalised silica nanoparticles and its contribution on oil recovery. These studies should focus on the surface chemistry or chemical interactions occurring between the crude oil, rock and nanofluids. Currently, oil recovery mechanisms, such as IFT reduction, log-jamming effect, generation of nanoparticle-stabilised emulsions in-situ and wettability alteration, were considered relevant for the studied nanoparticles. The effect of the studied nanofluids in EOR can be summarised as:

- The interfacial tension between crude oil and water is reduced by adding surface-modified silica NPs in seawater. However, the reduction is not in the orders of magnitude required for significant mobilisation of residual oil;
- In water-wet cores, nanofluids NF02-3 and NF02-4 appeared to affect wetting properties of the cores and increase oil recovery through the formation of stabilisation of oil-in-water emulsions. For samples NF02-6 and NF02-8, the main contributing EOR mechanism is likely the microscopic flow diversion due to plugging of the pore channels.
- In neutral-wet cores, nanofluids can generate nanoparticle-stabilised emulsions (NF02-3 and NF02-4) and induce plugging of the pores (NF02-6 and NF02-8); however, all nanofluids samples can change the wettability from neutral- to water-wet condition, which is probably the main oil drive mechanism for any of the samples.

7.2 Recommendations for Further Work

7.2.1 Design and testing of nanoparticles

The nanoparticles provided in this work performed good as an additives in the injection water for EOR in both water-wet and aged sandstone core samples. But most likely, the provided nanoparticles were not optimal for the rock and fluid system used in this project. It is possible to tailor make nanoparticles for oil recovery in a specific reservoir system. Most studies of nanofluid dispersion for oil recovery are performed by chemists and material scientists, where the application (of nanofluids) are investigated by reservoir engineers. To fill in this gap, the optimisation of NPs for oil recovery should be a task that requires a close cooperation between reservoir engineers, nano-materials specialists, chemists and others.

Such an optimisation effort could gradually lead to more knowledge about oil recovery mechanisms, and thereby a stepwise improvement of nanoparticles would be achieved. The final goal will be to develop a procedure for designing NPs that maximise oil recovery for a given crude oil/brine/rock system.

Present project gives the first indication on how this work can be started. As observed from the results, it will be necessary to develop the knowledge stepwise, starting from glass micromodels, then μ-CT studies and finally core scale flooding at simulated field conditions. The screening of NPs using glass micromodel should be done in engraved 2D rock pore system that mimic rock pore network structure and wettability of a specific reservoir rock. In such micromodels different NPs and fluid systems (with composition that resemble a specific oilfield) can be tested in relatively short time. Supplementary studies could be done in representative 3D glass micromodels in μ-CT. The next step will be nanofluid flooding in rock core samples.

The goal is to have a test procedure ready for optimising of recovery with nanofluid when an oil company want to evaluate a reservoir for this type of flooding. Given the type of rock, fluids and reservoir conditions, we should know, in broad sense, the suitable type of nanoparticles and the test procedure that should be applied for the final determination of the exact nanoparticle and concentration. We do not have such procedure today, leading to a lack of interest of this technology among oil companies. Nano-material companies must operate like the oil field chemistry companies and have a convincing proof at core scale that their products work.

7.2.2 Nanofluid EOR experiments

Future work is recommended to examine oil production and improve the understanding of recovery mechanisms of nanoparticles under variety of conditions. This should focus on:

- Characterisation of the surface charge of the NPs and charge of rock surface at the experimental conditions to predict the transport behaviour of nanoparticles; Moreover, characterisation and determination of bonding effect of nanoparticles with surface coating additives (i.e. surface activity and reactivity) is required to predict their interactions with fluid and rock during oil recovery process;
- Determine the optimum concentration that produces long-term stable dispersion of NPs and evaluate oil recovery in secondary and tertiary recovery modes at high temperature;
- Examine the effect of shut-in the cores at water flood residual saturation;

This is, inject NPs for 1-2 PVs after water flood residual oil saturation has been established and shut-in the system for some time (hours to days). After which, the injection can be continued with NPs or with water. Here, care should be taken to ensure no oil production before shut-in. That is why 1 to 2 PVs are suggested. The shut-in period should not exceed the onset of aggregation of NPs to avoid clogging of the pores.

References

Abdallah, W., Buckley, J. S., Carnegie, A., Edwards, J., Herold, B., Fordham, E., Graue, A., Habashy, T., Seleznev, N., and Signer, C. (1986). Fundamentals of wettability. *Technology*, 38(1125-1144):268.

Adil, M., Lee, K., Mohd Zaid, H., Ahmad Latiff, N. R., and Alnarabiji, M. S. (2018). Experimental study on electromagnetic-assisted zno nanofluid flooding for enhanced oil recovery (eor). *PLOS ONE*, 13(2):1–18.

Afolabi, R. O. and Yusuf, E. O. (2019). Nanotechnology and global energy demand: challenges and prospects for a paradigm shift in the oil and gas industry. *Journal of Petroleum Exploration and Production Technology*, 9(2):1423–1441.

Agi, A., Junin, R., and Gbadamosi, A. (2018). Mechanism governing nanoparticle flow behaviour in porous media: insight for enhanced oil recovery applications. *International Nano Letters*, 8(2):49–77.

Alagic, E., Spildo, K., Skauge, A., and Solbakken, J. (2011). Effect of crude oil ageing on low salinity and low salinity surfactant flooding. *Journal of Petroleum Science and Engineering*, 78(2):220 – 227.

Ali, J. A., Kolo, K., Manshad, A. K., and Mohammadi, A. H. (2018). Recent advances in application of nanotechnology in chemical enhanced oil recovery: Effects of nanoparticles on wettability alteration, interfacial tension reduction, and flooding. *Egyptian Journal of Petroleum*, 27(4):1371 – 1383.

Amott, E. (1959). Observations relating to the wettability of porous rock. *Society of Petroleum Engineers*.

Anderson, W. (1986). Wettability literature survey-part 2: Wettability measurement. *Journal of petroleum technology*, 38(11):1–246.

Anderson, W. G. (1987). Wettability literature survey-part 6: the effects of wettability on waterflooding. *Journal of petroleum technology*, 39(12):1–605.

Aurand, K. (2017). Enhanced oil recovery using silica nanoparticles: An experimental evaluation of oil production, recovery mechanisms and nanofluid stability. *PhD Thesis*.

Aurand, K., Dahle, S., and Torsæter, O. (2014). Comparison of oil recovery for six nanofluids in berea sandstone cores. In *International symposium of the society of core analysts*, pages 1–12.

Ayatollahi, S. and Zerafat, M. M. (2012). Nanotechnology-assisted eor techniques: New solutions to old challenges. In *SPE International Oilfield Nanotechnology Conference and Exhibition*. Society of Petroleum Engineers.

Baron, A. R., Desai, Dominguez, M., and Devon, Fernandez, M. (2008). Nanotechnology for the oil and gas industry. In *Nanotechnology*. Rice University.

Behzadi, A. and Mohammadi, A. (2016). Environmentally responsive surface-modified silica nanoparticles for enhanced oil recovery. *J. Nanoparticle Res.*, 18(9):266.

Bennetzen, M. V. and Mogensen, K. (2014). Novel applications of nanoparticles for future enhanced oil recovery. In *International petroleum technology conference*. International Petroleum Technology Conference.

Bera, A. and Belhaj, H. (2016). Application of nanotechnology by means of nanoparticles and nanodispersions in oil recovery-a comprehensive review. *Journal of Natural Gas Science and Engineering*, 34:1284–1309.

Berry, J. D., Neeson, M. J., Dagastine, R. R., Chan, D. Y., and Tabor, R. F. (2015). Measurement of surface and interfacial tension using pendant drop tensiometry. *Journal of colloid and interface science*, 454:226–237.

Binks, B. P. and Whitby, C. P. (2005). Nanoparticle silica-stabilised oil-in-water emulsions: improving emulsion stability. *Colloids and Surfaces A: Physicochemical and Engineering Aspects*, 253(1):105 – 115.

Bjorkum, P. and Nadeau, P. H. (1998). Temperature controlled porosity/permeability reduction, fluid migration, and petroleum exploration in sedimentary basins. *The APPEA Journal*, 38(1):453–465.

Buckley, J., Liu, Y., and Monsterleet, S. (1998). Mechanisms of wetting alteration by crude oils. *SPE journal*, 3(01):54–61.

Chatzis, I., Kuntamukkula, M., Morrow, N., et al. (1988). Effect of capillary number on the microstructure of residual oil in strongly water-wet sandstones. *SPE Reservoir Engineering*, 3(03):902–912.

Chatzis, I., Morrow, N. R., and Lim, H. T. (1983). Magnitude and detailed structure of residual oil saturation. *Society of Petroleum Engineers Journal*, 23(02):311–326.

Chengara, A., Nikolov, A., Wasan, D., Trokhymchuk, A., and Henderson, D. (2005). Spreading of nanoflulds driven by the structural disjoining pressure gradient. *J. Colloid Interface Sci.*, 280:192–201.

Chevalier, Y. and Bolzinger, M.-A. (2013). Emulsions stabilized with solid nanoparticles: Pickering emulsions. *Colloids and Surfaces A: Physicochemical and Engineering Aspects*, 439:23 – 34. Nanoparticles@interfaces.

Choi, S. K., Son, H. A., Kim, H. T., and Kim, J. W. (2017). Nanofluid enhanced oil recovery using hydrophobically associative zwitterionic polymer-coated silica nanoparticles. *Energy & Fuels*, 31(8):7777–7782.

Craig, F. F. (1971). *The reservoir engineering aspects of waterflooding*, volume 3. HL Doherty Memorial Fund of AIME New York.

Cuiec, L. (1984). Rock/crude-oil interactions and wettability: An attempt to understand their interrelation. In *SPE Annual Technical Conference and Exhibition*. Society of Petroleum Engineers.

Dai, C., Wang, X., Li, Y., Lv, W., Zou, C., Gao, M., and Zhao, M. (2017). Spontaneous imbibition investigation of self-dispersing silica nanofluids for enhanced oil recovery in low-permeability cores. *Energy & Fuels*, 31(3):2663–2668.

Dandekar, A. Y. (2013). *Petroleum reservoir rock and fluid properties*. CRC press.

Das, S. K., Choi, S. U., and Patel, H. E. (2006). Heat transfer in nanofluids—a review. *Heat transfer engineering*, 27(10):3–19.

Dehaghani, A. H. S. and Daneshfar, R. (2019). How much would silica nanoparticles enhance the performance of low-salinity water flooding? *Petroleum Science*, pages 1–15.

Denney, D. (2011). Nanosized particles for enhanced oil recovery. *Journal of Petroleum Technology*, 63(01):54–56.

DiCarlo, D. A., Aminzadeh, B., Roberts, M., Chung, D., Bryant, S. L., and Huh, C. (2011). Mobility control through spontaneous formation of nanoparticle stabilized emulsions. *Geophysical Research Letters*, 38(24).

Dimri, V., Srivastava, R., and Vedanti, N. (2012). Chapter 5 - reservoir geophysics: Some basic concepts. In Dimri, V., Srivastava, R., and Vedanti, N., editors, *Fractal Models in Exploration Geophysics*, volume 41 of *Handbook of Geophysical Exploration: Seismic Exploration*, pages 89 – 118. Pergamon.

Ding, H., Zhang, N., Zhang, Y., Wei, M., and Bai, B. (2019). Experimental data analysis of nanoparticles for enhanced oil recovery. *Industrial & Engineering Chemistry Research*.

Eide, Ø., Fernø, M., Nybø, S., and Graue, A. (2014). Waterflood stability in scal analysis. *Int. Symp. Soc. Core Anal. Held Avignon Fr.*

El-Diasty, A. I. (2015). The potential of nanoparticles to improve oil recovery in bahariya formation, egypt: An experimental study. In *SPE Asia Pacific Enhanced Oil Recovery Conference*. Society of Petroleum Engineers.

El-Diasty, A. I. and Aly, A. M. (2015). Understanding the mechanism of nanoparticles applications in enhanced oil recovery. In *SPE North Africa technical conference and exhibition*. Society of Petroleum Engineers.

Fakoya, M. F. and Shah, S. N. (2017). Emergence of nanotechnology in the oil and gas industry: Emphasis on the application of silica nanoparticles. *Petroleum*, 3(4):391–405.

Fletcher, A. and Davis, J. (2010). How eor can be transformed by nanotechnology. In *SPE improved oil recovery symposium*. Society of Petroleum Engineers.

Gbadamosi, A. O., Junin, R., Manan, M. A., Yekeen, N., Agi, A., and Oseh, J. O. (2018). Recent advances and prospects in polymeric nanofluids application for enhanced oil recovery. *Journal of Industrial and Engineering Chemistry*, 66:1–19.

Green, D. W. and Willhite, G. P. (1998). *Enhanced oil recovery*, volume 6. Henry L. Doherty Memorial Fund of AIME, Society of Petroleum Engineers.

Hamon, G. (2016). Low-salinity waterflooding: Facts, inconsistencies and the way forward. *Petrophysics*, 57(01):41–50.

Heaviside, J., Black, C., et al. (1983). Fundamentals of relative permeability: experimental and theoretical considerations. In *SPE Annual Technical Conference and Exhibition*. Society of Petroleum Engineers.

Hendraningrat, L., Li, S., and Torsæter, O. (2013a). A coreflood investigation of nanofluid enhanced oil recovery. *Journal of Petroleum Science and Engineering*, 111:128–138.

Hendraningrat, L., Li, S., and Torsaeter, O. (2013b). Enhancing oil recovery of low-permeability berea sandstone through optimised nanofluids concentration. In *SPE enhanced oil recovery conference*. Society of Petroleum Engineers.

Hendraningrat, L., Li, S., and Torsater, O. (2013c). Effect of some parameters influencing enhanced oil recovery process using silica nanoparticles: an experimental investigation. In *SPE Reservoir Characterization and Simulation Conference and Exhibition*. Society of Petroleum Engineers.

Hendraningrat, L., Shidong, L., and Torsaeter, O. (2012). A glass micromodel experimental study of hydrophilic nanoparticles retention for eor project. In *SPE Russian Oil and Gas Exploration and Production Technical Conference and Exhibition*. Society of Petroleum Engineers.

Hendraningrat, L. and Torsæter, O. (2014). Effects of the initial rock wettability on silica-based nanofluid-enhanced oil recovery processes at reservoir temperatures. *Energy & Fuels*, 28(10):6228–6241.

Hendraningrat, L. and Torsaeter, O. (2014). Unlocking the potential of metal oxides nanoparticles to enhance the oil recovery. In *offshore technology conference-Asia*. Offshore Technology Conference.

Hendraningrat, L. and Torsæter, O. (2015). Metal oxide-based nanoparticles: revealing their potential to enhance oil recovery in different wettability systems. *Applied Nanoscience*, 5(2):181–199.

Hendraningrat, L. and Torsæter, O. (2016). A study of water chemistry extends the benefits of using silica-based nanoparticles on enhanced oil recovery. *Applied Nanoscience*, 6(1):83–95.

Høgnesen, E. J., Olsen, M., and Austad, T. (2006). Capillary and gravity dominated flow regimes in displacement of oil from an oil-wet chalk using cationic surfactant. *Energy & fuels*, 20(3):1118–1122.

Hu, Z., Azmi, S. M., Raza, G., Glover, P. W., and Wen, D. (2016). Nanoparticle-assisted water-flooding in berea sandstones. *Energy & Fuels*, 30(4):2791–2804.

Hua, X., Frechette, J., and Bevan, M. A. (2018). Nanoparticle adsorption dynamics at fluid interfaces. *Soft matter*, 14(19):3818–3828.

Huibers, B. M., Pales, A. R., Bai, L., Li, C., Mu, L., Ladner, D., Daigle, H., and Darnault, C. J. (2017). Wettability alteration of sandstones by silica nanoparticle dispersions in light and heavy crude oil. *Journal of Nanoparticle Research*, 19(9):323.

Humphry, K., Suijkerbuijk, B., A. van der Linde, H., Pieterse, S., and Masalmeh, S. (2014). Impact of wettability on residual oil saturation and capillary desaturation curves. *PETROPHYSICS*, 55:313–318.

Ju, B., Fan, T., and Ma, M. (2006). Enhanced oil recovery by flooding with hydrophilic nanoparticles. *China Particuology*, 4(1):41–46.

Khalil, M., Jan, B. M., Tong, C. W., and Berawi, M. A. (2017). Advanced nanomaterials in oil and gas industry: design, application and challenges. *Applied Energy*, 191:287–310.

Khanamiri, H. H. and Torsæter, O. (2017). Injected pore volume on lab and field scales. *International Society for Porous Media, Interpore*.

Khilar, K. C. and Fogler, H. S. (1998). *Migrations of fines in porous media*, volume 12. Springer Science & Business Media.

Kim, I., Worthen, A. J., Johnston, K. P., DiCarlo, D. A., and Huh, C. (2016). Size-dependent properties of silica nanoparticles for pickering stabilization of emulsions and foams. *Journal of Nanoparticle Research*, 18(4):82.

Kokubun, M. E., Radu, F. A., Keilegavlen, E., Kumar, K., and Spildo, K. (2019). Transport of polymer particles in oil–water flow in porous media: Enhancing oil recovery. *Transport in Porous Media*, 126(2):501–519.

Kondiparty, K., Nikolov, A., Wu, S., and Wasan, D. (2011). Wetting and spreading of nanofluids on solid surfaces driven by the structural disjoining pressure: statics analysis and experiments. *Langmuir*, 27(7):3324–3335.

Kuang, W., Saraji, S., and Piri, M. (2018). A systematic experimental investigation on the synergistic effects of aqueous nanofluids on interfacial properties and their implications for enhanced oil recovery. *Fuel*, 220:849–870.

Lake, L. W. and Venuto, P. B. (1990). A niche for enhanced oil recovery in the 1990s. *Oil & Gas Journal*, 88(17):62–67.

León-Pabón, J.-A., Mejía-Pilonieta, T.-J., Carrillo-Moreno, L.-F., Buendía-Lombana, H., Zapata, J.-F., and Díaz-Prada, C.-A. (2014). Experimental comparison for the calculation of rock wettability using the amott-harvey method and a new visual method. *CT&F-Ciencia, Tecnología y Futuro*, 5(5):5–22.

Li, S. (2016). An experimental investigation of enhanced oil recovery mechanisms in nanofluid injection process. *NTNU*.

Li, S., Hendraningrat, L., and Torsaeter, O. (2013). Improved oil recovery by hydrophilic silica nanoparticles suspension: 2 phase flow experimental studies. In *IPTC 2013: International Petroleum Technology Conference*.

Li, S. and Torsæter, O. (2014). An experimental investigation of eor mechanisms for nanoparticles fluid in glass micromodel. In *Paper SCA2014-022 was prepared for presentation at the International Symposium of the Society of Core Analysts held in Avignon, France*, pages 8–11.

Lim, S., Horiuchi, H., Nikolov, A. D., and Wasan, D. (2015). Nanofluids alter the surface wettability of solids. *Langmuir*, 31(21):5827–5835.

Liu, L. and Buckley, J. S. (1999). Alteration of wetting of mica surfaces. *Journal of Petroleum Science and Engineering*, 24(2):75 – 83.

Lock, E., Ghasemi, M., Mostofi, M., and Rasouli, V. (2012). An experimental study of permeability determination in the lab. *WIT Transactions on Engineering Sciences*, 80:221–230.

McPhee, C. and Arthur, K. (1994). Relative permeability measurements: an inter-laboratory comparison. In *European Petroleum Conference*. Society of Petroleum Engineers.

Metin, C., Bonnecaze, R., and Nguyen, Q. (2013). The viscosity of silica nanoparticle dispersions in permeable media. *SPE Reservoir Evaluation & Engineering*, 16(03):327–332.

Micronit, M. (2019). micronit/products/enhanced-oil-recovery.

Miranda, C. R., Lara, L. S. d., and Tonetto, B. C. (2012). Stability and mobility of functionalized silica nanoparticles for enhanced oil recovery applications. In *SPE International Oilfield Nanotechnology Conference and Exhibition*. Society of Petroleum Engineers.

Mohammadi, A. R. S. S. M. (2013). An evaluation of modified silica nanoparticles' efficiency in enhancing oil recovery of light and intermediate oil reservoirs. *Egypt. J. Pet.*, 22(3):427 – 433.

Mohammed, M. and Babadagli, T. (2015). Wettability alteration: A comprehensive review of materials/methods and testing the selected ones on heavy-oil containing oil-wet systems. *Advances in colloid and interface science*, 220:54–77.

Morrow, N. R. (1990). Wettability and its effect on oil recovery. *Journal of petroleum technology*, 42(12):1–476.

Muggeridge, A., Cockin, A., Webb, K., Frampton, H., Collins, I., Moulds, T., and Salino, P. (2014). Recovery rates, enhanced oil recovery and technological limits. *Philosophical Transactions of the Royal Society A: Mathematical, Physical and Engineering Sciences*, 372(2006):20120320.

Nazari Moghaddam, R., Bahramian, A., Fakhroueian, Z., Karimi, A., and Arya, S. (2015). Comparative study of using nanoparticles for enhanced oil recovery: wettability alteration of carbonate rocks. *Energy & Fuels*, 29(4):2111–2119.

Negin, C., Ali, S., and Xie, Q. (2016). Application of nanotechnology for enhancing oil recovery–a review. *Petroleum*, 2(4):324–333.

NPD (2019). Resource report for discoveries and fields. *http://www.npd.no/en/facts/publications/reports2/resource-report/resource-report-2019/fields/*.

Ogolo, N., Olafuyi, O., and Onyekonwu, M. (2012). Enhanced oil recovery using nanoparticles. *SPE 160847*.

Panneerselvam, S. and Choi, S. (2014). Nanoinformatics: emerging databases and available tools. *International journal of molecular sciences*, 15(5):7158–7182.

Paunov, V. N., Binks, B. P., and Ashby, N. P. (2002). Adsorption of charged colloid particles to charged liquid surfaces. *Langmuir*, 18(18):6946–6955.

Pei, H., Zhang, G., Ge, J., Zhang, J., Zhang, Q., and Fu, L. (2015). Investigation of nanoparticle and surfactant stabilized emulsion to enhance oil recovery in waterflooded heavy oil reservoirs. In *SPE Canada heavy oil technical conference*. Society of Petroleum Engineers.

Peng, B., Zhang, L., Luo, J., Wang, P., Ding, B., Zeng, M., and Cheng, Z. (2017). A review of nanomaterials for nanofluid enhanced oil recovery. *RSC Advances*, 7(51):32246–32254.

Ponnapati, R., Karazincir, O., Dao, E., Ng, R., Mohanty, K., and Krishnamoorti, R. (2011). Polymer-functionalized nanoparticles for improving waterflood sweep efficiency: Characterization and transport properties. *Industrial & Engineering Chemistry Research*, 50(23):13030–13036.

Ragab, A. M. S. and Hannora, A. E. (2015). An experimental investigation of silica nano particles for enhanced oil recovery applications. In *SPE North Africa technical conference and exhibition*. Society of Petroleum Engineers.

Ramakrishnan, T. and Cappiello, A. (1991). A new technique to measure static and dynamic properties of a partially saturated porous medium. *Chemical engineering science*, 46(4):1157–1163.

Rodriguez, E., Roberts, M., Yu, H., Huh, C., and Bryant, S. L. (2009). Enhanced migration of surface-treated nanoparticles in sedimentary rocks. In *SPE annual technical conference and exhibition*. Society of Petroleum Engineers.

Roustaei, A. (2014). Experimental study of surface-modified silica nanoparticles in enhancing oil recovery. *Petroleum Geoscience*, 20(4):393–400.

Roustaei, A. and Bagherzadeh, H. (2015). Experimental investigation of sio 2 nanoparticles on enhanced oil recovery of carbonate reservoirs. *Journal of Petroleum Exploration and Production Technology*, 5(1):27–33.

Roustaei, A., Moghadasi, J., Bagherzadeh, H., and Shahrabadi, A. (2012). An experimental investigation of polysilicon nanoparticles' recovery efficiencies through changes in interfacial tension and wettability alteration. In *SPE international oilfield nanotechnology conference and exhibition*. Society of Petroleum Engineers.

Ryles, R. (1988). Chemical stability limits of water-soluble polymers used in oil recovery processes. *SPE reservoir engineering*, 3(01):23–34.

Satter, A. and Iqbal, G. M. (2016). 7 - reservoir life cycle and role of industry professionals. In Satter, A. and Iqbal, G. M., editors, *Reservoir Engineering*, pages 127 – 136. Gulf Professional Publishing, Boston.

Schramm, L. L. (2000). *Surfactants: fundamentals and applications in the petroleum industry*. Cambridge University Press.

Seright, R. S., Campbell, A., and Mozley, P. (2009). Stability of partially hydrolyzed polyacrylamides at elevated temperatures in the absence of divalent cations. In *SPE International Symposium on Oilfield Chemistry*. Society of Petroleum Engineers.

ShamsiJazeyi, H., Miller, C. A., Wong, M. S., Tour, J. M., and Verduzco, R. (2014). Polymer-coated nanoparticles for enhanced oil recovery. *Journal of Applied Polymer Science*, 131(15).

Sheng, J. J. (2015). Status of surfactant eor technology. *Petroleum*, 1(2):97 – 105.

Shepherd, M. (2009). Factors influencing recovery from oil and gas fields. *AAPG Special Volumes*.

Skauge, T., Spildo, K., and Skauge, A. (2010). Nano-sized particles for eor. in 'spe improved oil recovery symposium, tulsa, oklahoma, usa, 24–28 april, 2010'. *Society of Petroleum Engineers*.

Smalley, P., Muggeridge, A., Dalland, M., Helvig, O., Høgnesen, E., Hetland, M., and Østhus, A. (2018). Screening for eor and estimating potential incre-

mental oil recovery on the norwegian continental shelf. In *SPE Improved Oil Recovery Conference*. Society of Petroleum Engineers.

Sofla, S. J. D., James, L. A., and Zhang, Y. (2019). Toward a mechanistic understanding of wettability alteration in reservoir rocks using silica nanoparticles. In *E3S Web of Conferences*, volume 89, page 03004. EDP Sciences.

Spildo, K., Skauge, A., Aarra, M. G., and Tweheyo, M. T. (2009). A new polymer application for north sea reservoirs. *SPE Reservoir Evaluation & Engineering*, 12(03):427–432.

Stosur, G. J., Hite, J. R., Carnahan, N. F., and Miller, K. (2003). The alphabet soup of ior, eor and aor: effective communication requires a definition of terms. In *SPE International Improved Oil Recovery Conference in Asia Pacific*. Society of Petroleum Engineers.

Suleimanov, B. A., Ismailov, F., and Veliyev, E. (2011). Nanofluid for enhanced oil recovery. *Journal of Petroleum Science and Engineering*, 78(2):431–437.

Sun, X., Zhang, Y., Chen, G., and Gai, Z. (2017). Application of nanoparticles in enhanced oil recovery: a critical review of recent progress. *Energies*, 10(3):345.

Tangparitkul, S., Charpentier, T., Pradilla, D., and Harbottle, D. (2018). Interfacial and colloidal forces governing oil droplet displacement: Implications for enhanced oil recovery. *Colloids and Interfaces*, 2(3):30.

Than, P., Preziosi, L., Josephl, D., and Arney, M. (1988). Measurement of interfacial tension between immiscible liquids with the spinning road tensiometer. *Journal of colloid and interface science*, 124(2):552–559.

Torsater, O., Engeset, B., Hendraningrat, L., and Suwarno, S. (2012). Improved oil recovery by nanofluids flooding: an experimental study. In *SPE Kuwait international petroleum conference and exhibition*. Society of Petroleum Engineers.

Wasan, D. and Nikolov, A. (2003). Spreading of nanofluids on solids. *Nature*, 423:156–9.

Xu, K., Zhu, P., Huh, C., and Balhoff, M. T. (2015). Microfluidic investigation of nanoparticles' role in mobilizing trapped oil droplets in porous media. *Langmuir*, 31(51):13673–13679.

Youssif, M. I., El-Maghraby, R. M., Saleh, S. M., and Elgibaly, A. (2018). Silica nanofluid flooding for enhanced oil recovery in sandstone rocks. *Egyptian Journal of Petroleum*, 27(1):105–110.

Yu, F., Chen, Y., Liang, X., Xu, J., Lee, C., Liang, Q., Tao, P., and Deng, T. (2017). Dispersion stability of thermal nanofluids. *Progress in natural science: Materials international*, 27(5):531–542.

Yu, J., An, C., Mo, D., Liu, N., and Lee, R. L. (2012). Study of adsorption and transportation behavior of nanoparticles in three different porous media. In *SPE improved oil recovery symposium*. Society of Petroleum Engineers.

Yu, W. and Xie, H. (2012). A review on nanofluids: preparation, stability mechanisms, and applications. *Journal of nanomaterials*, 2012:1.

Zallaghi, M., Kharrat, R., and Hashemi, A. (2018). Improving the microscopic sweep efficiency of water flooding using silica nanoparticles. *J. Pet. Explor. Prod. Technol.*, 8(1):259–269.

Zhang, H., Ramakrishnan, T., Nikolov, A., and Wasan, D. (2016). Enhanced oil recovery driven by nanofilm structural disjoining pressure: flooding experiments and microvisualization. *Energy & Fuels*, 30(4):2771–2779.

Zhang, T., Davidson, D., Bryant, S. L., and Huh, C. (2010). Nanoparticle-stabilized emulsions for applications in enhanced oil recovery. In *SPE improved oil recovery symposium*. Society of Petroleum Engineers.

Zhang, T., Murphy, M. J., Yu, H., Bagaria, H. G., Yoon, K. Y., Nielson, B. M., Bielawski, C. W., Johnston, K. P., Huh, C., and Bryant, S. L. (2015). Investigation of nanoparticle adsorption during transport in porous media. *SPE Journal*, 20(04):667–677.

Zhang, X., Servos, M. R., and Liu, J. (2012). Ultrahigh nanoparticle stability against salt, ph, and solvent with retained surface accessibility via depletion stabilization. *J. Am. Chem. Soc.*, 134(24):9910–9913.

Zhou, X., Morrow, N. R., and Ma, S. (2000). Interrelationship of wettability, initial water saturation, aging time, and oil recovery by spontaneous imbibition and waterflooding. *SPE Journal*, 5(02):199–207.

APPENDIX A

Glass Micromodel Flooding Results

Table A.1 presents the results of 23 nanoparticles injection from start (at S_{wi}) using uniform pore network glass micromodels. Measured data for polymer-based fluid #28 is also included. The secondary EOR injection tests were conducted until there was no change in oil saturation. This was achieved for about 400 minutes. Step-wise images were taken over time to determine residual oil saturation in the micromodel using the Matlab script.

Table A.1: Percentage of oil remaining in the glass micromodel over the injection time for twenty-three nanofluid samples plus one polymer sample.

Time‡	**02-1**	**02-2**	**02-3**	**02-4**	**02-5**	**02-6**	**02-7**	**02-8**	**02-9**	**02-10**	**02-11**	**02-12**	**02-13**	**02-14**	**02-15**	**16**	**17**	**18**	**19**	**20**	**21**	**22**	**23**	**28**†
0	100	100	100	100	100	100	100	100	100	100	100	100	100	100	100	100	100	100	100	100	100	100	100	100
5	42.23	19.40	11.00	47.14	38.62	54.39	22.06	49.02	27.92	25.75	18.25	12.26	15.63	22.33	24.99	27.79	26.88	10.01	46.28	29.66	38.97	40.19	34.59	1.36
10	13.23	9.94	7.68	6.85	30.69	36.63	5.72	18.20	11.91	9.11	10.09	13.42	9.79	10.38	11.27	22.54	20.97	9.25	20.85	21.36	18.24	26.07	16.26	0.81
15	12.24	10.65	6.03	9.69	28.97	37.97	6.07	12.87	10.59	8.60	9.39	13.24	10.54	10.19	10.98	21.08	17.55	8.38	19.77	19.25	16.97	24.32	15.75	1.44
20	12.31	10.60	6.13	9.22	24.21	32.82	6.35	9.28	11.07	7.94	9.93	12.74	9.17	11.25	11.30	21.00	16.23	7.13	19.49	16.85	17.09	23.53	16.17	1.49
25	12.42	11.02	6.04	9.42	23.10	31.52	6.63	8.42	10.67	7.92	9.18	12.09	9.38	10.91	11.04	21.02	16.25	6.21	19.20	17.19	17.04	22.49	16.52	1.61
30	12.34	11.23	6.13	9.15	21.85	31.33	7.06	8.99	10.53	7.24	9.11	11.49	9.26	11.05	10.19	21.02	16.25	3.66	18.87	17.38	17.18	22.40	16.67	1.63
60	12.37	11.08	5.47	8.40	19.62	30.48	8.44	9.04	9.17	8.79	8.94	10.74	9.10	9.72	11.09	21.01	16.25	5.89	18.03	17.64	17.14	22.38	17.27	1.68
90	12.23	10.69	5.49	8.73	19.51	30.33	8.07	9.51	9.10	7.33	8.50	10.54	9.07	9.99	11.03	20.93	16.19	2.74	17.79	18.29	17.44	22.96	17.04	1.64
120	12.31	9.35	5.27	8.45	18.59	29.17	7.64	9.45	8.92	8.51	7.83	10.95	8.96	9.93	10.57	20.87	16.30	2.00	17.87	18.32	17.87	22.55	16.99	1.68
180	12.26	9.43	5.46	8.05	18.26	28.83	7.58	8.77	9.09	8.35	7.71	11.00	9.02	9.70	10.56	20.82	16.27	0.79	17.37	18.51	17.95	22.44	15.21	1.71
240	12.37	9.40	5.32	7.45	18.23	29.07	7.37	8.77	8.71	7.99	7.31	11.15	9.02	9.62	12.26	20.74	16.12	0.49	17.00	19.25	18.04	22.36	15.40	1.51
300	12.22	9.07	5.16	7.31	17.85	27.65	7.27	9.10	8.56	8.07	7.25	10.17	9.05	9.02	11.84	20.72	16.10	0.46	17.08	18.61	17.99	22.52	15.27	1.47
360	12.46	8.83	5.18	7.18	17.65	27.52	7.18	7.56	8.42	7.87	7.06	10.82	8.85	8.84	10.53	20.66	16.03	0.26	17.08	18.55	17.93	22.43	15.25	1.41
400	12.47	8.92	5.10	7.25	-	27.34	7.19	7.52	8.50	7.36	7.10	10.84	8.84	8.91	10.50	20.63	16.05	0.22	17.03	18.47	17.91	22.34	15.20	1.19

† Polymer
‡ In minutes

APPENDIX B

Petrophysical Properties of the Core Plugs

Table B.1: Petrophysical properties of water-wet cores. The initial water saturation and OOIP were determined by core flooding method. These cores were used for flooding experiment in section 5.5.1. The porosity and pore volume were determined by saturation method.

Core ID	NF type	D (cm)	l (cm)	ϕ (%)	k_{liq} (mD)	PV (ml)	OOIP (ml)	S_{wi} (%)
B9-1	02-3	3.75	4.6	17.74	407	8.82	5.60	36.50
B9-2		3.75	4.5	17.17	378	8.53	5.70	33.17
B9-3	02-4	3.75	4.5	16.96	322	8.53	5.65	33.78
B9-4		3.75	4.5	18.07	277	8.98	5.40	39.85
B9-5	02-6	3.80	4.5	16.54	300	8.24	5.95	27.75
B9-6		3.75	4.5	17.66	318	8.74	6.55	25.04
B9-7	02-7	3.76	4.5	16.53	265	8.24	6.00	27.15
B9-8		3.77	4.5	17.17	292	8.52	6.10	28.38
B9-9	02-8	3.75	4.5	17.25	302	8.57	5.60	34.66
B9-10		3.75	4.4	17.01	343	8.48	6.70	20.94
B9-11	02-9	3.75	4.5	16.75	250	8.34	6.35	23.85
B9-12		3.75	4.5	18.29	352	9.10	6.50	28.62
B9-13	02-13	3.75	4.5	16.93	264	8.41	6.50	22.72
B9-14		3.75	4.5	16.03	261	7.96	6.45	19.61
B9-15	18	3.75	4.5	16.73	247	8.29	6.60	20.43
B9-16		3.75	4.6	17.66	319	8.74	6.23	29.03
B9-17	23	3.80	4.6	16.83	272	8.37	6.20	25.88
B9-18		3.75	4.7	17.70	299	8.85	6.50	20.56

Table B.2: Petrophysical properties of the aged cores (neutral-wet) and initial water saturation obtained by the centrifuge. All of the cores were used for nanofluid flooding as secondary oil recovery experiment in section 5.5.2. The porosity and pore volume were determined by saturation method.

Core ID	NF type	D (cm)	l (cm)	ϕ (%)	k_{liq} (mD)	PV (ml)	OOIP (ml)	S_{wi} (%)
B9-19	02-3	3.75	4.5	17.13	351	8.51	7.65	10.15
B9-20		3.75	4.5	17.60	330	8.73	7.65	12.33
B9-21	02-4	3.75	4.46	17.61	299	8.67	7.80	10.08
B9-22		3.75	4.49	17.32	318	8.59	7.60	11.51
B9-23	02-6	3.75	4.75	15.44	256	7.88	7.00	11.17
B9-24		3.75	4.5	17.13	226	8.51	7.20	15.44
B9-25	18	3.76	4.5	18.22	297	9.11	7.40	18.74
B9-26		3.76	4.5	17.61	291	8.80	7.40	15.91
B9-27	28	3.75	4.5	17.50	292	8.74	7.40	15.33
B9-28		3.75	4.5	17.37	309	8.68	7.60	12.45
B9-29	31	3.75	4.5	17.48	244	8.69	7.40	14.83
B9-30		3.75	4.5	17.79	194	8.80	7.40	15.91

Table B.3: Petrophysical properties of water-wet cores used in part three of the screening process, i.e. tertiary core flooding section 5.5.5. Initial water saturation and OOIP were established by core flooding method. The porosity and pore volume were determined by saturation method.

Core ID	NF type	D (cm)	l (cm)	ϕ (%)	k_{liq} (mD)	PV (ml)	OOIP (ml)	S_{wi} (%)
M1	02-3	3.76	6.0	17.72	315	11.81	7.80	33.93
M2		3.76	6.0	18.03	283	12.00	9.10	24.22
M3	02-4	3.76	5.99	17.64	395	11.68	8.80	24.68
M4		3.76	6.0	18.35	329	12.23	9.70	20.68
M5	02-6	3.76	6.0	17.15	324	11.42	8.30	27.34
M6		3.76	6.0	16.66	331	11.10	8.80	20.73
B9-31	02-8	3.75	4.5	16.14	390	8.02	6.10	23.97
B9-32		3.75	4.5	16.81	394	8.33	6.80	18.41

Table B.4: Petrophysical properties of the aged cores (neutral-wet); initial water saturation was established by the centrifuge. The cores plugs were used during nanofluid flooding experiments in section 5.5.6. The porosity and PV were determined by saturation method.

Core ID	NF type	D (cm)	l (cm)	ϕ (%)	k_{liq} (mD)	PV (ml)	OOIP (ml)	S_{wi} (%)
B9-33	02-3	3.75	4.5	15.62	228	7.82	7.0	10.49
B9-34		3.75	4.5	16.32	234	8.11	6.8	16.19
B9-35	02-4	3.75	4.5	16.34	238	8.12	7.5	8.0
B9-36		3.75	4.5	16.62	256	8.29	7.5	10.0
B9-37	02-6	3.75	4.5	17.68	248	8.83	7.0	20.75
B9-38		3.75	4.5	17.22	270	8.6	7.2	16.30
B9-39	02-8	3.76	4.5	16.92	233	8.45	6.4	24.29
B9-40		3.75	4.5	17.23	234	8.59	7.3	15.02
B9-41	18	3.75	4.5	16.45	230	8.22	7.0	14.82
B9-42		3.75	4.5	18.13	247	9.05	7.0	22.73
B9-43	28	3.75	4.5	17.83	278	8.93	7.2	19.38
B9-44		3.75	4.5	18.11	223	9.10	7.2	20.45
B9-45	31	3.75	4.5	17.15	251	8.53	7.2	15.59
B9-46		3.75	4.5	17.18	234	8.51	6.9	18.89

Table B.5: Petrophysical properties of water-wet cores used for nanofluid flooding tests in Section 5.5.7. The S_{wi} and OOIP were established by core flooding method. The porosity and PV were determined by saturation method.

Core ID	NF type	D (cm)	l (cm)	ϕ (%)	k_{liq} (mD)	PV (ml)	OOIP (ml)	S_{wi} (%)
B9-L1	02-3	3.76	10	19.31	488	21.37	16.1	24.68
B9-L2		3.75	10	19.78	490	21.84	14.8	32.23
B9-L3	02-4	3.75	10	15.85	434	17.55	15.7	10.53
B9-L4		3.75	10	16.22	521	17.90	16.0	10.64
B9-L5	02-6	3.76	10	17.11	601	18.94	16.0	15.51
B9-L6		3.75	10	16.75	603	18.49	15.4	16.73
B9-L7	02-8	3.76	10	18.40	391	20.31	16.5	18.76
B9-L8		3.75	10	18.31	156	20.29	16.5	18.71

Table B.6: Petrophysical properties of neutral-wet cores used for nanofluid flooding tests in section 5.5.9. The S_{wi} and OOIP were established by core flooding method. The porosity and PV were determined by saturation method.

Core ID	NF type	D (cm)	l (cm)	ϕ (%)	k_{liq} (mD)	PV (ml)	OOIP (ml)	S_{wi} (%)
B9-L9	02-3	3.76	10	17.61	324	19.25	14.5	24.66
B9-L10		3.75	10	17.23	384	19.55	15.00	21.32
B9-L11	02-4	3.75	10	17.4	360	19.22	16.10	16.24
B9-L12		3.75	10	17.56	434	19.39	16.20	16.45
B9-L13	02-6	3.76	10	17.96	460	119.83	16.3	17.81
B9-L14		3.75	10	17.29	411	119.10	16.3	15.0
B9-L15	02-8	3.76	10	17.43	425	19.25	16.6	14.0
B9-L16		3.75	10	17.0	376	18.78	15.10	19.60

APPENDIX C

Core Flooding Results

In this Appendix C, the results of the core flood are presented in detail. Oil recovery and pressure profile across the core are plotted as a function of pore volumes injected for each test conducted. The properties of the core plugs used are given in Table B.1-B.4.

C.1 Secondary Nanofluid Flooding in Water-wet cores

Table C.1: Summary of secondary nanofluid (NF02-3 and NF02-4) flooding results in water-wet cores.

Core ID	Sample	wt.%	PV@BT	RF @BT	V_o (ml)	RF (%)	S_{or} (%)
B9-1	02-3	0.10	0.58	47.37	2.80	50.00	31.75
B9-2			0.47	44.64	3.07	53.86	30.83
B9-3	02-4	0.10	0.45	47.20	2.95	52.21	31.64
B9-4			0.41	47.79	2.76	51.11	29.40

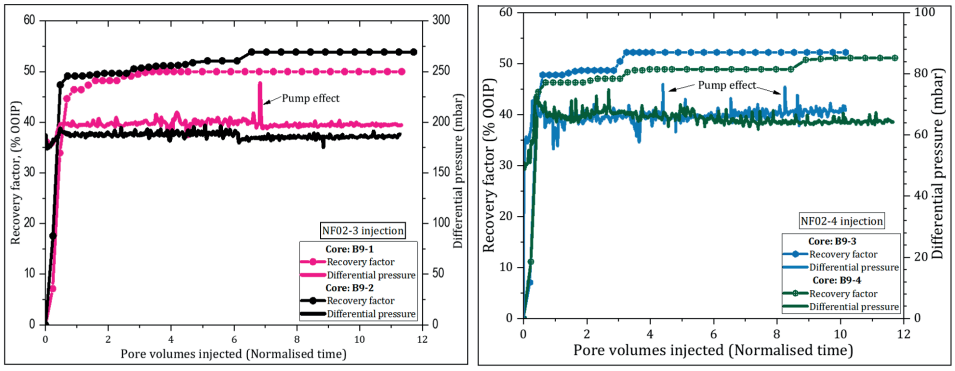

(a) **(b)**

Figure C.1: Secondary oil recoveries and dP versus PVs recorded throughout flooding tests. Two tests were conducted for each nanofluid type. (a) NF02-3 flooding; (b) NF02-4 flooding.

Table C.2: Absolute permeability and porosity measured before and after nanofluid core-flooding. The permeability was measured by gas permeameter and the Klinkenberg correction and the porosity by Helium porosimeter.

Core	**Absolute Permeability (mD)**			**Porosity (%)**		
ID	Before	After	% difference	Before	After	% difference
B9-1	407	385	-5	19	14	-25
B9-2	378	350	-7	18	15	-17
B9-3	322	309	-4	19	12	-35
B9-4	277	270	-3	18	13	-25

Table C.3: Summary of secondary nanofluid (NF02-6 and NF02-7) flooding results in water-wet cores.

Core ID	Sample	wt.%	PV@BT	RF @BT	V_o (ml)	RF (%)	S_{or} (%)
B9-5	02-6	0.10	0.49	50.42	3.17	53.28	33.75
B9-6			0.46	52.75	3.65	55.73	33.19
B9-7	02-7	0.10	0.49	41.67	2.84	47.33	38.37
B9-8			0.47	40.98	2.71	44.43	39.80

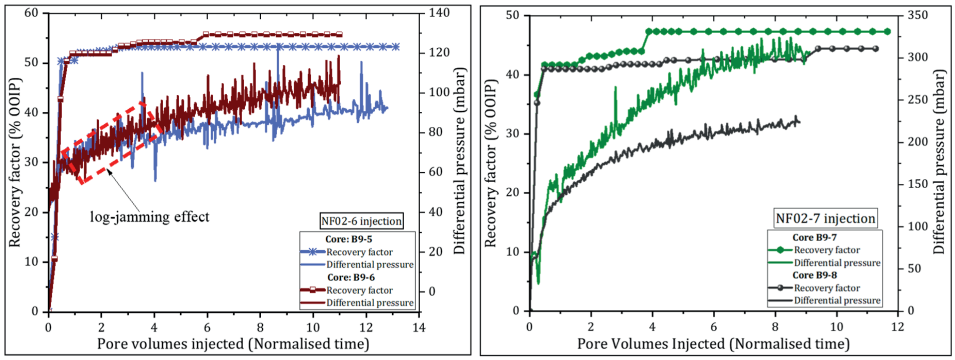

(a) **(b)**

Figure C.2: Secondary oil recoveries and dP versus PVs recorded throughout flooding tests. Two tests were conducted for each nanofluid type. (a) NF02-6 flooding; (b) NF02-7 flooding.

Table C.4: Absolute permeability and porosity measured before and after nanofluid core-flooding. The permeability was measured by gas permeameter and the Klinkenberg correction and the porosity by Helium porosimeter.

Core	**Absolute Permeability (mD)**			**Porosity (%)**		
ID	Before	After	% difference	Before	After	% difference
B9-5	300	265	-11	18	11	-36
B9-6	318	269	-15	19	14	-25
B9-7	265	186	-30	18	14	-18
B9-8	292	190	-35	18	15	-17

Table C.5: Summary of secondary nanofluid (NF02-8 and NF02-9) flooding results in water-wet cores.

Core ID	Sample	wt.%	PV@BT	RF @BT	V_o (ml)	RF (%)	S_{or} (%)
B9-9	02-8	0.10	0.47	45.18	2.82	50.36	32.44
B9-10			0.47	40.15	3.06	45.67	42.95
B9-11	02-9	0.10	0.48	42.52	2.95	46.46	40.77
B9-12			0.43	41.54	2.92	44.92	39.31

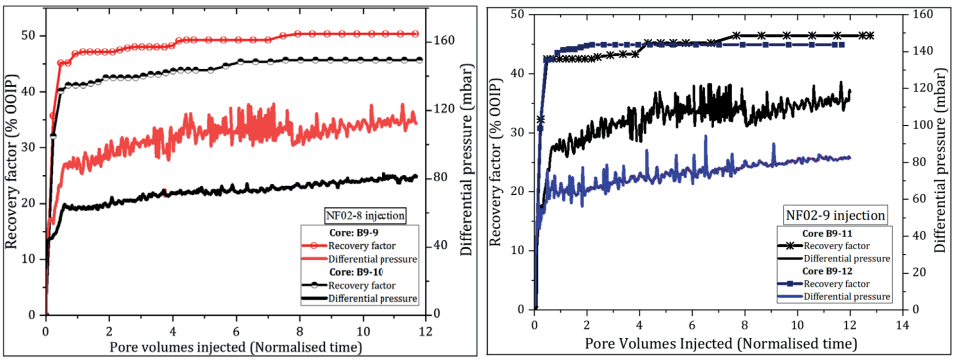

(a) **(b)**

Figure C.3: Secondary oil recoveries and dP versus PVs recorded throughout flooding tests. Two tests were conducted for each nanofluid type. (a) NF02-8 flooding; (b) NF02-9 flooding.

Table C.6: Absolute permeability and porosity measured before and after nanofluid core-flooding. The permeability was measured by gas permeameter and the Klinkenberg correction and the porosity by Helium porosimeter.

Core	**Absolute Permeability (mD)**			**Porosity (%)**		
ID	Before	After	% difference	Before	After	% difference
B9-9	302	249	-18	18	14	-25
B9-10	343	280	-18	18	14	-25
B9-11	250	186	-25	17	13	-22
B9-12	352	310	-12	20	15	-23

Table C.7: Summary of secondary nanofluid (NF02-13 and NF18) flooding results in water-wet cores.

Core ID	Sample	wt.%	PV@BT	RF @BT	V_o (ml)	RF (%)	S_{or} (%)
B9-13	NF02-13	0.10	0.40	36.92	3.02	46.50	41.38
B9-14			0.35	40.92	3.11	48.59	41.32
B9-15	NF18	0.10	0.41	40.15	3.36	50.91	39.06
B9-16			0.46	45.16	3.10	50.00	35.49

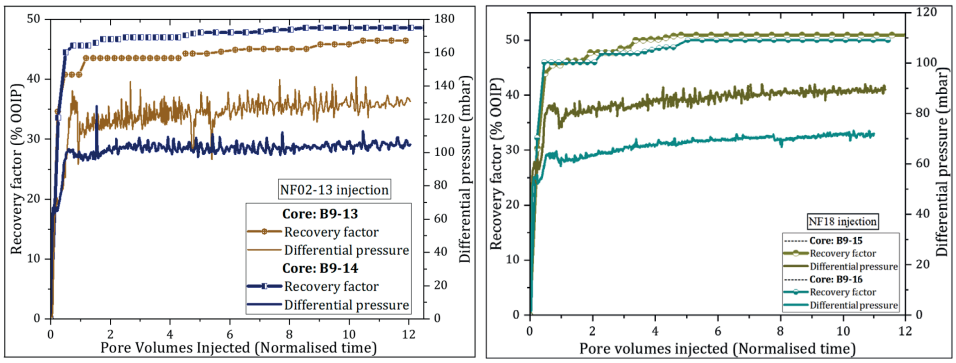

(a) **(b)**

Figure C.4: Secondary oil recoveries and dP versus PVs recorded throughout flooding tests. Two tests were conducted for each nanofluid type. (a) NF02-13 flooding; (b) NF18 flooding.

Table C.8: Absolute permeability and porosity measured before and after nanofluid flooding. The permeability was measured by gas permeameter and the Klinkenberg correction and the porosity by Helium porosimeter.

Core	**Absolute Permeability (mD)**			**Porosity (%)**		
ID	Before	After	% difference	Before	After	% difference
B9-13	264	234	-11	19	14	-27
B9-14	261	300	15	19	14	-28
B9-15	247	197	-20	18	12	-29
B9-16	319	357	12	18	14	-23

Table C.9: Summary of secondary nanofluid "NF23" flooding results in water-wet cores.

Core ID	Sample	wt.%	PV@BT	RF @BT	V_o (ml)	RF (%)	S_{or} (%)
B9-17	NF23	0.10	0.42	38.71	2.75	44.35	41.34
B9-18			0.43	34.29	3.06	47.07	38.90

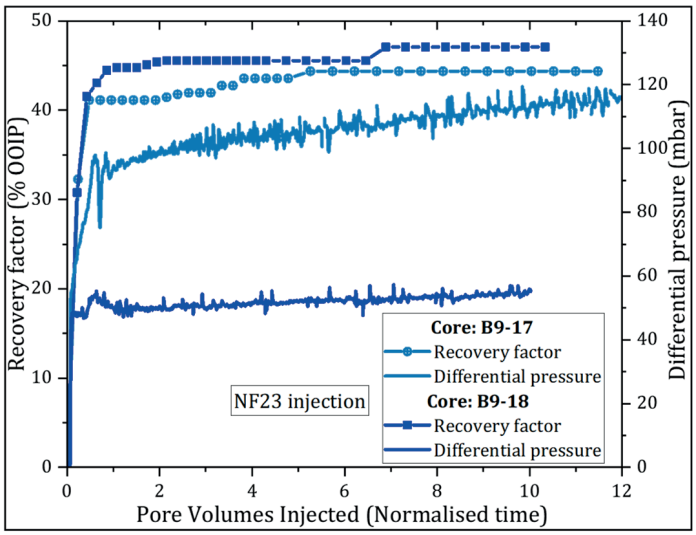

Figure C.5: Secondary oil recoveries factors and dP versus PVs recorded throughout the injection of nanofluid NF23 in neutral-wet cores for two tests conducted for tests #1 and #2.

Table C.10: Absolute permeability and porosity measured before and after nanofluid core flooding. The permeability was measured by gas permeameter and the Klinkenberg correction and the porosity by Helium porosimeter.

Core	**Absolute Permeability (mD)**			**Porosity (%)**		
ID	Before	After	% difference	Before	After	% difference
B9-17	272	-	-	17	15	-16
B9-18	299	359	+20	19	15	-23

C.2 Secondary Nanofluid Flooding in Neutral-wet cores

Table C.11: Oil recovery factors and residual oil saturation achieved at the end of secondary nanofluid "NF02-3" and "NF02-4" injection.

		Nanofluid Flood					Water Flood			
Core ID	NF type	PV (ml)	RF (%)	V_o (ml)	RF (%)	S_o (%)	V_o (ml)	RF (%)	S_o (%)	RF (%)
B9-19	NF02-3	0.35	40.52	4.60	60.13	35.83	-	-	-	60.13
B9-20		0.39	44.44	4.81	62.87	32.55	0.05	0.66	31.97	63.53
B9-21	NF02-4	0.34	42.31	4.61	59.10	36.78	-	-	-	59.10
B9-22		0.33	40.79	4.52	59.50	35.86	0.11	1.42	34.58	60.92

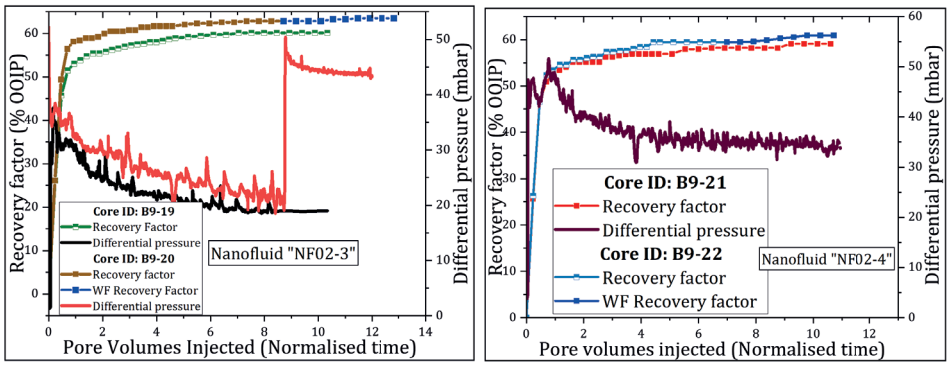

(a) **(b)**

Figure C.6: Secondary oil recovery factors and dP versus PVs recorded throughout flooding experiment; two tests were conducted for each nanofluid type at 0.2 ml/min. Water flooding was applied in one of the two cores at 0.5 ml/min. (a) "NF02-3" flooding; (b) "NF02-4" flooding, the dP failed to record properly for in the replicate test.

Table C.12: Oil recovery factors and residual oil saturation achieved at the end of secondary NF02-6 and NF18 injection.

		Nanofluid flood					Water flood			
Core ID	NF type	PV (ml)	RF (%)	V_o (ml)	RF (%)	S_o (%)	V_o (ml)	RF (%)	S_o (%)	RF (%)
B9-23	NF02-6	0.43	50.00	4.28	61.14	34.52	0.15	2.15	32.19	63.29
B9-24		0.36	47.22	4.31	59.89	33.92	-	-	-	59.89
B9-25	NF18	0.37	47.29	5.37	72.57	22.29	-	-	-	72.57
B9-26		0.34	41.89	5.21	70.40	24.89	0.12	1.63	23.52	72.03

Table C.13: Polymer-based fluid "#28" oil recovery factors and residual oil saturation achieved at the end of core-flooding.

		Polymer flood					Water flood			
Core ID	Fluid type	PV (ml)	RF (%)	V_o (ml)	RF (%)	S_o (%)	V_o (ml)	RF (%)	S_o (%)	RF (%)
B9-27	#28	0.31	41.22	4.88	65.95	28.83	-	-	-	65.95
B9-28		0.33	36.10	5.08	66.83	29.03	0.16	2.12	27.18	58.95
B9-29	#31	0.32	38.50	4.78	64.59	30.15	-	-	-	64.59
B9-30		0.33	36.36	4.32	66.83	38.02	0.27	3.51	34.99	59.61

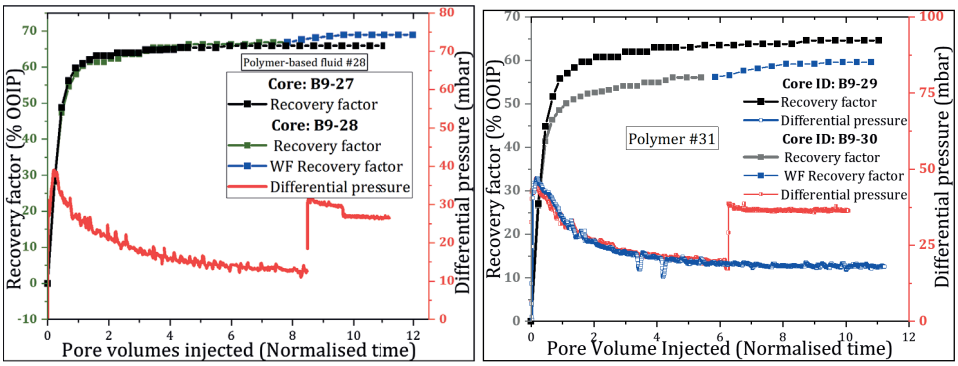

(a) **(b)**

Figure C.7: Secondary oil recovery factors and dP versus PVs recorded throughout flooding experiment; two tests were conducted for each polymer type at 0.2 ml/min. Water flooding was applied in one of the two cores at 0.5 ml/min. (a) Polymer-based fluid #28 flooding; (b) Polymer-based fluid #31 flooding.

C.3 Tertiary Nanofluid Flooding in Water-wet Cores

Table C.14: Oil recovery factors (expressed as % of OOIP) of water- and Nanofluid flooding and the respective residual oil saturation achieved at the end of core-flooding in water-wet cores.

Core	Water flood			NF	Nanofluid flood			Total
ID	V_o (ml)	RF	S_{or} (%)	type	V_o (ml)	RF	S_{or} (%)	RF (%)
B9-M1	3.36	43.08	37.61	NF02-3	0.36	4.61	34.55	47.69
B9-M2	3.54	38.90	46.29		0.66	7.25	40.83	46.15
B9-M3	3.36	43.08	37.61	NF02-4	0.36	4.61	34.55	47.69
B9-M4	3.54	38.90	46.29		0.66	7.25	40.83	46.15
B9-M5	3.38	40.72	43.07	NF02-6	0.72	8.67	36.78	49.39
B9-M6	3.34	37.91	49.22		0.86	9.77	41.47	47.68
B9-M7	2.14	35.08	49.35	NF02-8	0.58	9.51	42.14	44.59
B9-M8	2.76	40.58	48.48		0.45	6.62	43.09	47.20

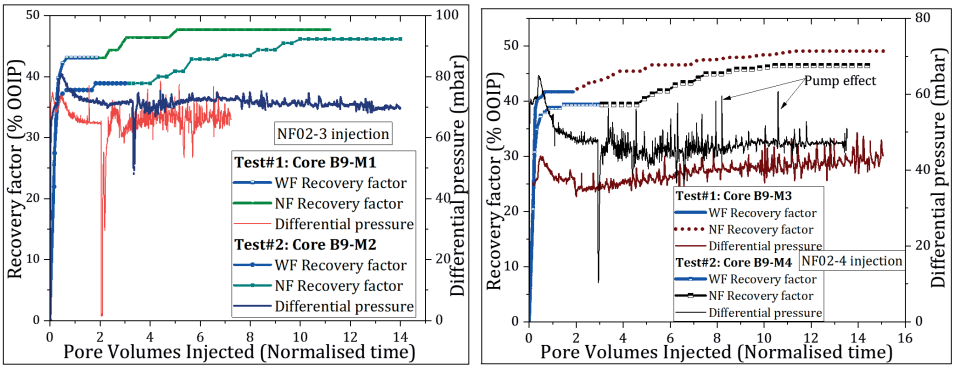

(a) **(b)**

Figure C.8: Oil recovery factors and dP recorded as function of PVs throughout the injection of nanofluid as tertiary EOR in water-wet cores. Both flooding schemes were conducted at 0.2 ml/min. Two tests were conducted for each nanofluid type. (a) NF02-3 flooding: In test#1, the first oil appeared at 0.5 PV of nanofluid injection resulting in RF of 1.33%; at ≈ 1PV the RF to 3.33%. Test#2, the first oil appeared at 1.33 PV and the RF was 1.1% of OOIP; (b) NF02-4 flood: In test#1, the first oil appeared at 0.51 PV of nanofluid injection resulting in RF of 0.6%; at ≈ 1PV the recovery increased to 2.16%. Test#2, the first oil appeared at ≈ 1.8 PV, resulting in recovery of 1.03% of OOIP.

C.4 Tertiary Nanofluid Flooding in Neutral-wet Cores

Table C.15: Oil recovery factors (expressed as % of OOIP) of water- and Nanofluid flooding and residual oil saturation achieved at the end of core-flooding in neutral-wet cores.

Core	Water flood			Nanofluid	Nanofluid flood			Total
ID	V_o (ml)	RF	S_{or} (%)	type	V_o (ml)	RF	S_{or} (%)	RF (%)
B9-33	4.12	58.86	36.83	NF02-3	0.19	2.71	34.39	61.57
B9-34	3.52	51.80	40.38		-	-	-	51.80
B9-35	4.60	61.33	35.72	NF02-4	0.25	3.33	32.64	64.67
B9-36	4.10	54.70	40.96		0.25	3.36	37.98	58.03
B9-37	4.15	59.29	32.26	NF02-6	0.23	3.29	29.66	62.57
B9-38	4.18	58.05	35.10		0.30	4.17	31.62	62.22
B9-39	3.17	49.59	38.16	NF02-8	0.28	4.40	34.80	54.03
B9-40	4.08	55.97	37.41		0.38	5.21	32.99	61.17

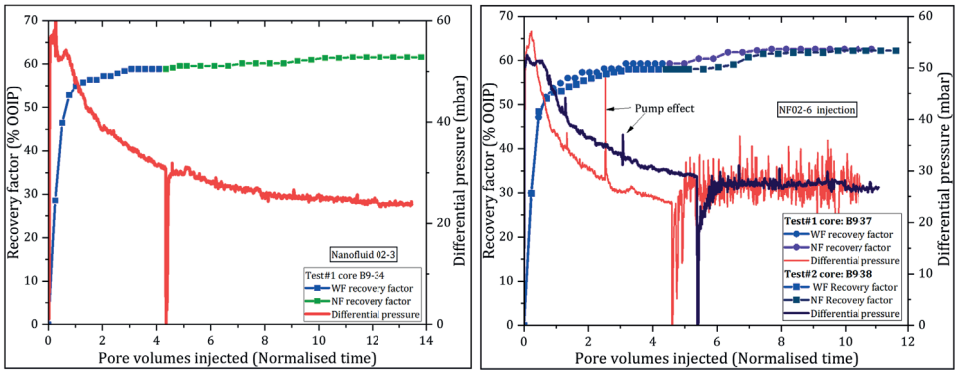

(a) **(b)**

Figure C.9: Oil RF and dP recorded as function of PVs during tertiary nanofluid injection in neutral-wet cores. Two tests were conducted for each nanofluid type. (a) NF02-3 flooding: In test#1, the first oil occurred at ≈ 0.51 PV of nanofluid injection and at 1PV the recovery increased to 0.71%. Tests#2 failed.; (b) NF02-6 flooding: The oil production occurred ≈ 1.4 and 1.63 PVs, resulting in recovery of about 1.14 and 0.41 of OOIP for test #1 and #2, respectively.

Table C.16: Oil recovery (expressed as % of OOIP) of water- and nanofluid "18"-flooding and the respective residual oil saturation achieved at the end of core-flooding in neutral-wet cores.

Core	Water flood			Nanofluid flood			Total
ID	V_o (ml)	RF (%)	S_{or} (%)	V_o (ml)	RF (%)	S_{or} (%)	RF
B9-41	4.01	57.29	36.38	0.20	2.85	33.94	60.14
B9-42	4.14	59.14	31.57	0.18	2.57	29.58	61.71

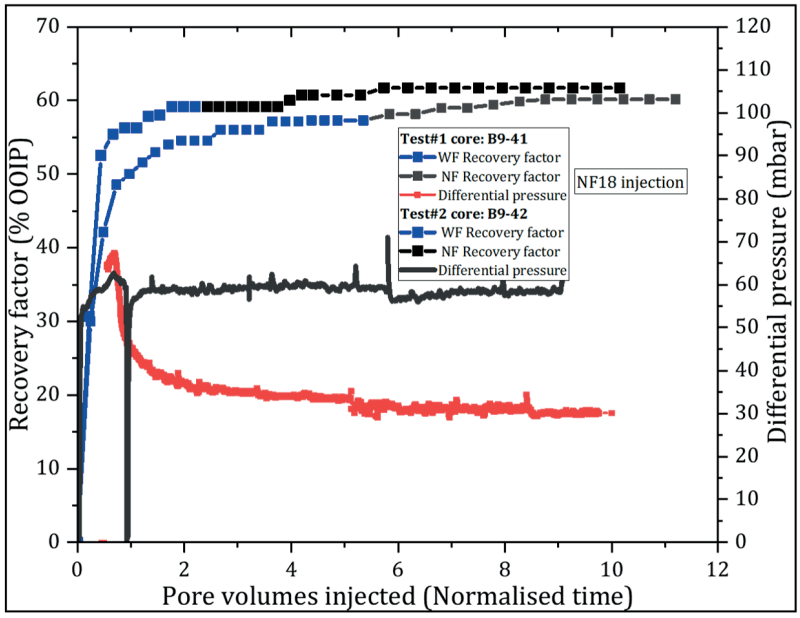

Figure C.10: Oil recovery factors and differential pressure recorded as a function of PVs during the injection of nanofluid NF18 as tertiary EOR in neutral-wet cores. Both flooding schemes were conducted at 0.2 ml/min. At 1PV test#1 and test#2 produced about 1% of oil and it was lower 1% OOIP.

Table C.17: Oil recovery (expressed as % of OOIP) of water- and polymer-based fluids injection and the respective residual oil saturation achieved at the end of core flooding in neutral-wet cores.

Core	Water flood			Polymer	Nanofluid flood			Total
ID	V_o (ml)	RF	S_{or} (%)	type	V_o (ml)	RF	S_{or} (%)	RF
B9-43	4.51	62.64	30.12	#28	0.13	1.81	28.67	64.44
B9-44	4.59	63.75	28.84		0.20	2.78	26.63	66.53
B9-45	4.45	61.81	32.24	#31	0.06	0.83	31.54	62.64
B9-46	3.75	54.28	37.09		0.19	2.82	34.86	57.03

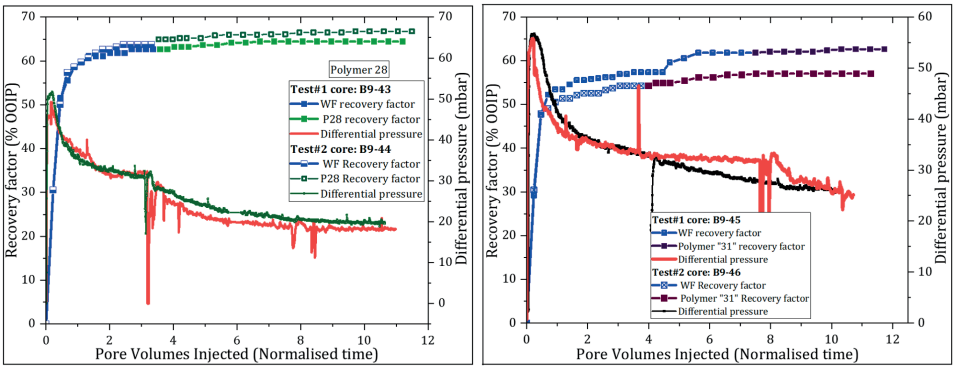

(a) **(b)**

Figure C.11: Oil recovery factors and dP recorded as a function of PVs during the injection of polymer as tertiary EOR in neutral-wet cores. Both flooding schemes were conducted at 0.2 ml/min. Two tests were conducted for each polymer type. (a) Polymer-based fluid #28 injection: The recover factor at 1PV was lower than 1% for both test#1 and test#2; (b) Polymer-based fluid #31 injection: The recover factor at 1PV was lower than 1% for both test#1 and test#2.

C.5 Tertiary Nanofluid Flood in Water-wet Cores at High Temperature

Table C.18: Oil recovery (expressed as % of OOIP) of water- and nanofluid "NF02-3" and the respective residual oil saturation achieved at the end of core-flooding in water-wet cores.

	Water flood				Nanofluid flood				Total
Core ID	V_o[1] (ml)	V_o[2] (ml)	RF (%)	S_o (%)	V_o[1] (ml)	V_o[2] (ml)	RF (%)	S_o (ml)	RF (%)
L1	7.2	0.4	47.20	39.77	1.4	0.2	9.94	35.59	57.14
L2	6.5	0.6	47.97	31.57	1.1	0.6	11.08	27.75	59.05

[1, 2] Volume of oil produced at low rate (0.2 ml/min) and at high rate (2 ml/min), respectively.

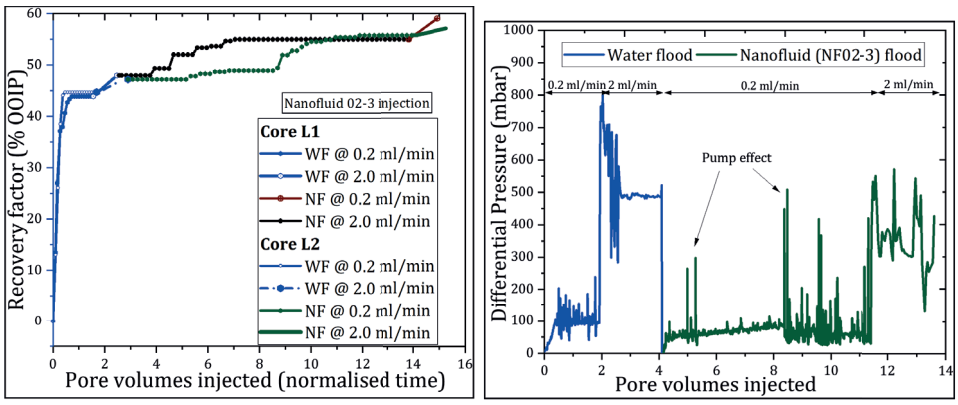

(a) **(b)**

Figure C.12: Oil recovery factor and dP recorded as a function of PVs injected (NF02-3) in water-wet cores. (a) The first oil due nanofluid flood was produced after 2.2 PVs and was 0.62% OOIP for test#1; for test#2, the first oil ocurred after 1.5 PVs and the RF was 1.35% of OOIP; (b) Differential pressure behaviour at each flooding stage for test#2.

Table C.19: Oil recovery (expressed as % of OOIP) of water- and nanofluid "NF02-4" and the respective residual oil saturation achieved at the end of core flooding in water-wet cores.

	Water flood				Nanofluid flood				Total
Core ID	V_o[1] (ml)	V_o[2] (ml)	RF (%)	S_o (%)	V_o[1] (ml)	V_o[2] (ml)	RF (%)	S_o (ml)	RF (%)
L3	8.1	0.7	56.11	39.27	0.8	0.5	8.40	31.86	64.40
L4	8.1	0.6	54.10	41.05	1.85	0.4	14.06	28.48	68.13

[1, 2] Volume of oil produced at low rate (0.2 ml/min) and at high rate (2 ml/min), respectively.

Table C.20: Oil recovery (expressed as % of OOIP) of water- and nanofluid "NF02-6" and the respective residual oil saturation achieved at the end of core-flooding in water-wet cores.

	Water flood				Nanofluid flood				Total
Core ID	V_o[1] (ml)	V_o[2] (ml)	RF (%)	S_o (%)	V_o[1] (ml)	V_o[2] (ml)	RF (%)	S_o (ml)	RF (%)
L5	8.0	0.7	54.06	38.81	1.4	0.3	10.31	30.10	64.38
L6	7.2	0.6	50.91	44.34	0.7	0.4	7.00	35.09	57.86

[1, 2] Volume of oil produced at low rate (0.2 ml/min) and at high rate (2 ml/min), respectively.

Table C.21: Oil recovery (expressed as % of OOIP) of water- and nanofluid "NF02-8" and the respective residual oil saturation achieved at the end of core-flooding in water-wet cores.

	Water flood				Nanofluid flood				
Core ID	V_o[1] (ml)	V_o[2] (ml)	RF (%)	S_o (%)	V_o[1] (ml)	V_o[2] (ml)	RF (%)	S_o (ml)	RF (%)
L7	8.2	0.7	53.64	37.67	1.4	0.1	9.09	30.03	62.73
L8	8.7	0.5	55.15	36.46	1.2	0.5	10.30	28.08	65.46

[1, 2] Volume of oil produced at low rate (0.2 ml/min) and at high rate (2 ml/min), respectively.

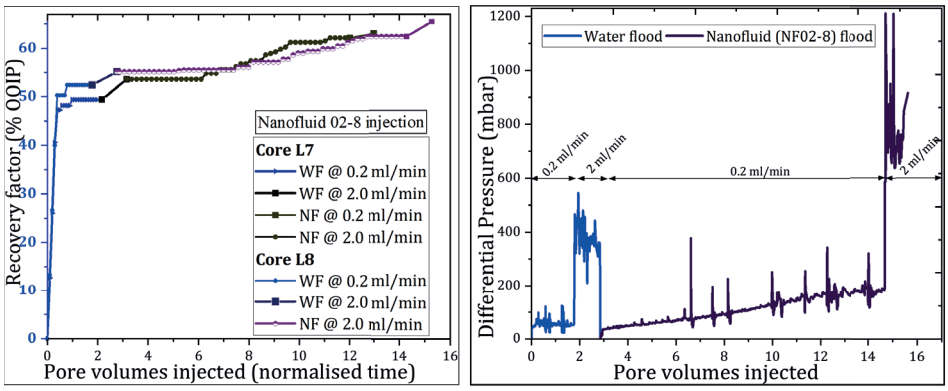

(a) **(b)**

Figure C.13: Oil recovery factors and dP recorded as a function of PVs injected for NF02-8 in water-wet cores. (a) Test#1: the first oil from nanofluid flood was produced after 3.7 PVs and it was ≈ 2% OOIP; for test#2, the first oil was produced after 2.5 PVs and the RF was ≈ 0.24% of OOIP ; (b) Differential pressure behaviour at each flooding stage for test#1.

C.6 Tertiary Nanofluid Flood in Neutral-wet Cores at High Temperature

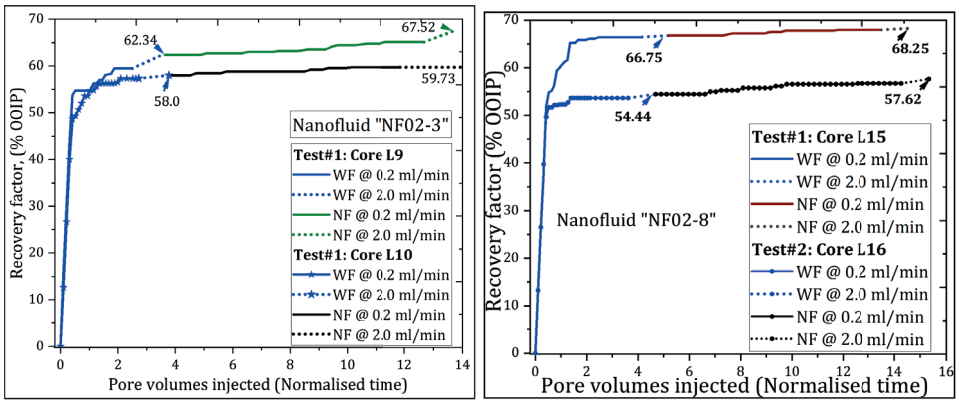

(a) **(b)**

Figure C.14: Effect of nanofluid injection on oil recovery during low rate and bump rate injections: (a) Sample NF02-3: Test#1 the first oil production occurred ≈1.56 PVs and the RF ≈0.41% OOIP; Test#2 produced ≈ 0.4% OOIP at 1 PV. (b) Sample NF02-8: Test#1 and Test#2 produced the first oil ≈2 PVs and the RF were ≈0.24% OOIP and ≈0.53% OOIP, respectively.

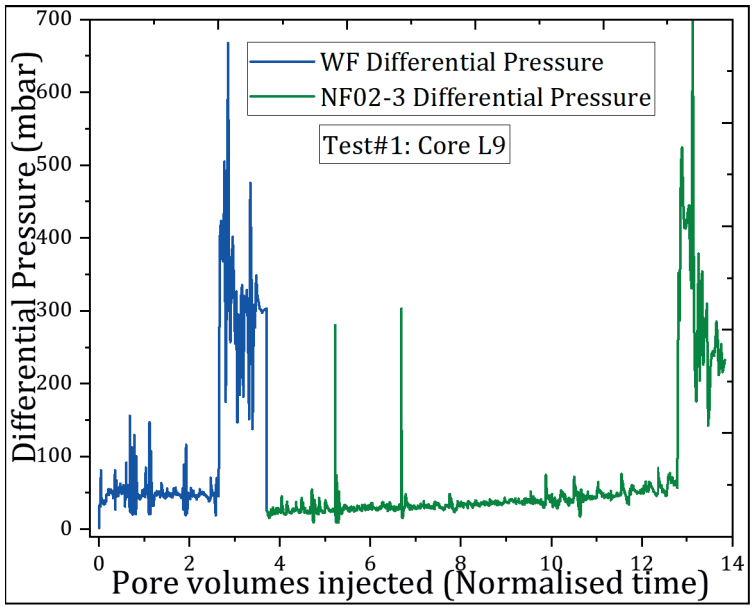

Figure C.15: Differential pressure recorded during water and nanofluid (NF02-3) flooding.

APPENDIX D

Amott Wettability Indices

Table D.1: Amott wettability indices determined on the cores after secondary nanofluid flooding. The cores were initially water-wet, then they were soaked in injected nanofluid (S_{or}) at 40 °C for 10 days.

Core ID	Sample	V_{o1} (cm^3)	V_{o2} (cm^3)	V_{w1} (cm^3)	V_{w2} (cm^3)	I_w	I_o	WI
B9-W1[a]	-	3.90	0.50	0.00	6.00	0.89	0.00	0.89
B9-W2[a]		3.90	0.60	0.00	5.80	0.87	0.00	0.87
B9-1	NF02-3	3.10	1.90	0.00	6.20	0.62	0.00	0.62
B9-2		3.10	2.20	0.00	6.30	0.58	0.00	0.58
B9-3	NF02-4	3.00	2.20	0.00	5.80	0.58	0.00	0.58
B9-4		2.90	2.10	0.00	5.80	0.58	0.00	0.58
B9-5	NF02-6	2.80	2.40	0.00	5.80	0.54	0.00	0.54
B9-6		3.00	2.20	0.00	6.00	0.58	0.00	0.58
B9-7	NF02-7	2.10	2.10	0.00	4.90	0.50	0.00	0.50
B9-8		2.60	2.20	0.00	5.60	0.54	0.00	0.54
B9-9	NF02-8	2.50	2.30	0.00	5.90	0.52	0.00	0.52
B9-10		2.70	2.20	0.00	5.70	0.55	0.00	0.55
B9-11	NF02-9	2.90	1.80	0.00	5.30	0.62	0.00	0.62
B9-12		3.00	2.30	0.00	6.00	0.57	0.00	0.57
B9-13	NF02-13	2.80	1.80	0.00	5.50	0.61	0.00	0.61
B9-14		2.80	2.00	0.00	5.40	0.58	0.00	0.58
B9-15	NF18	2.80	2.30	0.00	5.40	0.55	0.00	0.55
B9-16		3.40	2.30	0.00	5.80	0.60	0.00	0.60
B9-17	NF23	3.50	2.10	0.00	6.40	0.63	0.00	0.63
B9-18		2.50	1.50	0.00	5.80	0.63	0.00	0.63

[a] Reference WI of the cores prior to nanofluid flood.

Table D.2: Amott wettability indices evaluated after secondary nanofluid-flooding on initially neutral-wet cores.

Core ID	Sample	V_{o1} (cm^3)	V_{o2} (cm^3)	V_{w1} (cm^3)	V_{w2} (cm^3)	I_w	I_o	WI
A1[b]		0.0	4.5	0.3	3.0	0.00	0.09	-0.09
A2[b]	-	0.1	6.0	0.5	4.0	0.01	0.11	-0.10
A3[b]		0.0	3.0	0.3	4.0	0.00	0.07	-0.07
A4[b]	-	0.0	6.5	0.5	4.0	0.00	0.11	-0.11
A5[b]		0.1	6.5	0.5	4.0	0.01	0.11	-0.10
A6[b]	-	0.0	4.0	0.4	2.0	0.00	0.17	-0.17
B9-19[c]	02-3	3.80	1.40	0.10	6.20	0.73	0.02	0.71
B9-20		3.80	1.80	0.00	1.00	0.68	0.00	0.68
B9-21[c]	02-4	3.80	1.90	0.00	1.80	0.67	0.00	0.67
B9-22		3.40	2.00	0.00	6.20	0.63	0.00	0.63
B9-23	02-6	3.40	1.40	0.00	5.20	0.71	0.00	0.71
B9-24[c]		3.80	1.00	0.00	5.40	0.79	0.00	0.79
B9-25[c]	18	3.50	1.00	0.22	6.60	0.78	0.03	0.75
B9-26		2.70	3.50	0.05	6.80	0.44	0.01	0.43

[b] Reference WI of the cores prior to nanofluid flooding indicating neutral wettability.
[c] Cores soaked in the injected nanofluid at 40 °C for 10 days, then evaluated for wettability.

Table D.3: Amott water indices evaluated after tertiary nanofluid flooding in initially water-wet cores. There was no oil imbibition during tests.

Core ID	Sample	V_{o1} (cm^3)	V_{o2} (cm^3)	V_{w1} (cm^3)	V_{w2} (cm^3)	I_w	I_o	WI
M2	02-3	4.1	1.1	-	-	0.78	-	-
M4	02-4	3.0	0.50	-	-	0.58	-	-
M6	02-6	2.9	2.5	-	-	0.54	-	-
B9-32	02-8	2.80	1.30	-	-	0.68	-	-

Table D.4: Wettability indices obtained after tertiary nanofluid flooding in initially neutral-wet cores.

Core ID	**Sample**	$\mathbf{V}_{o1}$ (cm^3)	$\mathbf{V}_{o2}$ (cm^3)	$\mathbf{V}_{w1}$ (cm^3)	$\mathbf{V}_{w2}$ (cm^3)	$\mathbf{I}_w$	$\mathbf{I}_o$	**WI**
B9-33	02-3	3.60	1.30	0.05	5.20	0.73	0.01	0.73
B9-34[c]		3.80	1.20	0.55	5.20	0.76	0.10	0.66
B9-35[c]	02-4	3.30	2.10	0.90	5.20	0.61	0.15	0.46
B9-36		4.00	1.20	0.50	6.20	0.77	0.07	0.69
B9-37[c]	02-6	3.20	1.80	0.30	6.00	0.64	0.05	0.59
B9-38		3.80	2.20	0.80	5.80	0.63	0.12	0.51
B9-39[c]	02-8	3.20	1.50	0.30	5.30	0.68	0.05	0.63
B9-40		2.20	1.50	0.10	5.20	0.59	0.02	0.58
B9-41[c]	18	3.10	2.00	0.30	5.10	0.61	0.06	0.55
B9-42		2.90	2.40	0.00	1.20	0.55	0.00	0.55

[c] Cores soaked in the injected nanofluid at 40°C for 10 days, then evaluated for wettability.